# Experiments on the Transformation of Mud Flocs in Turbulent Suspensions

Duc Tran

Dissertation submitted to the Faculty of the
Virginia Polytechnic Institute and State University
in partial fulfillment of the requirements for the degree of

Doctor of Philosophy
in
Civil Engineering

Kyle B. Strom, Chair
Jennifer L. Irish
Nina Stark
Brian W. Romans

May 03, 2018
Blacksburg, Virginia

Keywords: Flocculation, Sediment Transport Modeling, Settling Velocity, Sand Clay Interaction, Equilibrium Floc Size

# Experiments on the Transformation of Mud Flocs in Turbulent Suspensions

Duc Tran

ACADEMIC ABSTRACT

This dissertation aims to better understand how floc aggregate characteristics and behaviors are modified under different local conditions and how such alterations impact the floc settling velocity, which is one of the most crucial parameters influencing sediment transport modeling.

A series of laboratory experiments were conducted to examine the impact of suspended sediment concentration, mixes of clay and silt, and resuspension process to equilibrium floc size and floc settling velocity. In order to observe floc size evolution, a new floc imaging acquisition was first developed. This new method allows flocs in suspended sediment concentration up to $C$ = 400 mg/L can be imaged non intrusively. This new method was applied in all three individual studies, which are composed of this dissertation.

The first chapter investigates the behaviors of flocs under constant and decay suspended sediment concentrations within a steady turbulent suspension. In the constant-concentration set of experiments, floc size time series were measured for 12 h for each of the concentration $C$ = 15, 25, 50, 100, 200, 300, and 400 mg/L. In the decay-concentration experiments, clear water was introduced to the mixing tank, simultaneously the suspension was drained out of the mixing tank at the same rate to make the suspended sediment concentration reduce while the turbulent shear was remained unchanged. The data shows that the equilibrium floc size is a weak, positive function of concentration. For example, in order to increase 20% of floc size ($\approx$ 22 $\mu$m) the concentration needs to be increased by 700% (going from 50 to 400 mg/L). The data also illustrates that during the decrease of concentration from $C$ = 400 to 50 mg/L, the floc size responses to the changes of concentration in the order of 10 min or less.

The second chapter examines how silt particles and clay aggregates interact in a turbulent suspension. Floc sizes and settling velocity of three different suspensions, i.e., pure clay, pure silt, and a mixture of clay and silt, were monitored. The floc size data show that the presence of silt particles does not have significant impacts on clay aggregate sizes. Silt particles, however, get bound up within floc aggregates, which in turn increase the settling velocity of the floc by at least 50%.

The third chapter examines whether any changes in floc properties during the deposition and resuspension processes. The floc sizes and shapes in a set of experiments with different consolidation times, concentrations, and shear patterns were measured. The conditions at which the flocs deposited or resuspended were maintained the same. The data reveal that floc size and shape of freshly deposited and after resuspended are unchanged. The erosion rate and concentration is a function of consolidation time and the applied shear stress during the deposition phase. Hence, there is a small reduction in resuspended concentration resulting in a slight decrease in resuspension floc size since floc size is also a function of concentration.

# Experiments on the Transformation of Mud Flocs in Turbulent Suspensions

Duc Tran

GENERAL AUDIENCE ABSTRACT

Sediment transport is a narrative poem from mother nature telling us about the evolution of ancient and modern rivers, deltas, and estuaries. For thousands of years, mankind has been examining the coarser part of the poem, the gravel and sand. The finer part, the mud, has not been systematically investigated until the last 60 years. The key difference between sand and mud is the capability of mud to aggregate and form flocs which have sizes, densities, and shapes that are vastly different from the original constitutive particles. This flocculation process adds a layer of dynamics to the erosion, deposition, and transport of mud that is not present in the transport of sand.

Therefore, the primary motivations for this dissertation are 1) to better understand the behavior of floc size under different conditions, e.g., in the estuaries, and 2) to provide high-quality data of floc characteristics and size evolution for model development, testing, and calibration purposes. Laboratory studies are conducted to measure the floc size and in some cases settling velocity, as a function of time under different turbulent, concentration, and sediment mixture. The findings in this dissertation help to fill the gaps of knowledge in cohesive sediment transport processes. This dissertation also suggests how floc behaviors should be accounted for under different conditions. Such information is valuable for projects such as management of sediment supplies, mitigation of land loss, restoration, and land-building diversions, e.g., on the Mississippi and Atchafalaya Rivers.

Data associated with this dissertation are also available on GitHub under https://github.com/FluidSedDynamics.

## Acknowledgments

I would like to express my sincere appreciation to my advisor Dr. Kyle Strom. He has been an excellent mentor over the last five years. I am truly grateful for all of his guidance, support, and trust given in my research explorations.

I would also like to thank my other advisory committee members, Dr. Brian Romans, Dr. Nina Stark, and Dr. Jennifer Irish. Thank you for taking time out to serve on my committee and I appreciate the different perspectives you brought to my studies.

Thanks to ExxonMobil Upstream Research Company for funding this work.

Additionally, I would like to thank my fellow graduate students with special appreciation to Mohamad Rouhnia, Hossein Hosseiny, Paul Hamilton, and Brandon Dillon for their time and help with my studies and laboratory experiments. My thanks go out to Chengzhao Zhang, Fong-Shu Jao, Jassim Jaf, Celso Castro Bolinaga, Nilay Iscen, Rachel Kuprenas, Christian Mooneyham and Jeffrey Culp whose friendship has made my graduate life especially memorable.

Last, but certainly not least, I would like to thank my wife, Van, for her support, patience, and encouragement.

## Contents

## List of Figures

## List of Tables

# 1 Introduction

## 1.1 Overview

Any water body generally consists of water, coarse non-cohesive sediment, and fine cohesive sediment. Existing hydrodynamic and morphordynamic models allow one to predict the transport of the first two phases, i.e., water and coarse non-cohesive sediment, within reasonable bounds. Yet, our current knowledge of flocculation processes is insufficient to quantitatively predict the fate of fine-grained sediment transport. This is because, when it comes to predicting the transport and depositional fate of suspended sediment, the accuracy of such models depends heavily on the selection of an appropriate sediment settling velocity, $w_s$ (Dyer, 1989; Winterwerp et al., 2002; Geyer et al., 2004; Harris et al., 2005; Partheniades, 2009; Chen et al., 2010). For sands, estimating the settling velocity is comparatively straightforward because $w_s$ is a function of the size, density, and shape of the particles found in the deposit (Rubey, 1933; Dietrich, 1982; Ferguson and Church, 2004). The settling velocity of mud is essentially a function of the same properties of size, density, shape, and porosity (Strom and Keyvani, 2011). However, the flocculation process complicates the estimation of these properties at the time of deposition for muds since suspensions of flocs can have sizes, densities, and shapes that are vastly different from the constitutive, or primary, particles found in the deposit or the water column at a particular moment in time (Krone, 1963; Dyer, 1989; Winterwerp and van Kesteren, 2004;

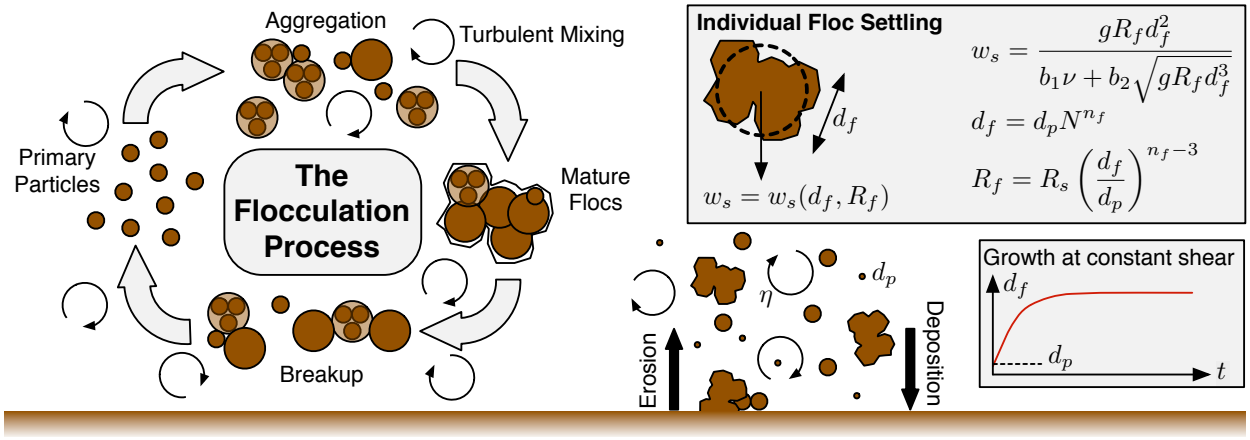


**Figure 1.1:** Schematic of the flocculation process. Floc settling velocity is a function of floc size, $d_f$ and floc submerged specific gravity, $R_f$ — which is related to the floc size and the size of the primary particles, $d_p$, through the 3D fractal dimension, $n_f$. The settling velocity equation shown is that of Strom and Keyvani (2011).

Partheniades, 2009). Therefore, understanding the flocculation process and its impact on settling velocity is crucial for sediment transport modeling of muds in rivers, estuaries, the shelf, and the deep ocean.

Flocculation is a process of simultaneous aggregation and breakup of cohesive particles within the water column (Krone, 1962; Winterwerp and van Kesteren, 2004), and is an important mechanism in a variety of fields of study, including: chemical and environmental engineering, oceanography, and river and estuarine mechanics (Argamam and Kaufman, 1970; Kranck, 1973; Gibbs, 1985; McAnally and Mehta, 2000; Biggs et al., 2003; Manning et al., 2010). In general, clay particles in suspension aggregate when they are brought close enough to each other for their overall net repulsive force (generated by a positively charged ion atmosphere) to be overcome by van der Waals attractive forces. Whether or not particles brought into proximity of each other aggregate is a function of the clay type, the actual distance between the particles, and the thickness of the diffuse ion atmosphere surrounding the particles.

Figure 1.1 depicts a few key elements related to flocs. The first key element to note is that there is a typical pattern to a time series of floc growth in a field of constant turbulent mixing. If one considers the growth of a suspension of primary particles from an unflocculated state up to a flocculated state, then the time series for the average floc size in the suspension will typically progress as shown in the bottom right panel of Figure 1.1. Initially, there will be a period of growth at a near constant rate. Following this, the rate of increase in size decreases as a steady-state size is asymptotically approached. Similar behavior is observed in the floc size distribution as a whole.

The second key element to note about mature flocs is that they are comprised of a large number of smaller particles and flocs that are packed together in a seemingly random way. This leads to irregularity in floc shape. It also leads to a floc density that is dependent on the packing arrangement of the constituent particles and the size of the floc itself. Observations have shown that, in general, floc density decreases with size following a power law decay (McCave, 1975). One mathematical framework used to view floc structure and theoretically account for this power-law decay in floc density is fractal geometry (Jiang and Logan, 1991; Kranenburg, 1994; Maggi and Winterwerp, 2004; Maggi, 2008). Under this framework, larger flocs are considered to be made up of smaller flocs which are composed of aggregates smaller yet and so-forth down to the so-called primary particles, or the smallest constituent particles within a flow (Winterwerp and van Kesteren, 2004) (Figure 1.1). One of the main advantages of treating flocs as fractal structures is that it allows for floc size, $d_f$, to be related to the size of the primary particles, $d_p$, and the total number of primary particles within the floc, $N$, through a 3D frac-

tal dimension, $n_f$ (the second equation, upper-right of Figure 1.1). This in turn allows for floc submerged specific gravity, $R_f = (\rho_f - \rho)/\rho$ (where $\rho_f$ is the floc density and $\rho$ is the water density), to be expressed as a function of floc size, the size of the primary particles, and the fractal dimension (Jiang and Logan, 1991; Kranenburg, 1994) (the third equation in the upper right of Figure 1.1). For a solid particle, $n_f = 3$, i.e., $R_f = R_s$. However, for flocs, $n_f$ is always less than 3. This means that $R_f$ will decrease with floc size following a negative power-law trend. The smaller the fractal dimension, the more loosely packed and irregularly shaped the flocs will be and the more rapidly $R_f$ will decrease with size. $n_f$ is therefore a useful index for quantifying the packing arrangement of particles within flocs.

There are at least three primary ways that flocculation impacts on settling have been incorporated into numerical models of sediment transport. In the first – the *size-based approach* – the floc size is modeled as a function of the hydrodynamic and suspension characteristics. The changes in floc size are then used along with a floc settling velocity equation, which uses the floc size and submerged specific gravity, to produce a dynamic settling velocity in the suspended sediment advection diffusion transport equation. The dynamic floc size is modeled either as a single, average floc size (Winterwerp, 1998; Winterwerp et al., 2006; Son and Hsu, 2008, e.g.) or a size population (e.g., McAnally and Mehta, 2000; Maggi, 2007; Verney et al., 2011). In general, these methods produce either a single (for the one size class) or multiple (for the multi-size class) PDEs whose solution yields the spatiotemporal floc size information. The methods are based on the principle of conservation of mass and use rate equations for aggregation and breakup of flocs based on particle collision theory and heuristic floc erosion models. Use of the

size-based approach for including flocculation effects in sediment transport models has largely been confined to the realm of academics. This is due to the increased computational cost demanded by the additional PDEs and the lack of floc size data needed for testing and calibrating the models.

In the second class of methods – the *steady-state approach* – the same governing equations for floc size are simplified through a steady-state assumption. The result is a model for the equilibrium floc size based on the aggregation and break up rate kernels. The settling velocity is then again calculated using a standard settling velocity equation. Because the approach neglects any time dependence, there is a built in assumption that flocs respond instantaneously to changes in local conditions.

The third method for producing a flocculations-influenced settling velocity is through the use of *empirical relations* between local turbulence and suspension characteristics and observed net settling behavior (Hwang and Mehta, 1989; van Leussen, 1999; Teeter, 2001). In some cases, such models are based on *in situ* estimates of suspension settling speeds and sometimes they are based on observations from stagnant tanks. By definition, the empirical relations assume that the settling properties of the suspension, and hence floc sizes, are in equilibrium with the locally-measured fluid and suspension properties. A practical advantage of the empirical relations approach is that no new PDEs need to be solved when modeling transport. The reason for this is that the relations link the local fluid and suspension properties, such as fluid shear rate and suspended sediment concentration, directly to a suspension settling velocity. The disadvantage of these methods is that key physics are often lost, and local conditions may

not best represent the historical conditions experienced by a floc that led to its current size and density. Because they are easy to implement, all practical modeling platforms that I am aware of, such as MIKE (DHI) and Delft3D (Deltares), use the empirical relations method for including flocculation influences when modeling mud transport.

## 1.2 Study Motivation

The incorporation of floc size modeling in sediment transport simulations has been limited, in part, because of the added computational expense associated with solving for floc size. Such limitations will be resolved in time as computational power and methods improve. However, the more fundamental limitation to inclusion of flocculation dynamics in sediment transport simulations is that there is very little time series data of floc size in turbulent suspensions with respect to key drivers. Without such data, it is difficult to test the conceptual models for flocculation that have been proposed. For instance, there is still uncertainty regarding the role that suspended sediment concentration plays in setting the equilibrium floc size, and few, if any, data has ever been collected to examine whether the presence of silts and sands in suspended muds impact floc properties such as size and density. Furthermore, current floc models have a number of water and sediment specific user-set coefficients; yet very little floc data exists in a form that is suitable for calibration or validation purposes.

Therefore, this dissertation broadly focuses on: (1) experimentally investigating the change in floc size with time in turbulent suspensions under the influence of different water column and sediment conditions; and (2) providing high-quality data of floc characteristics and size evolution under such conditions for floc size model development, testing, and calibration pur-

poses. The next section presents the specific research questions and hypotheses followed by an overview of the approaches used to test these hypotheses.

### 1.3 Research Questions and Hypotheses

In this section, a brief summary of three research questions, the hypotheses and a background introduction associated with each question are presented. The next chapters, Chapter 2, 3, and 4 are self-contained papers on the topics of 1) suspended sediment concentration influences floc growth rate and equilibrium floc size, 2) the impact of suspended silt on mud floc sizes and settling velocity, and 3) floc sizes and entrainment rates after repeated cycles of deposition and entrainment, respectively. The full background information and rational behind these hypotheses can be found in the self-contained papers in Chapter 2, 3, and 4. As of the writing of this dissertation, Chapter 2 and 3 both have been published in the Continental Shelf Research; Chapter 4 is in preparation and will be submitted soon.

In Chapter 2, we examine the question: How do changes in suspended sediment concentration alone influence the size of mud flocs under steady turbulent shearing? We hypothesize that (1) concentration exerts a strong control on the rate of floc growth, but (2) that it only exerts a weak control on the ultimate, equilibrium floc size.

The influence of suspended sediment concentration on floc growth, size, and density has been discussed in many studies (Burban et al., 1989; Chen and Eisma, 1995; Milligan and Hill, 1998; Shi, 2010). However, not all studies report the same impact on flocculation with changes in suspended sediment concentration. A positive relation between suspended concentration and equilibrium floc size has been observed in several studies (Eisma and Li, 1993; Berhane

et al., 1997; van Leussen, 1999; Gratiot and Manning, 2004; Law et al., 2013). However, there are other studies that show floc size can reduce with increasing concentration (Tsai et al., 1987; Burban et al., 1989). Furthermore, several other studies have not observed any relation between flocculation rate or equilibrium floc size and suspended sediment concentration (Milligan and Hill, 1998; Kumar et al., 2010). Chapter 2 investigates the relationship between suspended sediment concentration and floc sizes.

In Chapter 3, we investigate the question: Do suspended clay and silt size fractions act independently or dependently when it comes to settling in a turbulent flow? We hypothesize that are: (1) that the addition of silt will decrease the equilibrium floc size; (2) that a fraction of the silt will be bound within the flocs; and (3) that the addition of silt particles within the floc will produce an increase in the overall floc density and settling velocity.

To the best of our knowledge, whether or not this interaction does or does not occur has never been investigated in a turbulent suspension. Treating mixtures of suspended cohesive and non-cohesive sediment – like mixtures of clay and silt – independently is the commonly used approach in hydrodynamic and sediment transport models such as Delft3D, MIKE, and ROMS. The most essential assumptions made in such models is that concentration profiles of silt and clay are not impacted by other and are therefor linearly additive. Chapter 3 examines whether silt and clay in suspension can be treated independently or dependently.

Chapter 4 investigates: How do floc characteristics change once they have deposited to a bed, and how, if at all, are they modified during re-entrainment? The hypotheses are that (1) flocs grow in size once deposited on a bed; and (2) that re-entrainment efficiency plays a crucial

role in dictating re-suspension concentration which in turn influences the floc growth rate and equilibrium floc sizes after resuspension.

In many environments, recently deposited flocs (< 1 day) can be reentrained by increases in stress at the bed. For example, flocs deposited to the bed during high or low slack may experience significant erosive forces during the ebb or flood. Being able to properly characterize this reentrainment process is important for adequately modeling mud transport in systems that see either simultaneous erosion and deposition of flocs (such as in a river or turbidity current) or systems that have periodic erosion and deposition (such as estuaries and fresh shelf deposits that are reworked by waves).

### 1.4 Research Approach

Laboratory studies will be conducted to address the research questions by testing the hypotheses described above. A unifying quantity the work will seek to measure is the floc size, and in some cases settling velocity, as a function of time under different conditions of shear rate, concentration, consolidation time and sediment mixture. Experiments will primarily be carried out inside a mixing chamber where the turbulent shear rate, suspended sediment concentration, salt levels, and sediment type can be tightly controlled. Suspended sediment concentration will be measured with optical backscatter sensors (OBSs). Flocs sizes as a function of time and conditions will be measured using a floc camera system that is capable of photographing flocs while they are in suspension. When needed, the settling velocity of the flocs will be measured using an insulated settling column. Figure 1.2 illustrates the apparatus and setup of a typical experiment in this dissertation. The function and specifications of each devices in Figure 1.2

are highlighted in each individual Chapter.

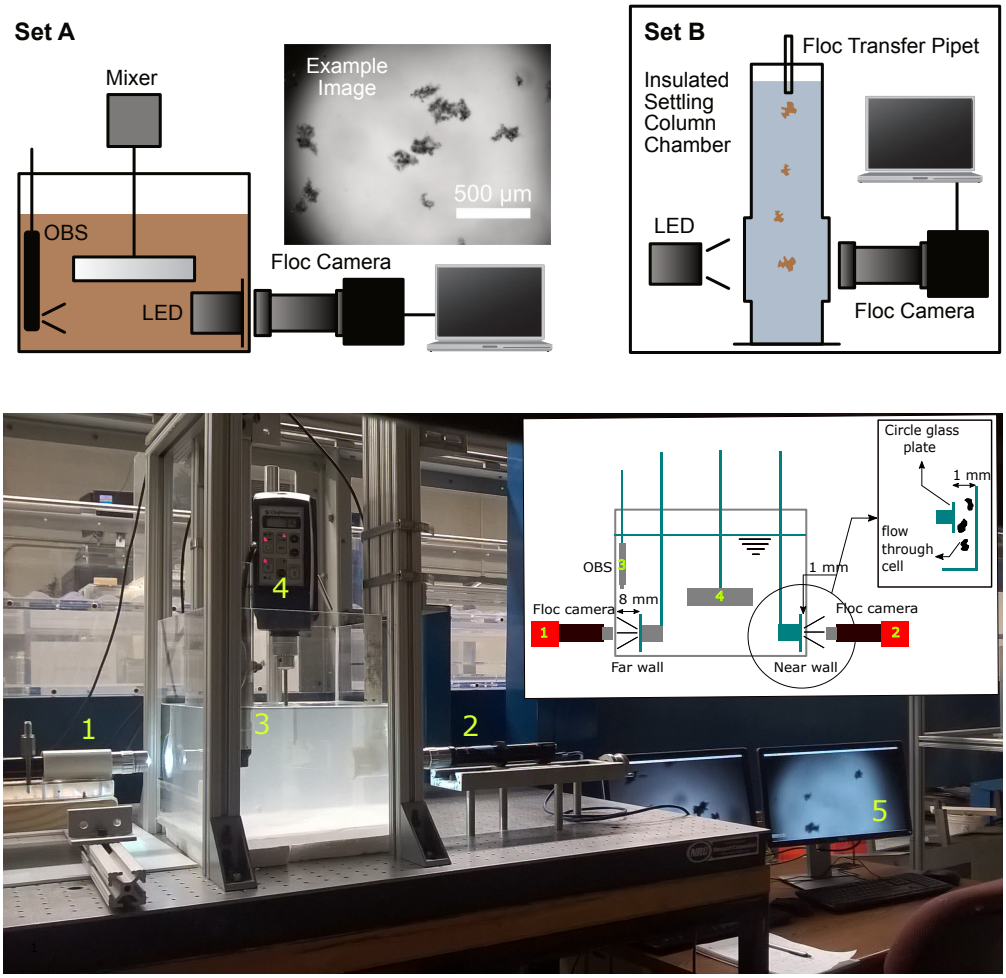


**Figure 1.2:** Upper panel: Schematic of the mixing tank and floc camera setup (Set A), and settling column (Set B). Lower panel: Schematic and picture of the Near Wall setup. The flow through cell results in slowing the speed and reducing the number of flocs being imaged.

A key to being able to obtain the data needed to test the hypotheses is the ability to collect time series measurements of floc sizes within a turbulent suspension over a range of suspended sediment concentration. Until now, both commercially manufactured and laboratory-built floc imaging systems have been confined to making measurements in concentrations less than 100 mg/L. The only way to make estimates of floc size in concentrations higher than this has been

to use proxy measurements such as those made with a LISST 100x, or to use other methods that can significantly alter the size of the flocs from that of what they may have been within the suspension, e.g., sizing with a Malvern mastersizer and pipet-sample-and-image-elsewhere methods. Therefore, the first task of this work was to develop a new method for making image-based measurements of flocs in suspensions up to concentrations of 400 mg/L. The new method, what I refer to as the Near Wall method (Figure 1.2 lower panel), created a flow-through cell by placing a round glass plate close to the wall. The placement of the glass near the wall both slowed the speed of the flocs and reduced the number of flocs between the light source and the tank wall. As a result, the Near Wall method significantly improves the quality of the floc images and also increases concentration in which the floc camera can be used. Details of the Near Wall method development and verification are presented in the Appendix of Chapter 2.

### 1.5 Dissertation Organization

The rest of this dissertation is organized into three primary chapters. Chapter 2 discusses the impact of concentration alone to equilibrium floc size and floc growth rate. This chapter also introduces a new image processing acquisition that allow us to capture floc images in suspension under concentration of $C$ = 400 mg/L. Chapter 2 was published in Continental Shelf Research as Tran et al. (2018). Chapter 3 examines the interaction of silt and clay under different shear conditions and different ratios of clay:silt in suspension. Chapter 3 was also published in Continental Shelf Research as Tran and Strom (2017). The third primary chapter, Chapter 4, investigates the changes, if any, of floc characteristics before deposit and after resuspension. Following this, the last chapter, Chapter 5, provides a summary of prominent findings from each individual

paper in the scope of how local conditions dictate floc behaviors and our recommendations of how to integrate such behaviors in flocculation models.

## Bibliography

Argamam, Y. and Kaufman, W. J. (1970). Turbulence and flocculation. *Journal of Sanitary Engineering, ASCE*, 96(SA2):223–241.

Berhane, I., richard W. Sternberg, Kineke, G. C., Milligan, T. G., and Kranck, K. (1997). The variability of suspended aggregates on the Amazon Continental Shelf. *Continental Shelf Research*, 17(3):267–285.

Biggs, C. A., Lant, P. A., and Hounslow, M. (2003). Modelling the effect of shear history on activated sludge flocculation. *Water Science and Technology*, 47(11):251–257.

Braithwaite, K. M., Bowers, D. G., Nimmo Smith, W. A. M., and Graham, G. W. (2012). Controls on floc growth in an energetic tidal channel. *Journal of Geophysical Research: Oceans*, 117(C2).

Burban, P.-Y., Lick, W., and Lick, J. (1989). The flocculation of fine-grained sediments in estuarine waters. *Journal of Geophysical Research*, 94(C6):8323–8330.

Chen, S. and Eisma, D. (1995). Fractal geometry of in situ flocs in the estuarine and coastal environments. *Netherlands Journal of Sea Research*, 33(2):173 – 182.

Chen, S.-N., Geyer, W. R., Sherwood, C. R., and Ralston, D. K. (2010). Sediment transport and

deposition on a river-dominated tidal flat: An idealized model study. *Journal of Geophysical Research*, 115(C10040).

Clark, M. M. and Flora, J. R. (1991). Floc restructuring in varied turbulent mixing. *Journal of Colloid and Interface Science*, 147(2):407 – 421.

de Lucas Pardo, M., Sarpe, D., and Winterwerp, J. C. (2015). Effect of algae on flocculation of suspended bed sediments in a large shallow lake. consequences for ecology and sediment transport processes. *Ocean Dynamics*, 65:889–903.

Dietrich, W. E. (1982). Settling velocity of natural particles. *Water Resources Research*, 18(6):1615–1626.

Dyer, K. R. (1989). Sediment processes in estuaries: future research requirements. *Journal of Geophysical Research*, 94(C10):14327–14339.

Eisma, D. and Li, A. (1993). Changes in suspended-matter floc size during the tidal cycle in the Dollard estuary. *Netherlands Journal of Sea Research*, 31(2):107–117.

Ferguson, R. and Church, M. (2004). A simple universal equation for grain settling velocity. *Journal of Sedimentary Research*, 74(6):933–937.

García, M. H. (2008). *Sediment Transport and Morphodynamics. Sedimentation Engineering*, chapter 2 Sediment Transport and Morphodynamics, pages 21–163. ASCE Manuals and Reports on Engineering Practice No. 110. ASCE.

Geyer, W. R., Hill, P. S., and Kineke, G. C. (2004). The transport, transformation and dispersal of sediment by buoyant coastal flows. *Continental Shelf Research*, 24(7-8):927 – 949.

Gibbs, R. J. (1985). Estuarine flocs: Their size, settling velocity and density. *Journal of Geophysical Research*, 90(C2):3249–3251.

Grabowski, R. C., Droppo, I. G., and Wharton, G. (2011). Erodibility of cohesive sediment: The importance of sediment properties. *Earth-Science Reviews*, 105(3-4):101 – 120.

Gratiot, N. and Manning, A. J. (2004). An experimental investigation of floc characteristics in a diffusive turbulent flow. *Journal of Coastal Research*, 41:105–113.

Harris, C. K., Traykovski, P. A., and Geyer, W. R. (2005). Flood dispersal and deposition by near-bed gravitational sediment flows and oceanographic transport: A numerical modeling study of the Eel River shelf, northern California. *Journal of Geophysical Research*, 110(C09025).

Hill, P. S., Milligan, T. G., and Rockwell Geyer, W. (2000). Controls on effective settling velocity of suspended sediment in the Eel River flood plume. *Continental Shelf Research*, 20(16):2095–2111.

Hill, P. S. and Nowell, A. R. M. (1995). Comparison of two models of aggregation in continental-shelf bottom boundary layers. *Journal of Geophysical Research*, 100(C11):22749–22763.

Hwang, K. N. (1989). Erodibility of fine sediment in wave dominated environments. Master's thesis, University of Florida, Gainesville, FL USA.

Hwang, K.-N. and Mehta, A. J. (1989). Fine sediment erodibility in Lake Okeechobee, Florida. Report ufl/coel-89/019, Department of Coastal and Oeanographic Enginnering, University of Florida.

Jiang, Q. and Logan, B. E. (1991). Fractal dimensions of aggregates determined from steady-state size distributions. *Environmental Science & Technology*, 25(12):2031–2038.

Keyvani, A. and Strom, K. (2013). A fully-automated image processing technique to improve measurement of suspended particles and flocs by removing out-of-focus objects. *Computers & Geosciences*, 52:189–198.

Keyvani, A. and Strom, K. (2014). Influence of cycles of high and low turbulent shear on the growth rate and equilibrium size of mud flocs. *Marine Geology*, 354(0):1 – 14.

Kranck, K. (1973). Flocculation of suspended sediment in the sea. *Nature*, 246(5432):348–350.

Kranenburg, C. (1994). The fractal structure of cohesive sediment aggregates. *Estuarine, Coastal and Shelf Science*, 39(5):451 – 460.

Krone, R. B. (1962). Flume studies of the transport of sediment in estuarial shoaling processes. Technical report, Hydraulic Engineering Laboratory and Sanitary Engineering Research Laboratory, University of California, Berkely, CA.

Krone, R. B. (1963). A study of rheological properties of estuarine sediments. Committee on Tidal Hydraulics Final Report 63-88, Waterways Experiment Station, Corps of Engineers, US Army.

Kumar, R. G., Strom, K. B., and Keyvani, A. (2010). Floc properties and settling velocity of San Jacinto Estuary mud under variable shear and salinity conditions. *Continental Shelf Research*, 30(20):2067–2081.

Law, B., Milligan, T., Hill, P., Newgard, J., Wheatcroft, R., and Wiberg, P. (2013). Flocculation on a muddy intertidal flat in willapa bay, washington, part i: A regional survey of the grain size of surficial sediments. *Continental Shelf Research*, 60, Supplement(0):S136 – S144.

Logan, B. E. (1999). *Environmental Transport Processes*. John Wiley & Sons.

Maggi, F. (2007). Variable fractal dimension: A major control for floc structure and flocculation kinematics of suspended cohesive sediment. *Journal of Geophysical Research*, 112(C07012).

Maggi, F. (2008). Stochastic flocculation of cohesive sediment: Analysis of floc mobility within the floc size spectrum. *Water Resources Research*, 44(W01433).

Maggi, F. and Winterwerp, J. C. (2004). Method for computing the three-dimensional capacity dimension from two-dimensional projections of fractal aggregates. *Physical Review E*, 69:011405.

Manning, A., Langston, W., and Jonas, P. (2010). A review of sediment dynamics in the Severn estuary: Influence of flocculation. *Marine Pollution Bulletin*, 61:37–51.

Manning, A. J. and Dyer, K. R. (1999). A laboratory examination of floc characteristics with regard to turbulent shearing. *Marine Geology*, 160(1-2):147 – 170.

McAnally, W. H. and Mehta, A. J. (2000). Aggregation rate of fine sediment. *Journal of Hydraulic Engineering*, 126(12):883–892.

McCave, I. (1975). Vertical flux of particles in the ocean. *Deep Sea Research and Oceanographic Abstracts*, 22(7):491 – 502.

Milligan, T. and Hill, P. (1998). A laboratory assessment of the relative importance of turbulence, particle composition, and concentration in limiting maximal floc size and settling behaviour. *Journal of Sea Research*, 39(3–4):227 – 241.

Milligan, T., Hill, P., and Law, B. (2007). Flocculation and the loss of sediment from the po river plume. *Continental Shelf Research*, 27(3-4):309 – 321.

Moriarty, J., Harris, C., Rabouille, C., Fennel, K., Friedrichs, M., and Xu, K. (2017). The roles of resuspension, diffusion and biogeochemical processes on oxygen dynamics offshore of the Rhone River, France: a numerical modeling study. *Biogeosciences*, 14:1919–1946.

Partheniades, E. (2009). *Cohesive Sediments in Open Channels*. Butterworth-Heinemann/Elsevier, Burlington, MA.

Rubey, W. W. (1933). Settling velocity of gravel, sand, and silt particles. *American Journal of Science*, 25(148):325–338.

Salehi, M. and Strom, K. (2012). Measurement of critical shear stress for mud mixtures in the San Jacinto estuary under different wave and current combinations. *Continental Shelf Research*, 47:78–92.

Sharif, A. and Atkinson, J. (2012). Model for surface erosion of cohesive soils. *Journal of Hydraulic Engineering*, 138(7):581–590.

Shi, J. Z. (2010). Tidal resuspension and transport processes of fine sediment within the river plume in the partially-mixed changjiang river estuary, china: A personal perspective. *Geomorphology*, 121(3–4):133 – 151.

Son, M. and Hsu, T.-J. (2008). Flocculation model of cohesive sediment using variable fractal dimension. *Environmental Fluid Mechanics*, 8(1):55–71.

Soulsby, R., Manning, A., Spearman, J., and Whitehouse, R. (2013). Settling velocity and mass settling flux of flocculated estuarine sediments. *Marine Geology*, 339:1 – 12.

Spicer, P. T., Pratsinis, S. E., Raper, J., Amal, R., Bushell, G., and Meesters, G. (1998). Effect of shear schedule on particle size, density, and structure during flocculation in stirred tanks. *Powder Technology*, 97:26–34.

Strom, K. and Keyvani, A. (2011). An explicit full-range settling velocity equation for mud flocs. *Journal of Sedimentary Research*, 81(12):921–934.

Strom, K. and Keyvani, A. (2016). Flocculation in a decaying shear field and its implications for mud removal in near-field river mouth discharges. *Journal of Geophysical Research: Oceans*, 121:2142–2162.

Teeter, A. M. (2001). Clay-silt sediment modeling using mulitple grain classes. part I: Settling

and deposition. In McAnally, W. H. and Mehta, A. J., editors, *Coastal And Estuarine Fine Sediment Processes*, pages 157–171. Elsevier.

Tran, D. and Strom, K. (2018). How do changes in suspended sediment concentration alone influence the size of mud flocs under steady turbulent shearing? *in Continental Shelf Research*, 158:1–14.

Tran, D. and Strom, K. (2017b). Suspended clays and silts: Are they independent or dependent fractions when it comes to settling in a turbulent suspension? *Continental Shelf Research*, 138:81–94.

Tsai, C.-H., Iacobellis, S., and Lick, W. (1987). Flocculation of fine-grained lake sediments due to a uniform shear stress. *Journal of Great Lakes Research*, 13(2):135–146.

van Leussen, W. (1994). *Estuarine macroflocs and their role in fine-grained sediment transport*. PhD thesis, University of Utrecht, The Netherlands.

van Leussen, W. (1999). The variability of settling velocities of suspended fine-grained sediment in the Ems estuary. *Journal of Sea Research*, 41:109–118.

Verney, R., Lafite, R., and Brun-Cottan, J.-C. (2009). Flocculation potential of estuarine particles: The importance of environmental factors and of the spatial and seasonal variability of suspended particulate matter. *Estuaries and Coasts*, 32(4):678–693.

Verney, R., Lafite, R., Brun-Cottan, J. C., and Hir, P. L. (2011). Behaviour of a floc population

during a tidal cycle: Laboratory experiments and numerical modelling. *Continental Shelf Research*, 31(10):S64–S83.

Voulgaris, B. and Trowbridge, J. H. (1998). Evaluation of the acoustic Doppler velocimeter (ADV) for turbulence measurements. *Journal of Atmospheric and Oceanic Technology*, 15:272–289.

Wiberg, P. L., Law, B. A., Wheatcroft, R. A., Milligan, T. G., and Hill, P. S. (2013). Seasonal variations in erodibility and sediment transport potential in a mesotidal channel-flat complex, Willapa Bay, WA. *Continental Shelf Research*, 60, Supplement(0):S185 – S197.

Winterwerp, J. C. (1998). A simple model for turbulence induced flocculation of cohesive sediment. *Journal of Hydraulic Research*, 36(3):309–326.

Winterwerp, J. C., Bale, A. J., Christie, M. C., Dyer, K. R., Jones, S., Lintern, D. G., Manning, A. J., and Roberts, W. (2002). Flocculation and settling velocity of fine sediment. *Proceedings in Marine Science*, 5:25–40.

Winterwerp, J. C., Manning, A. J., Martens, C., de Mulder, T., and Vanlede, J. (2006). A heuristic formula for turbulence-induced flocculation of cohesive sediment. *Estuarine, Coastal and Shelf Science*, 68:195–207.

Winterwerp, J. C. and van Kesteren, W. G. M. (2004). *Introduction to the physics of cohesive sediment in the marine environment*, volume 56 of *Developments in Sedimentology*. Elsevier, Amsterdam, The Netherlands.

Ariathurai, R. and Krone, R. B. (1976). Finite element model for cohesive sediment transport. *Journal of Hydraulics Division*, 102(3):323–338.

Berhane, I., richard W. Sternberg, Kineke, G. C., Milligan, T. G., and Kranck, K. (1997). The variability of suspended aggregates on the Amazon Continental Shelf. *Continental Shelf Research*, 17(3):267–285.

Braithwaite, K. M., Bowers, D. G., Nimmo Smith, W. A. M., and Graham, G. W. (2012). Controls on floc growth in an energetic tidal channel. *Journal of Geophysical Research: Oceans*, 117(C2).

Burban, P.-Y., Lick, W., and Lick, J. (1989). The flocculation of fine-grained sediments in estuarine waters. *Journal of Geophysical Research*, 94(C6):8323–8330.

Burt, T. N. (1986). Field settling velocities in estuarine muds. In Mehta, A. J., editor, *Estuarine Cohesive Sediment Dynamics*, pages 126–150. Springer New York.

Chen, S. and Eisma, D. (1995). Fractal geometry of in situ flocs in the estuarine and coastal environments. *Netherlands Journal of Sea Research*, 33(2):173 – 182.

Chen, S.-N., Geyer, W. R., Sherwood, C. R., and Ralston, D. K. (2010). Sediment transport and deposition on a river-dominated tidal flat: An idealized model study. *Journal of Geophysical Research*, 115(C10040).

Cuthbertson, A. J. S., Ibikunle, O., McCarter, W. J., and Starrs, G. (2016). Monitoring and characterisation of sand-mud sedimentation processes. *Ocean Dynamics*, 66:867–891.

Dietrich, W. E. (1982). Settling velocity of natural particles. *Water Resources Research*, 18(6):1615–1626.

Dyer, K., Christie, M., and Manning, A. (2004). The effects of suspended sediment on turbulence within an estuarine turbidity maximum. *Estuarine, Coastal and Shelf Science*, 59:237–248.

Dyer, K. R. (1989). Sediment processes in estuaries: future research requirements. *Journal of Geophysical Research*, 94(C10):14327–14339.

Eisma, D., Bernard, P., Cadee, G., Ittekkot, V., Kalf, J., Laane, R., Martin, J., Mook, W., van Put, A., and Schuhmacher, T. (1991). Suspended-matter particle size in some West-European estuaries; Part II: A review on floc formation and break-up. *Netherlands Journal of Sea Research*, 28(3):215–220.

Eisma, D. and Kalf, J. (1996). In situ particle (floc) size measurements with the Nioz in situ camera system. *Journal of Sea Research*, 36(1-2):49–53.

Eisma, D. and Li, A. (1993). Changes in suspended-matter floc size during the tidal cycle in the Dollard estuary. *Netherlands Journal of Sea Research*, 31(2):107–117.

Ferguson, R. and Church, M. (2004). A simple universal equation for grain settling velocity. *Journal of Sedimentary Research*, 74(6):933–937.

Geyer, W. R., Hill, P. S., and Kineke, G. C. (2004). The transport, transformation and dispersal of sediment by buoyant coastal flows. *Continental Shelf Research*, 24(7-8):927 – 949.

Gratiot, N. and Manning, A. J. (2004). An experimental investigation of floc characteristics in a diffusive turbulent flow. *Journal of Coastal Research*, 41:105–113.

Guo, C., He, Q., Prooijen, B., Guo, L., Manning, A., and Bass, S. (2018). Investigation of flocculation dynamics under changing hydrodynamic forcing on an intertidal mudflat. *Marine Geology*, 395:120–132.

Harris, C. K., Traykovski, P. A., and Geyer, W. R. (2005). Flood dispersal and deposition by near-bed gravitational sediment flows and oceanographic transport: A numerical modeling study of the Eel River shelf, northern California. *Journal of Geophysical Research*, 110(C09025).

Hill, P. S., Milligan, T. G., and Rockwell Geyer, W. (2000). Controls on effective settling velocity of suspended sediment in the Eel River flood plume. *Continental Shelf Research*, 20(16):2095–2111.

Huang, H. (1994). Fractal properties of flocs formed by fluid shear and differential settling. *Physics of Fluids*, 6(10):3229–3234.

Hwang, K. N. (1989). Erodibility of fine sediment in wave dominated environments. Master's thesis, University of Florida, Gainesville, FL USA.

Hwang, K.-N. and Mehta, A. J. (1989). Fine sediment erodibility in Lake Okeechobee, Florida. Report ufl/coel-89/019, Department of Coastal and Oeanographic Enginnering, University of Florida.

Keyvani, A. (2013). *Flocculation processes in river mouth fluvial to marine transitions*. PhD thesis, University of Houston, Houston, TX.

Keyvani, A. and Strom, K. (2013). A fully-automated image processing technique to improve measurement of suspended particles and flocs by removing out-of-focus objects. *Computers & Geosciences*, 52:189–198.

Keyvani, A. and Strom, K. (2014). Influence of cycles of high and low turbulent shear on the growth rate and equilibrium size of mud flocs. *Marine Geology*, 354(0):1 – 14.

Kranenburg, C. (1994). The fractal structure of cohesive sediment aggregates. *Estuarine, Coastal and Shelf Science*, 39(5):451 – 460.

Krone, R. B. (1962). Flume studies of the transport of sediment in estuarial shoaling processes. Technical report, Hydraulic Engineering Laboratory and Sanitary Engineering Research Laboratory, University of California, Berkely, CA.

Krone, R. B. (1963). A study of rheological properties of estuarine sediments. Committee on Tidal Hydraulics Final Report 63-88, Waterways Experiment Station, Corps of Engineers, US Army.

Krone, R. B. (1978). Aggregation of suspended particles in estuaries. In Kjerfve, B., editor, *Estuarine transport processes*, pages 177–190. University of South Carolina Press.

Kumar, R. G., Strom, K. B., and Keyvani, A. (2010). Floc properties and settling velocity of San

Jacinto Estuary mud under variable shear and salinity conditions. *Continental Shelf Research*, 30(20):2067–2081.

Kuprenas, R., Tran, D., and Strom, K. (2017). A shear-limited flocculation model for dynamically predicting average floc size. *Journal of Geophysical Research: Oceans*, page Under review.

Law, B., Milligan, T., Hill, P., Newgard, J., Wheatcroft, R., and Wiberg, P. (2013). Flocculation on a muddy intertidal flat in willapa bay, washington, part i: A regional survey of the grain size of surficial sediments. *Continental Shelf Research*, 60, Supplement(0):S136 – S144.

Li, B., Eisma, D., Xie, Q., Kalf, J., Li, Y., and Xia, X. (1999). Concentration, clay mineral composition and Coulter counter size distribution of suspended sediment in the turbidity maximum of the Jiaojiang river estuary, Zhejiang, China. *Journal of Sea Research*, 42:105–116.

Lick, W. and Lick, J. (1988). Aggregation and disaggregation of fine-grained lake sediments. *Journal of Great Lakes Research*, 14(4):514 – 523.

Logan, B. E. (1999). *Environmental Transport Processes*. John Wiley & Sons.

MacDonald, D. G., Goodman, L., and Hetland, R. D. (2007). Turbulent dissipation in a near-field river plume: A comparison of control volume and microstructure observations with a numerical model. *Journal of Geophysical Research*, 112(C07026).

Maggi, F. (2015). Experimental evidence of how the fractal structure controls the hydrodynamic resistance on granular aggregates moving through water. *Journal of Hydrology*, 528:694–702.

Manning, A. J. and Dyer, K. R. (1999). A laboratory examination of floc characteristics with regard to turbulent shearing. *Marine Geology*, 160(1-2):147 – 170.

McAnally, W. H. and Mehta, A. J. (2000). Aggregation rate of fine sediment. *Journal of Hydraulic Engineering*, 126(12):883–892.

Mehta, A. J. and McAnally, W. H. (2008). *Sedimentation Engineering: Processes, Measurements, Modeling, and Practice*, chapter 4, pages 253–306. ASCE Manuals and Reports on Engineering Practice No. 110. American Society of Civil Engineering.

Mietta, F., Chassagne, C., and Winterwerp, J. (2009). Shear-induced flocculation of a suspension of kaolinite as function of pH and salt concentration. *Journal of Colloid and Interface Science*, 336(1):134–141.

Mikeš, D. and Manning, A. J. (2010). Assessment of flocculation kinetics of cohesive sediments from the Seine and Gironde estuaries, France, through laboratory and field studies. *Journal of Waterway, Port, Coastal, and Ocean Engineering*, 136(6):306–318.

Milligan, T. (1995). An examination of the settling behaviour of a flocculated suspension. *Netherlands Journal of Sea Research*, 33(2):163–171.

Milligan, T. and Hill, P. (1998). A laboratory assessment of the relative importance of turbulence, particle composition, and concentration in limiting maximal floc size and settling behaviour. *Journal of Sea Research*, 39(3–4):227 – 241.

Milligan, T., Hill, P., and Law, B. (2007). Flocculation and the loss of sediment from the po river plume. *Continental Shelf Research*, 27(3-4):309 – 321.

Oles, V. (1992). Shear-induced aggregation and breakup of polystyrene latex-particles. *Journal of Colloid and Interface Science*, 154(2):351–358.

Partheniades, E. (2009). *Cohesive Sediments in Open Channels*. Butterworth-Heinemann/Elsevier, Burlington, MA.

Rubey, W. W. (1933). Settling velocity of gravel, sand, and silt particles. *American Journal of Science*, 25(148):325–338.

Safak, I., Allison, M., and Sheremet, A. (2013). Floc variability under changing turbulent stresses and sediment availability on a wave energetic muddy shelf. *Continental Shelf Research*, 53(0):1 – 10.

Sahin, C., Guner, Anil, A. H., Ozturk, M., and Sheremet, A. (2017). Floc size variability under strong turbulence: Observations and artificial neural network modeling. *Applied Ocean Research*, 68:130–141.

Shi, J. Z. (2010). Tidal resuspension and transport processes of fine sediment within the river plume in the partially-mixed changjiang river estuary, china: A personal perspective. *Geomorphology*, 121(3–4):133 – 151.

Shi, Z. and Zhou, H. J. (2004). Controls on effective settling velocities of mud flocs in the changjiang estuary, china. *Hydrological Processes*, 18:28772892.

Smith, J. and Friedrichs, C. (2015). Image processing methods for in situ estimation of cohesive sediment floc size, settling velocity, and density. *Limnology and Oceanography: Methods*, 13:250–264.

Smith, S. J. and Friedrichs, C. T. (2011). Size and settling velocities of cohesive flocs and suspended sediment aggregates in a trailing suction hopper dredge plume. *Continental Shelf Research*, 31(10, Supplement):S50 – S63.

Strom, K. and Keyvani, A. (2011). An explicit full-range settling velocity equation for mud flocs. *Journal of Sedimentary Research*, 81(12):921–934.

Strom, K. and Keyvani, A. (2016). Flocculation in a decaying shear field and its implications for mud removal in near-field river mouth discharges. *Journal of Geophysical Research: Oceans*, 121:2142–2162.

Tambo, N. and Watanabe, Y. (1979). Physical aspect of flocculation process–I: fundamental treatise. *Water Research*, 13(5):429 – 439.

Tang, F. H., Alonso-Marroquin, F., and Maggi, F. (2014). Stochastic collision and aggregation analysis of kaolinite in water through experiments and the spheropolygon theory. *Water Research*, 53:180 – 190.

Tang, F. H. and Maggi, F. (2016). A mesocosm experiment of suspended particulate matter dynamics in nutrient- and biomass-affected waters. *Water Research*, 89:76 – 86.

Teeter, A. M. (2001). Clay-silt sediment modeling using mulitple grain classes. part I: Settling

and deposition. In McAnally, W. H. and Mehta, A. J., editors, *Coastal And Estuarine Fine Sediment Processes*, pages 157–171. Elsevier.

Tran, D. and Strom, K. (2017). Suspended clays and silts: Are they independent or dependent fractions when it comes to settling in a turbulent suspension? *Continental Shelf Research*, 138:81–94.

Tsai, C.-H., Iacobellis, S., and Lick, W. (1987). Flocculation of fine-grained lake sediments due to a uniform shear stress. *Journal of Great Lakes Research*, 13(2):135–146.

Van Der Lee, W. T. B. (1998). The impact of fluid shear and the suspended sediment concentration on the mud floc size variation in the Dollard estuary, The Netherlands. *Geological Society Special Publication*, 139:187–198.

van Leussen (1997). *Cohesive Sediments*, chapter The Kolmogorov microscale as a limiting value for the floc sizes of suspended fine-grained sediment in estuaries, pages 45–62. John Wiley Sons.

van Leussen, W. (1994). *Estuarine macroflocs and their role in fine-grained sediment transport*. PhD thesis, University of Utrecht, The Netherlands.

van Leussen, W. (1999). The variability of settling velocities of suspended fine-grained sediment in the Ems estuary. *Journal of Sea Research*, 41:109–118.

Verney, R., Lafite, R., Brun-Cottan, J. C., and Hir, P. L. (2011). Behaviour of a floc population

during a tidal cycle: Laboratory experiments and numerical modelling. *Continental Shelf Research*, 31(10):S64–S83.

Wendling, V., Legout, C., Gratiot, N., Michallet, H., and Grangeon, T. (2016). Dynamics of soil aggregate size in turbulent flow: Respective effect of soil type and suspended concentration. *Catena*, 141:66–72.

Winterwerp, J. C. (1998). A simple model for turbulence induced flocculation of cohesive sediment. *Journal of Hydraulic Research*, 36(3):309–326.

Winterwerp, J. C. (2002). On the flocculation and settling velocity of estuarine mud. *Continental Shelf Research*, 22:1339–1360.

Winterwerp, J. C., Manning, A. J., Martens, C., de Mulder, T., and Vanlede, J. (2006). A heuristic formula for turbulence-induced flocculation of cohesive sediment. *Estuarine, Coastal and Shelf Science*, 68:195–207.

Winterwerp, J. C. and van Kesteren, W. G. M. (2004). *Introduction to the physics of cohesive sediment in the marine environment*, volume 56 of *Developments in Sedimentology*. Elsevier, Amsterdam, The Netherlands.

Wolanski, E., Asaeda, T., and Imberger, J. (1989). Mixing across a lutocline. *Limnology and Oceanography*, 34(5):931–938.

Xia, X. M., Li, Y., Yang, H., Wu, C. Y., Sing, T. H., and Pong, H. K. (2004). Observations on the size

and settling velocity distributions of suspended sediment in the Pearl River Estuary, China. *Continental Shelf Research*, 24(16):1809–1826.

Xu, J., Sequeiros, O., and Noble, M. (2014). Sediment concentrations, flow conditions, and downstream evolution of two turbidity currents, Monterey Canyon, USA. *Deep-Sea Research I*, 89:11–34.

Zhang, J.-F. and Zhang, Q.-H. (2011). Lattice Boltzmann simulation of the flocculation process of cohesive sediment due to differential settling. *Continental Shelf Research*, 31:S94–S105.

# 2 How Do Changes in Suspended Sediment Concentration alone Influence the Size of Mud Flocs under Steady Turbulent Shearing?

## 2.1 Introduction

Engineers and scientists rely on physics-based numerical modeling to predict the transport and fate of sediment in river, estuarine, and coastal systems. In terms of predicting the transport and depositional fate of suspended sediment, the accuracy of such models depends heavily on the selection of an appropriate sediment settling velocity, $w_s$ (Dyer, 1989; Winterwerp, 2002; Geyer et al., 2004; Harris et al., 2005; Partheniades, 2009; Chen et al., 2010). For sands, estimating the settling velocity is comparatively straightforward because $w_s$ is a function of the size, density, and shape of the particles found in the deposit (Rubey, 1933; Dietrich, 1982; Ferguson and Church, 2004). The settling velocity of mud is essentially a function of the same properties of size, density, shape, and porosity (Krone, 1963; Dyer, 1989; Winterwerp and van Kesteren, 2004; Partheniades, 2009; Strom and Keyvani, 2011). However, the flocculation process complicates the estimation of these properties at the time of deposition for muds since suspensions of flocs can have sizes, densities, and shapes that are vastly different from the constitutive particles found in the deposit or the water column at a particular moment in time (Krone, 1963;

Chapter 2 was published in Continental Shelf Research as Tran et al. (2018)

Dyer, 1989; Winterwerp and van Kesteren, 2004; Partheniades, 2009). Therefore, understanding the flocculation process and its impact on settling velocity is crucial for sediment transport modeling of muds in rivers, estuaries, the shelf, and the deep ocean.

Flocculation is a process of simultaneous aggregation and breakup of cohesive particles within the water column (Krone, 1962; Winterwerp and van Kesteren, 2004). In general, clay particles in suspension aggregate when they move close enough for their net repulsive forces (generated by a positively charged ion atmosphere) to be overcome by van der Waals attractive forces. From a sediment transport perspective, the result of aggregation is that the mud settling velocity will increase due to the increase in floc size. Flocs can disaggregate due to fluid shear or ballistic impacts from other particles whenever these forces are sufficient to overcome inter-particle bond forces. The breakage of these bonds can occur around the exterior surface of the floc (erosion), or within the interior (fracture); either way, the breakup of flocs leads to a reduction in floc size and settling velocity.

The change in average floc size can be conceptualized as a rate problem (Winterwerp, 1998):

$$\frac{d(d_{f50})}{dt} = A - B \tag{2.1}$$

where $d_{f50}$ is the diameter of a floc in suspension for which 50% of the flocs are finer by volume, $A$ is the floc aggregation rate [L/t], and $B$ is a floc breakup rate [L/t]. If $A$ and $B$ are unequal, the floc size will change with time and move towards an equilibrium value, $d_{f50e}$, defined as the floc size when $d(d_{f50})/dt = 0$ or when $A = B$. Many factors, such as: the mineral and organic composition of the mud (Krone, 1963; Partheniades, 2009; Tang and Maggi, 2016), the time history

of exposure of the suspension to various levels of turbulent mixing (van Leussen, 1994; Mehta and McAnally, 2008; Keyvani and Strom, 2014), the chemical properties of the water (e.g., ion levels and pH) (Xia et al., 2004; Mietta et al., 2009), and suspended sediment concentration, $C$ (Krone, 1978; Van Der Lee, 1998; Manning and Dyer, 1999; Mikeš and Manning, 2010) all influence the $A$ and $B$ terms for any given suspension. In this paper, we focus on the role that suspended sediment concentration, $C$, plays in altering the size of suspended mud flocs within a turbulent suspension. To provide context for the work, we briefly discuss, in the next section, the terms and processes related to the growth rate (i.e., Equation 2.1) and equilibrium size, $d_{f50e}$ of mud flocs as it pertains to suspended sediment concentration. Then, an overview of past laboratory and field observations regarding the influence of $C$ on floc size and settling velocity is presented. Following this general discussion, the paper examines how the influence of $C$ can be incorporated into floc settling velocity equations used in sediment transport modeling.

## 2.2 Background

### 2.2.1 Overview

For a given mud mixture and fixed water chemistry, the floc growth rate is largely a function of the particle collision rate (McAnally and Mehta, 2000; Winterwerp and van Kesteren, 2004; Partheniades, 2009; Keyvani, 2013). Collisions can be driven by Brownian motion, differential settling, and/or turbulent mixing (Burban et al., 1989; Eisma et al., 1991; Huang, 1994). The mean turbulent shear rate, $G$, is a quantitative measure of turbulent energy and is defined as $G = \sqrt{\epsilon/\nu} = \nu/\eta^2$, where $\epsilon$ is the mean turbulent energy dissipation rate, $\nu$ is the kinematic viscosity of the fluid, and $\eta$ is the Kolmogorov micro length scale (Tambo and Watanabe, 1979).

Other factors that impact the collision rate are the particle number concentration, or the mass concentration, $C$, particle or floc diameter, $d_f$, and particle shape (Tang et al., 2014). Classic shear-driven collision kinetics show that the rate of collision is $\propto GC^2\rho_s^{-2}d_f^{-3}$, where $\rho_s$ is the sediment density (McAnally and Mehta, 2000). Taking the collision kinetics relationship given above to be true, it is easy to see that increases in $C$ (along with $G$) will promote collisions, and therefore the potential for an increase in the floc growth rate and floc size. This fact, coupled with empirical observations of suspension settling velocity in stagnant settling columns (e.g., Krone, 1962; Hwang, 1989; Teeter, 2001) have resulted in empirical floc settling velocity equations that take the settling velocity of floc-impacted mud suspensions to be a function of concentration, $w_s = w_s(C)$ (e.g., Wolanski et al., 1989; Hwang, 1989). An example of this style of relation is the three-part settling velocity equation of Hwang and Mehta (1989):

$$w_s = \begin{cases} w_{sf} & C < C_1 \\ a_w \dfrac{C^n}{(C^2 + b_w^2)^m} & C_1 < C < C_2 \\ \sim \text{negligible} & C_2 < C \end{cases} \tag{2.2}$$

Where $w_{sf}$ is free settling velocity, $a_w$ is velocity scaling coefficient, $n$ is flocculation settling exponent, $b_w$ is hindered settling coefficient, and $m$ is hindered settling exponent. Eq. 2.2 has a general parabolic form and accounts for the impact of flocculation (due to differential settling) and hindered settling on the net suspension settling velocity. In this formulation, if $C < C_1$, flocculation is thought to have no impact on $w_s$; the transitional concentration marking the boundary between floc influence and no floc influence is suggested to be around 100 to 300

mg/L (Mehta and McAnally, 2008). $C_2$ is the concentration associated with the peak in settling velocity (maximum floc size) and is stated to range from 1 to 15 g/L. For concentrations higher than $C_2$ floc enhanced settling rates start to decline due to hindered settling affects. While not all floc-settling-velocity equations take the exact form of Equation 2.2, many do take $w_s = w_s(C)$ (e.g., Ariathurai and Krone, 1976; Burt, 1986). Furthermore, many larger-scale sediment transport modeling platforms often use some sort of concentration-dependent settling velocity to account for flocculation (such as Eq. 2.2) in the transport of mud regardless of whether the equation is being applied to stagnant or turbulent water.

Relations such as Equation 2.2 assume that floc size will increase with $C$ without accounting for the level of fluid stress being applied to the flocs. This assumption is an outcome of the fact that all studies which have sought to examine the influence of $C$ on floc size or settling velocity have done so in stagnant settling columns (e.g., Krone, 1962; Huang, 1994; Teeter, 2001; Cuthbertson et al., 2016), or in suspensions for which the shearing or mixing has been turned off for a number of minutes before measurements were made (e.g., Manning and Dyer, 1999). Yet, it has also been shown that the level of turbulent energy, $G$, plays a key role in limiting the maximum size that a floc can obtain, and that this maximum size is proportional to the Kolmogorov micro length scale, $\eta$ (van Leussen, 1997; Milligan and Hill, 1998; Manning and Dyer, 1999; Kumar et al., 2010; Braithwaite et al., 2012; Tran and Strom, 2017). Therefore, it is reasonable to expect that both $d(d_{f50})/dt$ and $d_{f50e}$ could be a function of $C$ and $G$ (among other parameters). Or, at least that the function between floc size and $C$ could look different in a turbulent suspension than it would in a stagnant, or near stagnant, settling column or tank.

### 2.2.2 Prior Results and Equations Pertaining to the Influence of Concentration on the Equilibrium Floc Size and a Floc-impacted Settling Velocity

As discussed previously, the influence of $C$ on $d_{f50e}$ and $w_s$ has been examined primarily in stagnant settling columns, in suspensions for which turbulence had been reduced prior to the time of measurement, or in conditions where both $C$ and $G$ covary in the field or lab (Burban et al., 1989; Chen and Eisma, 1995; Milligan and Hill, 1998; Shi, 2010; Sahin et al., 2017). As might be expected, not all of these studies report the same relationship between concentration and $d_{f50e}$ and $C$ (Table 3.1). For example, most studies have shown that $d_{f50e}$ is positively related to $C$ (Oles, 1992; Eisma and Li, 1993; Berhane et al., 1997; Li et al., 1999; van Leussen, 1999; Gratiot and Manning, 2004; Shi and Zhou, 2004; Law et al., 2013). Yet, a few studies have also concluded that floc size can reduce with increasing concentration (Tsai et al., 1987; Burban et al., 1989; Safak et al., 2013; Sahin et al., 2017; Guo et al., 2018). For example, Burban et al. (1989) concluded that while increasing the concentration enhances the aggregation rate, the effect of disaggregation due to three-body collisions is significant enough to result in smaller equilibrium sizes. Furthermore, other studies have not observed any relation between flocculation rate or equilibrium floc size and $C$. This is especially true regarding the impact of $C$ on the equilibrium size, $d_{f50e}$ (Milligan and Hill, 1998; Manning and Dyer, 1999; Kumar et al., 2010; Mikeš and Manning, 2010; Zhang and Zhang, 2011; Braithwaite et al., 2012). One complicating factor in understanding the relationship between floc size and $C$ is that in the field, $C$ and $G$ typically covary, with $C$ being positively related to $G$ (Manning and Dyer, 1999; Gratiot and Manning, 2004; Safak et al., 2013; Sahin et al., 2017; Guo et al., 2018). Such covariance can make it difficult to determine if the observed change in floc size is due to a change in $C$ or a change in $G$. Table

| Source | Concentration $C$ [mg/L] | Shear $G$ [$s^{-1}$] | $w_s$ [mm/s] | Floc size $d_f$ [$\mu$m] | Salinity $S$ [ppt] | Sediment type | Relation to $C$ |
|---|---|---|---|---|---|---|---|
| Gratiot and Manning (2004) | 200 - 8,000 | 3, 7, 19 | 1 - 4.22 | 30 - 700 | 16.5 | Tamar & Gironde mud | $d_f \sim C$ |
| van Leussen (1999) | 10 - 1,000 | - | 0.008 - 2 | 5 - 25 | 0 - 35 | Ems mud | $d_f \sim C$ |
| Eisma and Li (1993) | 40 - 250 | - | - | 10 - 800 | 2 - 30 | Dollard mud | $d_f \sim C$ |
| Milligan and Hill (1998) | 50, 250 | 8 | 0.03 - 5.43 | 125 - 1,195 | 30 | Bentonite & drill-mud | None |
| Kumar et al. (2010) | 50, 150 | 2 - 50 | 0.2 - 4 | 20 - 350 | 0, 10, 15 | San Jacinto mud | None |
| Manning and Dyer (1999) | 80, 120, 160 | < 27.45<br>> 27.45 | 0.2 -1.05 | 36.5 - 255 | 10 ± 0.5 | Tamar mud | $d_f \sim C$<br>$d_f \sim 1/C$ |
| Burban et al. (1989) | 10 - 800 | 100 - 600 | - | 18 - 106 | - | Detroit River mud | $d_f \sim 1/C$ |
| Wendling et al. (2016) | 1,600 - 10,900 | 3, 7, 19 | - | 45.3 - 63.9 | 0 | Molasses and Clay | $d_f \sim 1/C$ |
| Safak et al. (2013) | 500 - 1,400 | 3 - 35 | - | 2.5 - 500 | - | Atchafalaya shelf mud | $d_f \sim 1/C$ |
| Sahin et al. (2017) | 500 - 20,000 | 0 - 4 | - | 10 - 400 | 25 - 30 | Atchafalaya shelf mud | $d_f \sim 1/C^{3/2}$ |

**Table 2.1:** Sample of different relations between concentration and floc size in literature.

3.1 provides a summary of past findings regarding the impact of $C$ on floc size.

The variability in the relationship of flocs size, or settling velocity, with $C$ is mirrored in the mathematical models used to account for the impact of flocs on mud settling velocity. For example, consider the equilibrium size-based models of Winterwerp (1998):

$$d_{f50e} = b + \frac{K_A}{K_B} G^{-1/2} C \tag{2.3}$$

and Lick and Lick (1988):

$$d_{f50e} = \alpha G^{-1/2} C^{-1/2} \tag{2.4}$$

In Equation 2.3, $b = d_p$, with $d_p$ being the size of the smallest, or primary, particles within the environment of interest and $K_A$ and $K_B$ are suspension-specific aggregation and breakup coefficients; $\alpha$ in Equation 2.4 is also a suspension-specific coefficient. The key item to note in these two equations is that $d_{f50e} \propto C$ in the Winterwerp (1998) formulation while is inversely related to $\sqrt{C}$ in the Lick and Lick (1988) formulation. Therefore, one model says that $d_{f50e}$ goes up with $C$ (due to increased collisions and therefore aggregation), and the other says it goes down with

$C$ (due to an increase in floc breakup under ballistic collisions).

The point of the comparison between Equations 2.3 and 2.4 is not to say that one model is correct and the other is not. Rather, the comparison is meant to highlight the fact that the dependence of the equilibrium floc size on $C$ is poorly constrained. One might obtain significantly different trends in mud deposition rates and zones of accumulation depending on the model's functionality between floc size and $C$. This could be particularly acute in zones where $C$ is continually changing due to deposition, resuspension, and/or entrainment of ambient fluid (such as in river mouth plumes and turbidity currents). For example, Strom and Keyvani (2016) made calculations of floc settling velocity in an idealized river mouth plume, using both a size-based floc model and empirical equations, and found that reductions in concentration due to entrainment (not settling) led to strong reductions in the modeled floc size, and hence in the suspension settling velocity, in the cross-shore direction. This runs counter to field observations, such as Hill et al. (2000) and Milligan et al. (2007), and perhaps reflects a defect in our understanding of the drivers of floc size in conditions of clear-water entrainment.

### 2.2.3 Research Questions and Hypotheses

Based on the current state of knowledge, we suggest that further laboratory and field experiments are needed to better constrain the relationship between $C$ and floc size. Certainly, it is true that floc size is a function of $C$ in stagnant settling columns, but how exactly floc size and $C$ are related to each other in a turbulent suspension is unclear. Toward this end, we experimentally investigate the influence of $C$ on the growth rate and equilibrium size of flocs in conditions of steady shear, $G \neq G(t)$, with both constant and time-varying $C$. The two primary questions

being investigated are as follows: (1) is there any relationship between $d_{f50e}$ and $C$ in a turbulent suspension under conditions of steady concentration at levels below those associated with hindered settling?; and (2) how fast do floc sizes respond, if at all, to changes in $C$, alone, within this range? In response to these questions, we hypothesize that: (1) concentration exerts a strong control on the rate of floc growth, but that it exerts only a weak control on the equilibrium floc size; and (2) that flocs size responds quickly to changes in $C$. Throughout the study, we will make measurements of the floc sizes directly within the turbulent suspension without transferring the samples to another location for measurement. Doing so will allows for less ambiguous understanding of the influence of $C$ alone on floc size in both steady and unsteady settings — providing data that will be useful for building better models of time dependent flocculation.

## 2.3 Methods

### 2.3.1 Approach

Two sets of laboratory experiments were conducted to examine the influence of concentration (over the range of $C$ = 15 to 400 mg/L) on floc growth rate and equilibrium size under conditions of steady turbulent shearing. In the first set of experiments (Set A), $C$ was held constant with time while flocs grew from an unflocculated state up to their equilibrium size. The Set A experiments were used to examine hypothesis 1. In the second set of experiments (Set B), flocs in equilibrium were subjected to a continual decay in $C$ with time to examine the influence of settling or clearwater ($C$ = 0 mg/L) entrainment on the size of flocs left in suspension, i.e., to test hypothesis 2. All experiments were run in a turbulent mixing tank (rather than a stagnant settling column); details on the experimental setup are given below. Data collected in all runs

consisted of time series measurements of concentration and the floc size distribution. Table 3.3 summarizes the experimental conditions.

To test the hypotheses, the ability to measure floc sizes over a range of suspended sediment concentrations is crucial. In general, using a camera system to make measurements of flocs within a turbulent suspension is the best way to preserve floc structure and provide high-fidelity data (Eisma and Kalf, 1996; Gratiot and Manning, 2004; Smith and Friedrichs, 2011; Keyvani and Strom, 2013; Maggi, 2015; Smith and Friedrichs, 2015). However, concentrations of suspended sediment that exceed 50 to 100 mg/L make the water so cloudy that it has previously been impossible to obtain good measurements of floc sizes without transferring a sample of the suspension to another dilution chamber for measurement (Gratiot and Manning, 2004; Strom and Keyvani, 2016). There are two reasons for this. The first is that $C \sim 100$ mg/L and greater limits the amount of light that makes it to the camera's sensor. The second is that it becomes nearly impossible to distinguish one floc from another in most setups since there can be thousands of flocs within the volume of fluid surrounding the focal plane in the image at these concentrations. To overcome these deficiencies, we have developed a small flow-through cell close to the wall of the tank where imaging can take place in a thin slice of fluid. A flow-through cell such as this reduces the number of flocs between the camera and the light source, thereby allowing more light to make it to the sensor and reducing the number of flocs within the imaged frame. The development and testing of this new method, the so-called Near-Wall Method, is presented in the Appendix. In the following sections, the equipment and experimental procedures for the two sets of experiments used to test the hypotheses are introduced.

| | | Set A: C = constant (mg/L) | | | | | | | Set B: C decays from 400 to 50 mg/L in (min) | | |
|---|---|---|---|---|---|---|---|---|---|---|---|
| | | 15 | 25 | 50 | 100 | 200 | 300 | 400 | 50 (min) | 100 (min) | 200 (min) |
| Time of monitoring (h) | [1]NPS | 12 | 12 | 12 | 12 | 12 | 12 | 12 | - | - | - |
| | [2]PS | 12 | 12 | 12 | 12 | 12 | 12 | 12 | 170 (min) | 220 (min) | 320 (min) |

**Table 2.2:** A summary of the experimental conditions. In Set B, all experiments started from NPS phase, similar to Set A, but this phase lasted only 2 hours and was not measured. Flocs measurement via imaging commenced during the PS phase of the Set B runs. [1]NPS stands for non prior shear. [2]PS stands for prior shear.

### 2.3.2 Experimental Equipment

All experiments were run in a 13 L mixing chamber that has dimensions of 27.5 x 27.5 x 25 cm. A rotating paddle mixer was used to generate turbulent shear. The shear rate can be related to the paddle and tank geometry as suggested by Logan (1999):

$$G = \left( \frac{52.3 b_{d,p} A_p s^3 R_p^3}{\nu_w V_T} \right)^{1/2} \tag{2.5}$$

where $b_{d,p}$ is the drag coefficient, $A_p$ is the area of the paddle in $m^2$, $R_p$ is the radius of the paddle in $m^2$, $s$ is the paddle speed (rotation per minute), $\nu$ is the fluid kinematic viscosity ($m^2/s$), and $V_T$ is the total volume of the fluid in the chamber in $m^3$. Our selected paddle rotation rates, 35 rpms, produced tank-averaged turbulent shears of approximately $G = 50\ s^{-1}$, such shear rate can be found in nature in rivers (Tran and Strom, 2017), energetic estuaries and bays (Dyer et al., 2004), the mouth regions of coastal river plumes (MacDonald et al., 2007), and turbidity currents (Xu et al., 2014), or under extreme events like storms, hurricanes.

A floc camera system was used to collect still images of flocs within the turbulent mixing chamber. The camera has a 2080 x 1552 pixel progressive scan, monochrome 8 mm CMOS

sensor fitted with a 2X primary magnification objective lens resulting in quantification of particle size over the range of 10 to 1000 $\mu$m. To provide illumination, a LED was fitted inside a waterproofed housing, sealed inside with a round glass plate, and placed inside the tank.

Two Optical Backscatter Sensors (OBS) were installed at 5 and 12 cm above the bottom of the mixing tank to monitor the concentration and stratification of the suspension. OBS calibration followed the protocol in Operation's Manual (2008 - 2012) for OBS-3+ and OBS300 Suspended Solids and Turbidity Monitors given by Campbell Scientific, Inc.. For our sediment mixture, the relationship between $C$ in (mg/L) and the OBS measurement of NTU is: $C = 0.9761(\text{NTU}) - 3.5794$ with the coefficient of determination, $R^2 = 0.99$. The suspension in all experiments consists of a mixture of 80% kaolinite and 20% montmorillonite, a mixture that has been used in past studies to mimic estuarine mud (Keyvani and Strom, 2014; Tran and Strom, 2017). The background water for all experiments was a base of tap water with enough salt added to bring the salinity to 8.5 ppt; we have empirically found that adding salt at 5 ppt and greater reduces variability in floc growth that may occur from run to run with unsalted tap water. The water was left at room temperature for 24 hours before being used.

Figure 4.1 shows a schematic of the mixing tank with the OBS and floc camera system in the Near Wall configuration for the Set A experiments. In the Set B experiments, the concentration in the tank was systematically reduced with time while $G$ was held constant. The decay in $C$ was accomplished by simultaneously introducing clearwater ($C = 0$ mg/L) to the top of the mixing tank while draining sediment-laden water from the bottom of the mixing tank. Control over the inflow and outflow was accomplished by introducing two additional tanks to the

system; one was placed above the mixing tank and the other below it (Fig. 2.2). This arrangement results in a gravity-driven system where the flow rate into and out of the mixing tank is controlled by a pair of needle valves and the elevation difference between the water surfaces in the tanks. To keep $G$ constant through the decay in $C$, the volume of fluid within the mixing tank must remain constant (Eq. 4.4); i.e., the inflow discharge of clear fluid to the mixing tank must equal the outflow discharge (Fig. 2.2). This steady volume condition is accomplished by ensuring that the water surface elevation difference between the top tank and the mixing tank, and between the mixing tank and the waste tank, are equal and that the valves are opened to the same position. For the experiments, the initial water surface elevation difference was set to 1.2 m. A reduction in the initial elevation differences does occur once the valves have been opened. However, the reduction in the elevation difference is the same between the mixing tank and both the upper and lower tanks. Hence, the volume in the mixing tank stays constant.

### 2.3.3 Procedures

All experiments began with the preparation of the mixture. The 80%/20% kaolinite and montmorillonite mixture (by dry mass) was first hydrated in a beaker with 150 mL of water and sonicated for 15 minutes to break the clay aggregates down to an average size of approximately 5 $\mu$m (Keyvani and Strom, 2014). The suspension was then introduced directly to clear water that was mixing at a rate of $G = 50$ s$^{-1}$in the mixing tank (Keyvani and Strom, 2014).

In Set A, mixing at $G = 50$ s$^{-1}$continued for 12 hrs following the introduction of the sediment to allow the flocs to grow up to an equilibrium size distribution; throughout this time, the suspension was continuously imaged at a rate of 0.5 Hz. After 12 hours, the paddle rotation rate

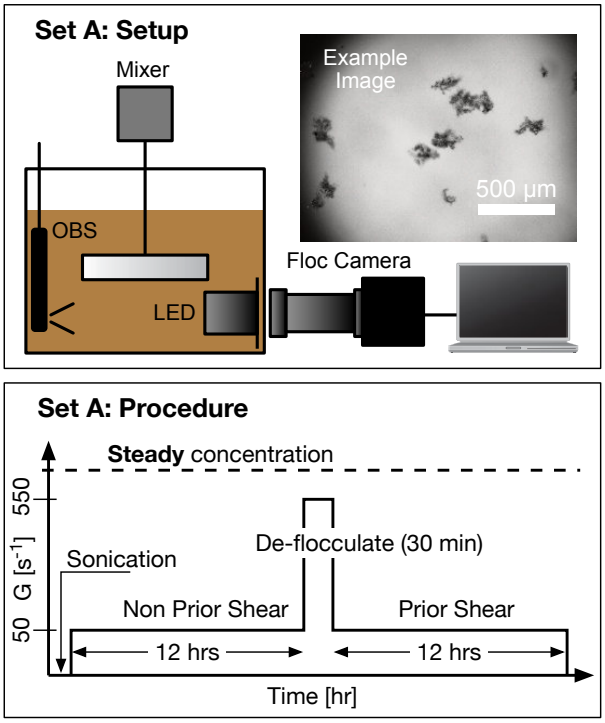


**Figure 2.1:** Schematic of tank setup and procedure time series of imposed turbulent shear, $G$, and suspended sediment concentration for the experiments run with constant concentration (Set A).

was increased to produce conditions of $G \approx 550\ \mathrm{s}^{-1}$. Mixing at this rate continued for 30 minutes to ensure that all flocs were broken down to a new primary particle suspension; mixing at this rate is larger than what would be experienced in any average flow environment. The purpose of this period of high shearing was to disaggregate the flocs and produce a turbulent-shear-generated initial condition for the suspension. Following the 30 min of high mixing, conditions were returned to $G = 50\ \mathrm{s}^{-1}$ for another 12 hrs (Fig. 4.1), and images of the suspension were collected at 0.5 Hz. This procedure was applied for the seven values of concentration used in the Set A experiments, i.e., $C = 15$, 25, 50, 100, 200, 300 and 400 mg/L.

The sequence of sediment preparation and mixing outlined above leads to two phases within each experiment. Following previous work, these phases are referred as the “non prior”

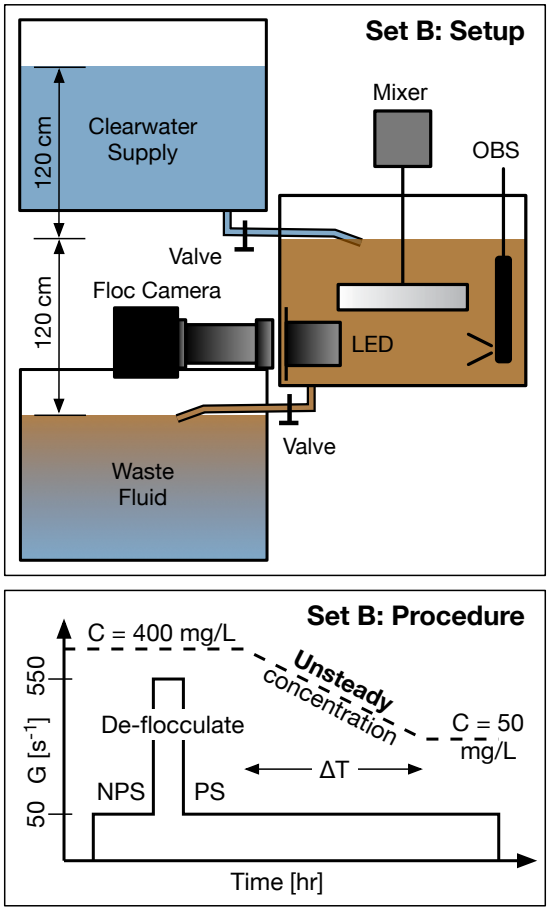


**Figure 2.2:** Schematic of tank setup and procedure time series of imposed turbulent shear, $G$, and suspended sediment concentration for the experiments run with an unsteady decay in concentration (Set B); the times over which the decay occur, $\Delta T$, are given in Table 3.3.

and "prior" shear phases (Keyvani and Strom, 2014; Tran and Strom, 2017). The non-prior-shear (NPS) phase refers to the growth of flocs from the sonified suspension (Fig. 4.1). The prior-shear (PS) phase refers to the growth of flocs following the end of vigorous mixing. A key difference between the two phases was that the non-prior-shear phase – deflocculated by ultra sound during sonication – starts with smaller clay particles ($d_p \approx 5$ $\mu$m) relative to the prior-shear phase ($d_p \approx 10-15$ $\mu$m), which was deflocculated by high turbulent shear.

The Set B experiments followed the same initial steps as those in Set A, but differed in

the length of the NPS phase and the steadiness of the concentration during the PS phase. The NPS phase in Set B was run for 2 hrs to produce mature flocs before creating the turbulent-shear-generated initial conditions for the PS phase ($G$ = 50 s$^{-1}$) via 30 min of vigorous mixing at $G \approx 550$ s$^{-1}$(Fig. 2.2). Following the vigorous mixing, the concentration was held steady for 1 hr of mixing at $G$ = 50 s$^{-1}$; which was more than enough time for the size distribution to reach an equilibrium. After 1 hr, the valves on the inflow and outflow tubes to the mixing tank were opened to a predetermined setting to produce a time-dependent decay in $C$ (Fig. 2.2). In all Set B runs, $C$ decreased from 400 mg/L to 50 mg/L over a set time of decay, $\Delta T$; values tested include $\Delta T$ = 50, 100, and 200 (min). Upon reaching $C$ = 50 mg/L, the valves on the inflow and outflow lines were closed and mixing was continued for another hour. Images of the suspension were recorded for both the steady and unsteady portion of the PS phase to allow for measurement of any change in the floc size distribution through the decay in $C$.

### 2.3.4 Image Processing

Time series of floc and general suspended particle sizes were extracted from images using automated procedures of Keyvani and Strom (2013). The routines remove out-of-focus flocs, by comparing the gradients of particles' grayscale values to an empirical threshold (Keyvani and Strom, 2013), and then combine the results from 30 images to yield size distributions of suspended particles every minute. Each 1-minute distribution contains several hundred to a few thousand particle measurements – depending on concentration and floc size. The raw by-number size distributions are then converted to a by-volume distribution (which is nearly equivalent to a by-mass distribution). Key floc size distribution statistics reported on in this

paper include: $d_{f5}$, $d_{f16}$, $d_{f50}$, $d_{f84}$, and $d_{f95}$. The statistics $d_{fX}$ always refers to the floc diameter for which X% of the material is finer than by volume.

### 2.3.5 Floc Size Uncertainty

Uncertainty in reported floc sizes comes from at least two sources, i.e., floc overlap in the images and experimental variation. First, images of flocs at higher concentrations, e.g. $C$ = 200, 300, and 400 mg/L, resulting in a significant number of flocs within the imaged plane. This can lead to what we refer to as "overlap" issues when running the automated image processing routines. The term overlap refers to automatically identified flocs in the image processing routines that appeared to be the superposition projection of two or several individuals, detached flocs (Fig. 2.10). These overlap "flocs" often appear larger and more irregularly shaped than the true flocs, and the inclusion of them in the size statistics can lead to overestimation of the floc size statistics. Our analysis (see Appendix) showed that the overlapping flocs do not significantly alter the shape of the floc size distribution, but that they do lead to slight overestimation of the average floc sizes, $d_{f50e}$. For example, the average overestimation of $d_{f50e}$ was found to be +3 $\mu$m for a concentration of 100 mg/L, up to +11 $\mu$m for concentrations of 400 mg/L (Fig. 2.11 and Table 2.4). An in-depth discussion on how overlap was quantified is presented in the Appendix.

Second, in previous work (Tran and Strom, 2017), we have conducted replicate experiments to quantify the variability inherent in experiments using this particular clay mixture and the experimental procedures of Set A. Data from these tests showed that even without overlap issues, the equilibrium size may vary up to ± 8 $\mu$m from run to run with $C$ = 100 mg/L. Therefore, it is important to keep in mind that the direct size data from the image processing proce-

dures are biased largely for $C > 100$ (i.e., Eq. 2.12 with max $+\Delta d_{f50}$ of 11 $\mu$m at $C = 400$ mg/L), and that there is inherent experimental variability of up to approximately $\pm$ 10 $\mu$m from run to run even without overlap. In the following Results section, we present the time-series data that is the direct result of the image processing procedures with no attempt to remove overlap bias. In the Discussion, we attempt to remove the overlap bias when considering the impact of concentration induced changes to $d_{f50e}$ and settling velocity.

## 2.4 Results

### 2.4.1 Set A: Floc Size Evolution under Steady Concentration

Figure 2.3 shows a sampling of flocs imaged at equilibrium condition under the NPS phases from the six different concentration experiments in Set A. Visually, it is evident that the number of flocs increase with $C$, and that the flocs in conditions of $C = 25$ mg/L are slightly smaller than the flocs that develop in higher concentrations (the size data confirms this observation). While this is true, it is difficult to decipher a clear difference in either the average floc size or shape among the images from other Set A experiments. The size differences are also apparent in the floc-size time series for the NPS phase (Fig. 2.4a) and the PS phase (Fig. 2.4b). That is, there is a general increase in the average floc size as $C$ goes up, with the increase in size being starkest between $C = 15$ to 25 mg/L and the rest of the runs ($C = 50$, 100, 200, and 400).

Overall the time series data for the NPS and PS phases show similar trends in that floc size and rate of growth both increase with $C$ (Fig. 2.4). However, comparing data from the two phases does reveal two differences. The first is that the average equilibrium floc size, $d_{f50e}$, from the NPS runs are $\approx 25$ $\mu$m larger than their PS phase counterparts at the same concentration.

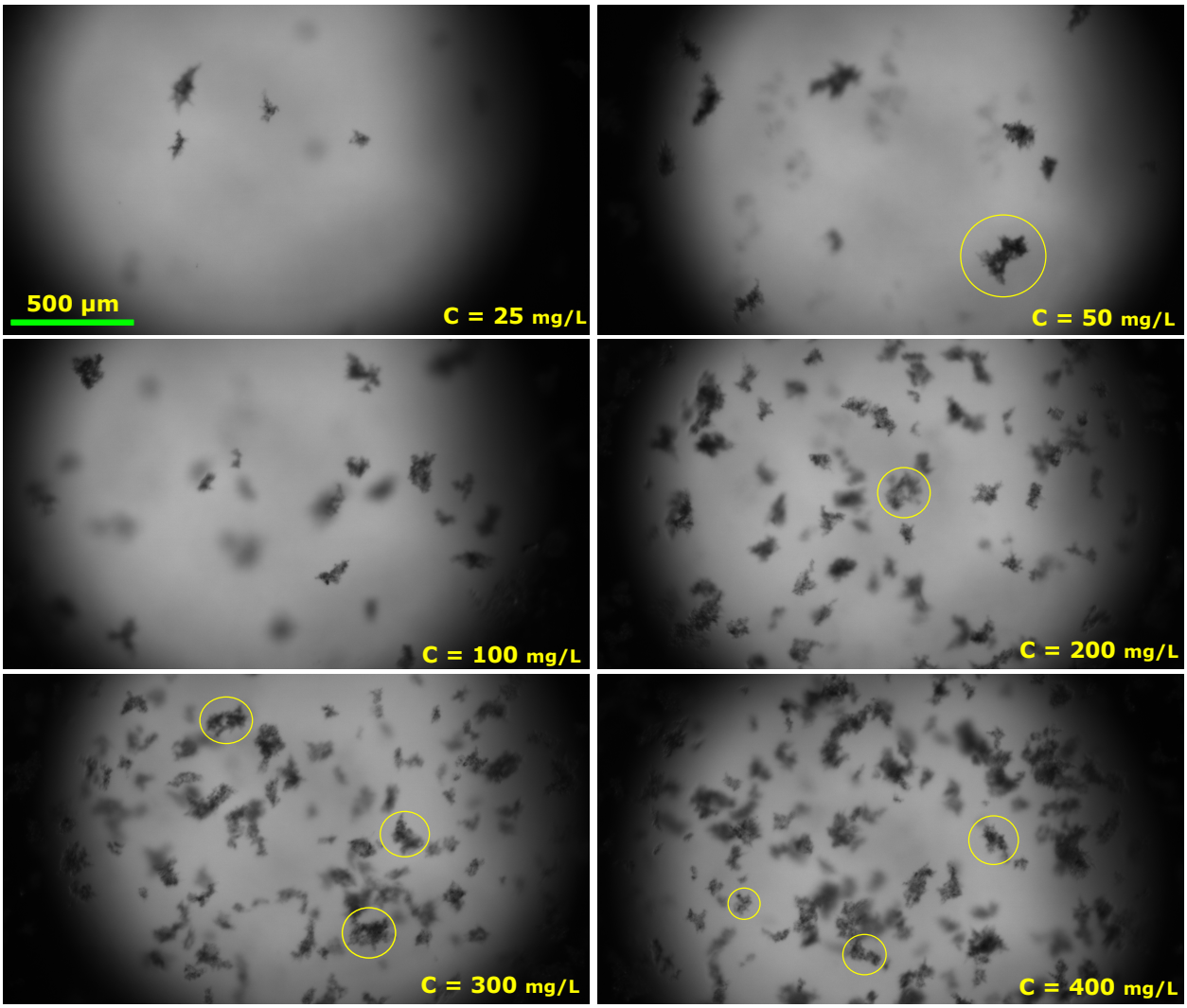


**Figure 2.3:** Samples of typical floc images at equilibrium (minute 720) in the NPS phase for the Set A runs (steady-state concentration). At higher concentrations, one can note that microflocs can occasionally be loosely bound to form macroflocs; some of these are circled.

Another difference between the phases is that the NPS phase has a peak in the time series for $d_{f50}$, whereas the PS phase does not (Fig. 2.4a,b). We expect that these differences are a manifestation of different initial primary particle sizes and shapes. Because the NPS phase starts with smaller primary particles that have been generated by sonication of the suspension, i.e., $d_p \approx 5$ $\mu$m, the particles comprising the flocs initially have a higher sticking efficiency and stronger bonding than they do during the PS phase. A consistent result of this is an initial peak in the floc sizes during the NPS phase followed by a slow drop down to an equilibrium size as the flocs are reworked by mixing (Keyvani and Strom, 2014). Suspensions that start from a state with larger primary particles, produced by turbulent mixing do not produce such behavior.

Figure 2.4c and 2.4d display floc size distribution characteristics measured within the last five minutes (minutes 716 to 720). These five minutes of data made for a total population of 13,673 individual flocs, unevenly distributed from several hundred for each lower concentration conditions to thousands of floc for each higher concentration conditions. At least two observations are evident from this set of size distribution data. The first is that $d_{f50}$ is clearly a function of $C$ (Fig. 2.4). Second, this change in $d_{f50}$ is primarily a result of a stretching of the distribution by adding in larger flocs; that is, the distributions are also getting more poorly sorted with $C$ (Fig. 2.4c, and 2.4d).

### 2.4.2 Set B: Floc Size Evolution under a Decay in Concentration

Figure 2.5 shows the concentration time series and corresponding change in the floc $d_{f50}$ from the three Set B experiments in which concentration was decreased linearly at three different rates from 400 mg/L down to 50 mg/L (Fig. 2.2); the time to go from $C$ = 400 mg/L to 50 mg/L,

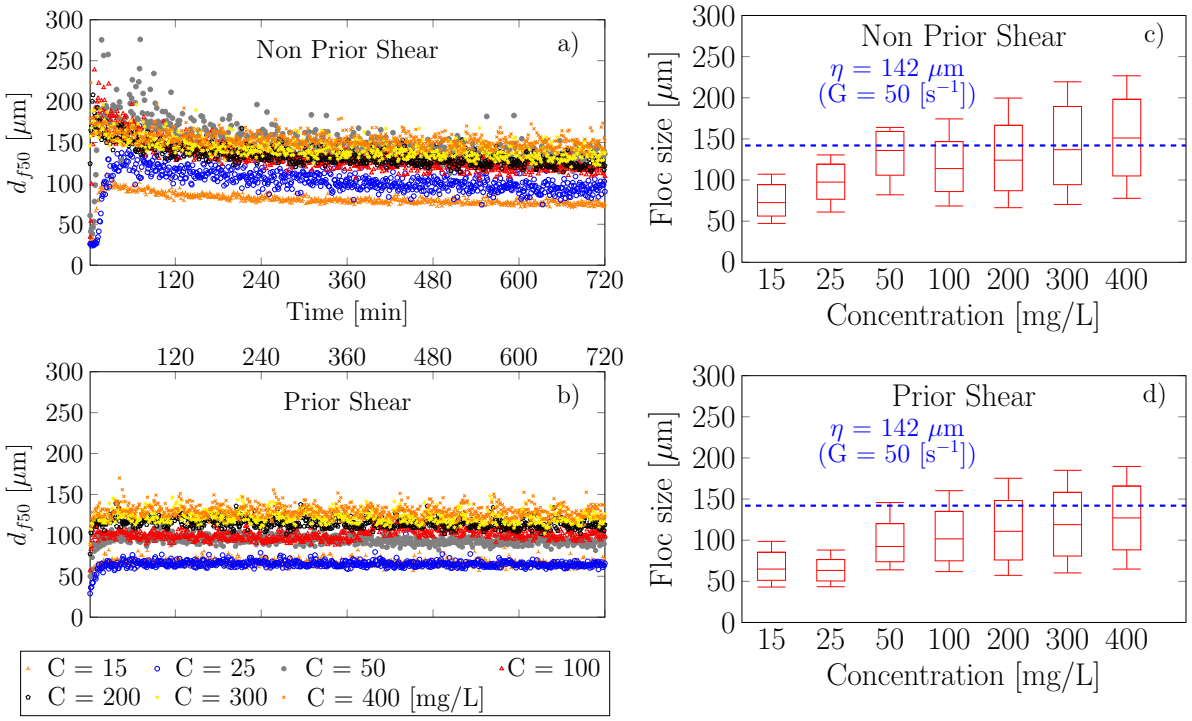


**Figure 2.4:** Measured floc size, $d_{f50}$, from Set A experiments (steady-state concentration). a) and b): time series data for NPS and PS, respectively. c) and d): boxplot of the last five minutes (minutes 716 to 720) of the time series data for NPS and PS, respectively. The bars in the boxplot from top to bottom present $d_{f95}$, $d_{f84}$, $d_{f50}$, $d_{f16}$, and $d_{f5}$.

$\Delta T$, was 50, 100 and 200 min respectively. For context, data shown in Figure 2.5 is from the PS phase of the experiment only; that is, from the time period following de-flocculation by strong mixing (Fig. 2.2). A few observations regarding the data from Set B (Fig. 2.5) are in order. First, it is clear that floc sizes decrease in time with the drop in concentration (Fig. 2.5 a-d). This outcome shows that flocs created at one concentration will change their size with a decrease in concentration even when the mixing conditions remain constant. Second, the differences in equilibrium floc size at $C$ = 400 mg/L to 50 mg/L between Set A and Set B are all within the range of experimental variation of ± 8 $\mu$m. Third, even throughout the concentration drop, there is little difference between the floc sizes at a particular concentration, e.g., 300, 200, or 100 mg/L,

and the equilibrium floc size at that concentration from the Set A experiments (Fig. 2.5 e-g). While the magnitude of the differences between the Set A and Set B sizes was small, there was a general trend of $d_{f50}$ at a particular concentration in the Set B runs being slightly larger than those in Set A. Fourth, there was no consistent trend in the $d_{f50}$ between the Set B runs at a particular concentration. We take this to indicate that, at least when averaged over a 5 minute window, average floc size $d_{f50}$ did not depend on the rate of decrease in concentration.

## 2.5 Discussion

The Set A (steady concentration) and Set B (unsteady concentration) experiments both show that the equilibrium and time-dependent floc size distribution is a function of concentration (Fig. 2.4, 2.5). Specifically, the data show that the size of the largest flocs increase with C (Set A) and that, similar to some other studies (e.g., Milligan, 1995), floc size responds rather quickly (within 20 min) to a time dependent decay in $C$. In this discussion section, we explore: (1) the relationship between $d_{f50e}$ and $C$; (2) the floc size differences at a given $C$ between experiments A (steady) and B (unsteady); (3) the impact of a change in $C$ on the calculated settling velocity of the flocs in suspension relative to changes in $G$ (turbulent shearing); and (4) the capabilities of empirical floc settling velocity equations to capture these relationships.

### 2.5.1 Relationship between $d_{f50e}$ and $C$

The data show that floc size, $d_{f50e}$, is a weak positive function of $C$. As discussed in section **??**, it is expected that $d_{f50e}$ can vary by $\pm$ 8 $\mu$m due to variability in the experiments. Furthermore, overlap can cause an overestimation of 3 to 11 $\mu$m depending on the concentration (Table 2.4

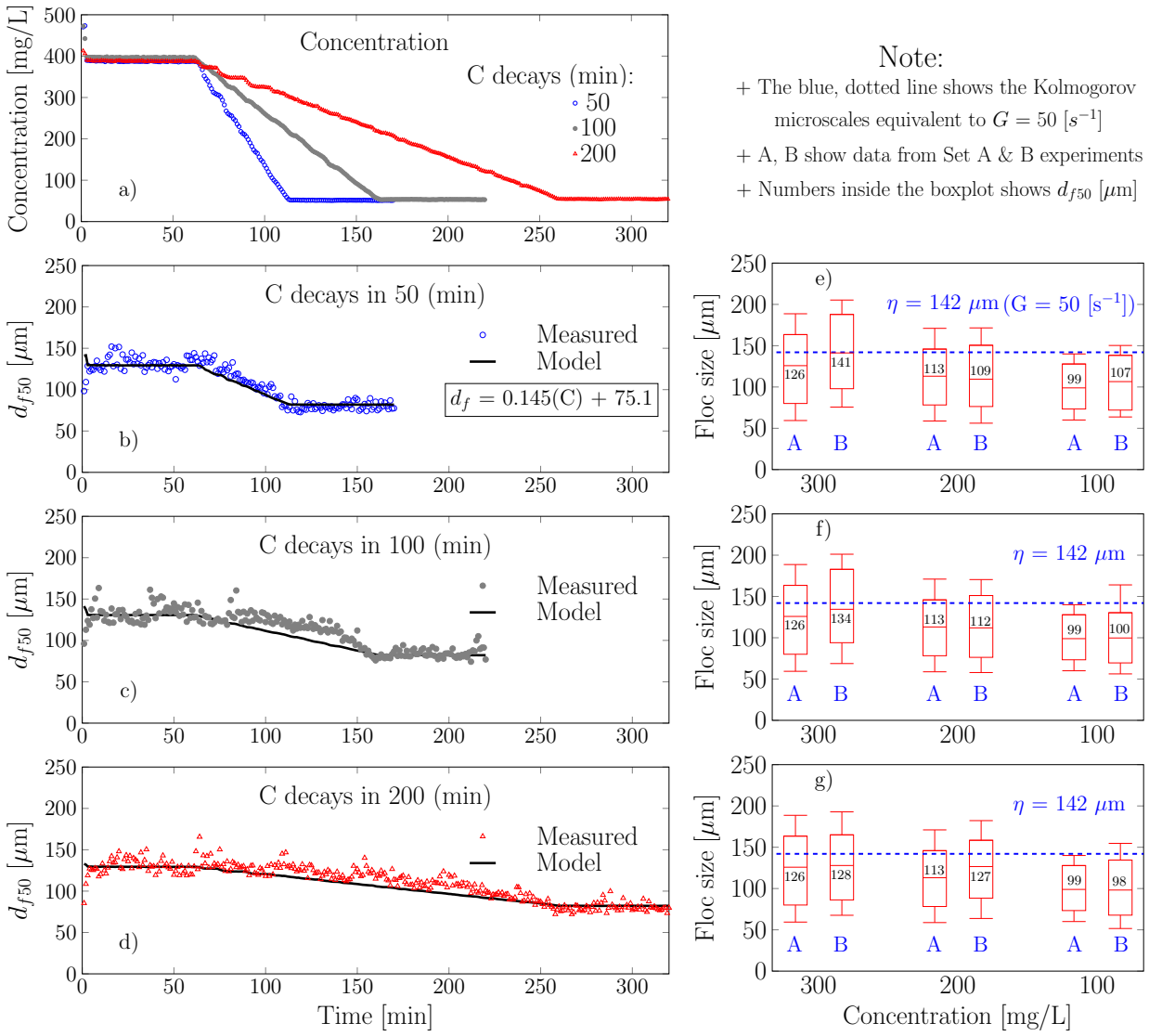


**Figure 2.5:** Data from the Set B experiments (change in floc size due to a steady rate of decrease in *C*). The diagrams on the left depict (a) the concentration time series and (b-d) the time series of $d_{f50}$ for each run. The correlation coefficients between the concentration and floc size are 0.94, 0.88 and 0.90 for 50, 100, and 200 minutes scenarios, respectively. Plots in the column to the right (e-g) shows the box-and-whisker plot of floc size characteristics at three different concentrations during the decay period. The data of equivalent concentrations from Set A are also presented for comparison. In all cases, the box plots were developed with 5 minutes of floc size data. The horizontal box-and-whisker markers from top to bottom correspond to: $d_{f95}$, $d_{f84}$, $d_{f50}$, $d_{f16}$, and $d_{f5}$.

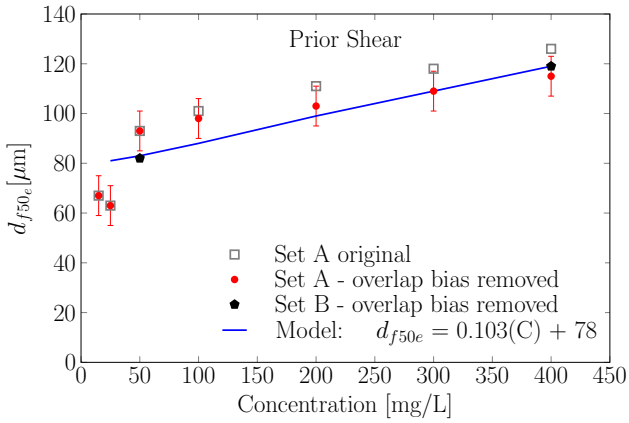


**Figure 2.6:** Floc size with overlap removed. The error bars show the experimental variations of ± 8 $\mu$m.

and Appendix). To provide context for these differences, the equilibrium size data from Set A is plotted in Figure 2.6 both with and without the overlap bias removed [via Equation 2.12]; the ± 8 $\mu$m experimental variation is also indicated via error bars. The differences among the experiments at different concentrations all reduces once the overlap bias has been removed. After removal of the overlap bias from the Set A data, the difference in $d_{f50e}$ between $C$ = 15 mg/L and $C$ = 400 mg/L is 48 $\mu$m; this difference reduces to 22 $\mu$m comparing only $C$ = 50 mg/L and $C$ = 400 mg/L (Fig. 2.6). Similarly, if the floc overlap bias is removed in the Set B data, [via Equation 2.12] the difference in floc size between 50 and 400 mg/L drops to approximately 35 $\mu$m. The equilibrium size data in Figure 2.6 also show that $d_{f50e}$ from Set B is close to that from Set A for $C$ = 400 mg/L (within the experimental variability), but that the sizes at $C$ = 50 mg/L are slightly smaller than their counterparts in Set A.

The equilibrium size model of Winterwerp (1998) (Eq. 2.3) suggests that $d_{f50e}$ should be proportional to $C$. Data from our experiments illustrates that this is reasonable if data from the $C$ = 15 and 25 mg/L experiment are neglected (Fig. 2.6). Fitting a line to all of the equilibrium

size data (both Set A and Set B) for which the overlap bias has been removed (using Eq. 2.12) gives:

$$d_{f50e} = 0.103(C) + 78, \quad (R^2 = 0.77) \tag{2.6}$$

Hereinafter, in all equations $C$ is in mg/L and $d_{f50e}$ is in $\mu$m, unless otherwise stated. Considering only data from $C = 50$ to 400 mg/L gives: $d_{f50e} = 0.08(C) + 85.73$ ($R^2 = 0.90$). These fits show that $d_{f50e}$ is linearly related to $C$ in the experiments, at least in the range of $C = 50$ to 400 mg/L. However, a direct comparison between Equation 2.6 and Equation 2.3 of Winterwerp (1998) is somewhat tenuous because a one-to-one comparison would suggest an interpretation of the intercept as being equal to the primary particle size in $\mu$m (i.e, $d_p = 78$ $\mu$m, which is significantly larger than the expected value of $d_p \approx 15$ $\mu$m. With either of the two linear fits, and assuming that the trends hold for much larger concentrations than the ones tested here, $C$ would need to increase from 100 to 1000 mg/L to produce a doubling of $d_{f50e}$.

### 2.5.2 Are Flocs in Equilibrium with the Local Conditions During a Time-dependent Decay in $C$

This section further examines the data from Set B experiments to determine how close the flocs sizes are during the unsteady decay in $C$ to their equilibrium values at the same concentration. That is, we explore the question of wether or not $d_{f50}$ at a concentration of $C_1$ ( $400 > C_1 > 50$ mg/L) is equal to the equilibrium value, $d_{f50e}(C = C_1)$, as determined by the Set A experiments.

Inherent in many empirical floc settling velocity equations, such as Equation 2.2, is the assumption that floc size and density, and hence settling velocity, are in equilibrium with the local concentration. That is, that $w_s$ is defined based solely on $C$ without any time dependence.

Figure 2.5 reveals that the $d_{f50}$ does respond to changes in concentration quickly. In fact, the correlation coefficients between the concentration decay and the reduction in floc size are 0.94, 0.88, and 0.90 for scenarios 50, 100, and 200 minutes, respectively. Hence, it seems reasonable to consider, at least for our experimental conditions, that the floc size is very close to being in equilibrium with the local conditions — even during periods of slow or fast reductions in $C$. Perhaps this outcome is partially due to the fact that the average equilibrium floc sizes over this range of $C$ and $G$ conditions are already reasonably close to each other. Unfortunately, our data does not say anything about how a mature floc size distribution responds to increases in $C$ with time.

In this section, we use the idea of a linear function between $d_{f50e}$ and $C$ for concentrations between 50 and 400 mg/L to examine how close to equilibrium the floc sizes are during the decay in $C$ within the Set B experiments. If the floc sizes are in equilibrium with the local conditions, then the size data through the decay in $C$ should be well approximated by a line resulting from a linear fit to the equilibrium size data. Fitting a line through the two points of $d_{f50e}$ at $C = 50$ and 400 mg/L (for the Set B data only) gives:

$$d_{f50e,m} = 0.145(C) + 75.1 \tag{2.7}$$

Concentration time series data from the OBS was used in Equation 2.7 to generate a theoretical time series of $d_{f50,m}$ for which the size is in equilibrium with the local concentration at every point in time. The comparison between this theoretical curve and the measured $d_{f50}$ data is shown in Figure 2.5. Strictly speaking, the size predicted by Equation 2.7 through the decay

is smaller at any given point in time than the measured data. In other words, there is a lag in time between when a particular size is reached in the measured data relative to the equilibrium model (Eq. 2.7). This observation may also be an artifact of using the measured floc sizes at $C = 400$ and 50 mg/L to develop the equilibrium model (Eq. 2.7).

### 2.5.3 The Impact of $C$ on Settling Velocity in a Turbulent Suspension

The data show that floc size changes with $C$. In this section, we explores how those changes in size might manifest in modifications in the floc effective settling velocity due to changes in concentration, $C$, and turbulent shearing, $G$. In the analysis, we assume that the floc's fractal dimension, $n_f$, is insensitive to variation in $C$ or $G$ and that $n_f = 2$; based on previous settling velocity measurements (Tran and Strom, 2017), a value of $n_f = 2$ is a reasonable estimate for this particular mixture of mud. Doing so allows for the computation of a floc effective settling velocity based on floc size. This calculation used the settling velocity equation of Strom and Keyvani (2011):

$$w_s = \frac{g R_f d_f^2}{b_1 \nu + b_2 \sqrt{g R_f d_f^3}} \tag{2.8}$$

where $g$ is the acceleration of gravity, $R_f = (\rho_f - \rho)/\rho$ is the submerged specific gravity of the floc or particle, $\rho_f$ is the density of the particle or floc, $\rho$ is the density of the ambient water, $d_f$ is the equivalent diameter of the floc or particle (in the analysis we use $d_f = d_{f50e}$), and $b_1$ and $b_2$ are coefficients that are dependent on particle shape and porosity (unless otherwise stated, we use $b_1 = 20$ and $b_2 = 1.26$). $R_f$ can be put as function of $R_s$ the submerged gravity of the sediment, $d_f$, $d_p$, and a fractal dimension, $n_f$ using the following relation: $R_f = R_s(d_f/d_p)^{n_f - 3}$ (Kranenburg, 1994). Considering the data with the overlap bias removed, the calculation reveals

that a 700% change in $C$ results in an ≈ 20% change in floc $w_s$ (i.e, going from 0.4 mm/s to 0.5 mm/s). Assuming that Equation 2.6 can be applied to higher concentrations, a doubling of the predicted effective settling velocity can be obtained by going from $C$ = 100 mg/L to 1,000 mg/L (from 0.38 mm/s to 0.76 mm/s).

In our present study, we have isolated the impact of steady-state and decaying suspended sediment concentration on time-dependent and equilibrium floc sizes under conditions of steady shear. However, numerous studies have shown that floc size is proportional to the Kolmogorv micro length scale, $\eta$, or that $d_{f50e} \propto G^{-1/2}$ (Lick and Lick, 1988; Winterwerp, 1998; Verney et al., 2011; Guo et al., 2018). Here we use this proportionality and data from previous studies to estimate the expected change in $w_{s(df50)}$ due to only changes in $G$. The purpose of doing so is to compare the magnitude of the change in settling velocity that might be expected from variation in $G$ to changes that might be expected from variations in $C$. These estimates are based on the following approximation:

$$d_{f50e,m} \approx 0.75\eta = 0.75\sqrt{\frac{\nu}{G}} \tag{2.9}$$

The factor of 0.75 in the proportionality between floc size and $\eta$ was chosen because it allowed for a reasonable match between Equation 2.9 and the equilibrium size data from the current experiments (at $G = 50$ s$^{-1}$) and the experiments of Tran and Strom (2017). Using Equations 2.9 and 3.1, one would expect to see a doubling of the effective settling velocity due to a decrease in shear only when going from $G = 50$ to 12 s$^{-1}$(from 0.46 mm/s up to 0.91 mm/s).

### 2.5.4 Can Current Equilibrium Models Capture the Observed Trend?

This section examines the ability of historic equilibrium floc size, or empirical floc settling velocity, equations to capture the basic trend in our data for $d_{f50e} = d_{f50e}(C)$. In the comparison Equation 3.1 was used to translate between $d_{f50e}$ and $w_s$. The models being tested are those of, Krone (1962), Teeter (2001), and the steady-state version of the Winterwerp (1998) floc size model. These three models were chosen because their basic structure represents the widest variety in relationship of such models while still maintaining some dependence of $d_{f50e}$, or $w_s$, on $C$.

The most basic form of a concentration dependent settling velocity is that of Krone (1962), who suggested that the flocculation impacted settling velocity relationship,

$$w_s = aC^n \tag{2.10}$$

described his experimental observations from a dilute suspension of San Francisco Bay mud. Here $a$ and $n$ are sediment and water chemistry specific parameters, equal to $a = 0.107$ and $n = 4/3$ for Krone's data where $w_s$ is in mm/s and $C$ is in g/l. Please note that the Krone (1962) flocculation-influenced settling velocity is solely a function of $C$. We would argue that the shear rate being experienced by the mixture strongly influences the size of the flocs and therefore the settling velocity of the mud. However, since the experiments presented in this paper were conducted under uniform conditions of $G$, it is possible that an equation like Equation 2.10 could do a good job of capturing the trends in our data.

In a previous study, Strom and Keyvani (2016) found that the van Leussen (1994) model could be calibrated to reasonably estimate the dependence of $w_s$ on changes in $G$ only. However, the van Leussen (1994) model does not have any dependence with $C$, and would therefore predict no difference in $w_s$ among our current set of experimental conditions. Therefore, we test the function of the Teeter (2001) model, which adds a concentration dependence to the basic structure of the van Leussen (1994) equation:

$$w_{s,i} = a_1 \left( \frac{C}{C_{ul}} \right)^{n_i} \left[ \left( \frac{1 + a_{2G}}{1 + a_3 G^2} \right) \exp\left( -a_4 \frac{C}{C_{ll}} \right) + 1 \right] \tag{2.11}$$

where $a_1$ through $a_4$ are general coefficients, $n_i$ is a power specific to each size class $i$, $C_{ll}$ is the the lower concentration limit below which flocculation is thought to be unimportant, and $C_{ul}$ is the upper limit past which hindered settling is important. The third model is given by the steady-state solution to the time-dependent model by Winterwerp (1998) (Eq. 2.3); which seems appropriate without modification because flocs in our experiments never settle.

Figure 2.7 displays the results from our analysis. Figure 2.7A compares the equilibrium floc size data from the prior shear experiments of Set A to the three models presented above, using the coefficients given by the original authors. As can be seen, when using the original model coefficient values, the three models underpredict the settling velocity calculated from the floc size measurements over the range of $C$ values tested. That is, the models predict very little influence due to flocculation in the 15 to 400 mg/L range. For this reason, we re-calibrated the model coefficients for each equation by fitting the models to our observed data. Figure 2.7B shows the models after they were calibrated with our data; the original and newly calibrated

coefficient values are given in Table 2.3. Because the Krone (1962) and Teeter (2001) models are both power functions, they can be calibrated to well match the observed data over the range of concentrations used in the experiments, and even down to smaller sizes as $C$ approaches 0 mg/L. However, because the Winterwerp (1998) equation is linear, it cannot capture the change in slope between $C = 0$ and 50 mg/L. Furthermore, setting the intercept equal to the primary particle size, $b = d_p$, in Equation 2.3, makes it impossible to capture the slope of the settling velocity curve for $C \geq 50$ mg/L. For these reasons, two types of calibration with $b$ and $K_A/K_B$ in Equation 2.3 were investigated. In the first, $b$ was set equal to $d_p$ and $K_A/K_B$ was determined by ensuring that the settling velocity predicted with Equation 2.3 and Equation 3.1 matched the value obtained with the experimental data at $C = 100$ mg/L. For the second, both $b$ and $K_A/K_B$ were varied to best fit the data in the range of $C \geq 50$ mg/L (Fig. 2.7B). Following the work in this study we proposed a modification of the limits floc sizes to that of the Kolmogorov micro length scale so that Winterwerp (1998) equation can better predict floc size at other level of concentrations, e.g., Figure 13 in (Kuprenas et al., 2017).

Once calibrated, all three of the models could reasonably describe the equilibrium floc size, or settling velocity, over the range of $C = 25$ to 100 mg/L. However, in all cases, the original model coefficients: (1) under predicted the influence of flocculation in the dilute suspension tested here (predicted a lower $w_s$ value than the data suggest), and (2) overpredicted the influence of $C$ on $w_s$ (or overpredicted the slope of the $w_s = w_s(C)$ function). This comparison shows that there are both empirical and semi-empirical equilibrium floc-size models that can adequately capture the relationship of floc settling velocity under conditions of constant shear.

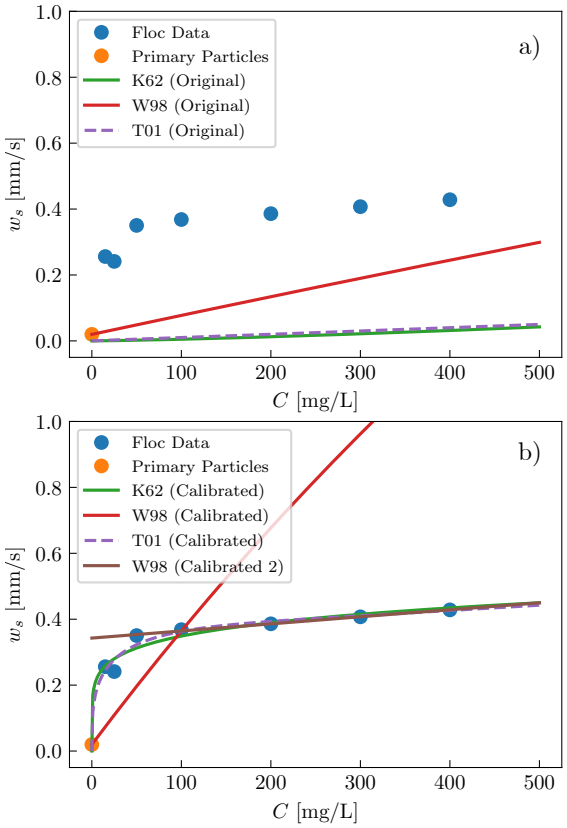


**Figure 2.7:** Comparison between the equilibrium floc data from Set A and the equilibrium models of Krone (1962) (K62), Winterwerp (1998) (W98), and Teeter (2001) (T01). Note, the assumption in this figure is that $w_s$ goes to the settling velocity of the primary particles as $C$ approaches 0 mg/l, which is very small. (a) comparison between the data and the models using the original calibration coefficients of the authors; (b) comparison between the data and the models using coefficients that were developed in calibrating the models to the data in this paper. Values for all coefficients in both panels (a) and (b) can be found in Table 2.3.

However, these models need calibration and, as of yet, cannot be used with off-the-shelf model coefficients. Of the three models tested here, we suggest that the Teeter (2001) and Winterwerp (1998), or the limited-residence-time model of Winterwerp et al. (2006), are better suited for describing the resulting impact of flocculation on $w_s$ because they also include a functionality with $G$.

| Model | Original Values | Calibrated Values |
|---|---|---|
| Krone (1962) | | |
| $a$ | 0.107 | 0.50 |
| $n$ | 1.33 | 0.16 |
| | | |
| Winterwerp (1998) | | |
| $K_A/K_B$ | 1.04 | 6.5 (0.43)* |
| $b$ [$\mu$m] | $d_p$ | $d_p$ (91)* |
| | | |
| Teeter (2001) | | |
| $w_{si,max}$ [mm/s] | 1 | 1 |
| $a_1$ | 266 | 300 |
| $a_2$ | 9 | 10 |
| $a_3$ | 0.80 | 0.05 |
| $n_i$ | 1 | 0.89 |
| $C_{ll}$ [mg/l] | 100 | 10 |
| $C_{ul}$ | 10000 | 10000 |

**Table 2.3:** Coefficient values for the settling velocity equations presented section 2.5.4. *values in parenthesis represents the best fit of both the slope ($K_A/K_B$) and intercept, $b$, of Equation 2.3 using only data from $C$ = 50 mg/L and larger.

## 2.6 Conclusions

This study investigated the influence of suspended sediment concentration, alone, on (1) the equilibrium floc size, and (2) the rate of adjustment in size within a suspension in response to a decay in concentration mimicking that of clearwater entrainment. The investigation was carried out through two sets of experiments, one of which maintained a steady concentration (Set A), while the other was configured so that concentration decreased with time (Set B). The newly-developed "near wall" imaging method allowed us to directly image flocs in concentrations up to $C$ = 400 mg/L without removing any samples from the turbulent suspension.

The data suggest that equilibrium floc size is a function of $C$, but that the dependence is weak–at least when the turbulent shearing is relatively strong (i.e., $G = 50\ s^{-1}$) and $C \geq$50 mg/L.

For example, a 700% increase in concentration (going from 50 to 400 mg/L) only led to a change in the floc size of 22 $\mu$m (a $\approx$ 20% change in size). The increase in equilibrium floc size with $C$ was found to be linear within the range of $C$ = 50 to 400 mg/L. Furthermore, increases in $C$ were found to enhance the growth rate of flocs in the NPS phase; yet this pattern was not discernible in the PS phase since floc re-equilibrated very quickly during the PS phase.

In these experiments, it seems reasonable to take the PS floc behavior as being a more accurate representation of flocs in natural water bodies. Under this paradigm, the Set B experiments showed that floc sizes respond quickly to decreases in $C$, making the time dependent flocs size nearly equal to the equilibrium floc size predicted by the conditions in the tank at any instant. In the strict sense, flocs were out of equilibrium with the local conditions. However, factoring in experimental error and a natural variability in floc size data, we conclude that for the water and sediment conditions tested in our experiment, the floc size, and hence settling velocity, could be treated as being in equilibrium with the local conditions for process or computational time scales on the order of minutes to tens of minutes and larger.

## 2.7 Appendix

### 2.7.1 Development of Near-wall Method

In this study, we suggest an alteration to the setup we have used in the past to allow for measurement of floc sizes within suspensions of up to $C$ = 400 mg/L. As mentioned previously, to provide illumination, a LED was fitted inside a waterproofed housing, sealed inside with a round glass plate, and placed inside the tank. The glass plate served two functions. First, it allowed light to pass out of the waterproofed housing. Second, placing the LED in the tank such

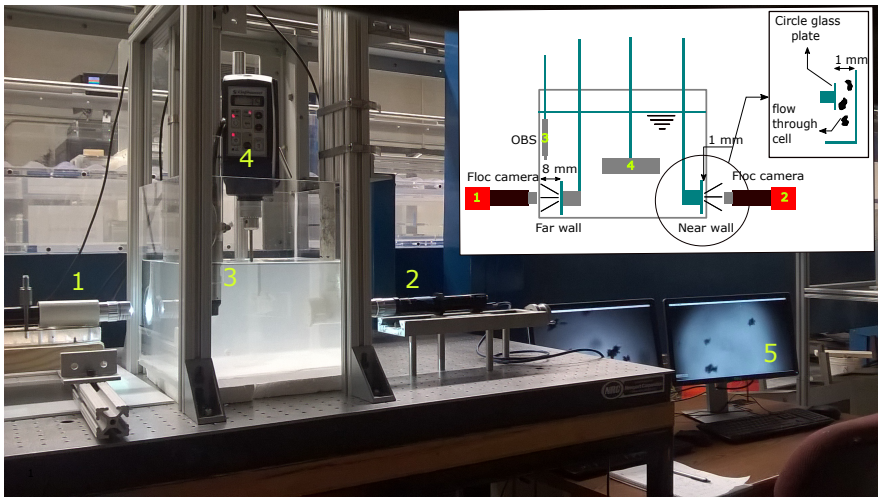


**Figure 2.8:** Schematic and picture of the Near wall setup. The flow through cell results in slowing the speed and reducing the number of flocs being imaged.

that the glass plate was parallel to the mixing tank wall produced a thin, (≈ 1 mm) flow-through cell where flocs could be imaged. The flow-through cell both slowed the speed of the flocs and reduced the number of flocs between the light source and tank wall. The combined effect was that flocs could be imaged with a constant (as opposed to flashed) light source, and flocs could be imaged in concentrations up to 400 mg/L (Figure 2.8). Without the glass plate, the maximum concentration in which flocs could be imaged is ≈ 100 mg/L (Strom and Keyvani, 2016).

### 2.7.2 Comparison Between the Near-wall and Standard, Far-wall, Methods

The new glass plate, flow-through cell was tested extensively to ensure that it did not filter out larger flocs, cause a breakup, or increase floc size due to congestion in the cell. To conduct this test, we used two identical floc camera systems within the same mixing tank. Both light sources were fitted with the glass plate described above and placed within the tank. One was placed at 1 mm from the wall (i.e., the “near-wall” setup), and the other was placed at 8 mm from the wall; the one placed at 8 mm from the wall is referred to as the *far-wall* method. Experiments on floc

growth, with procedures identical to those of Set A, were run with this setup under conditions of $C$ = 25, 50, and 100 mg/L; note that the camera with the light source 8 mm away cannot capture meaningful data when $C$ >100 mg/L. Images from both cameras were run through the image processing routines to produce floc-size populations and average-size time series. The sizes captured with the two different camera setups were then compared. Data from the three experiments showed very little difference in floc size or rate of growth between the two cameras (Fig. 2.9). Based on these experiments, we conclude that the near-wall method creates a climate for collecting reasonable floc-size data when the floc's diameters are less than about half of the flow-through cell gap.

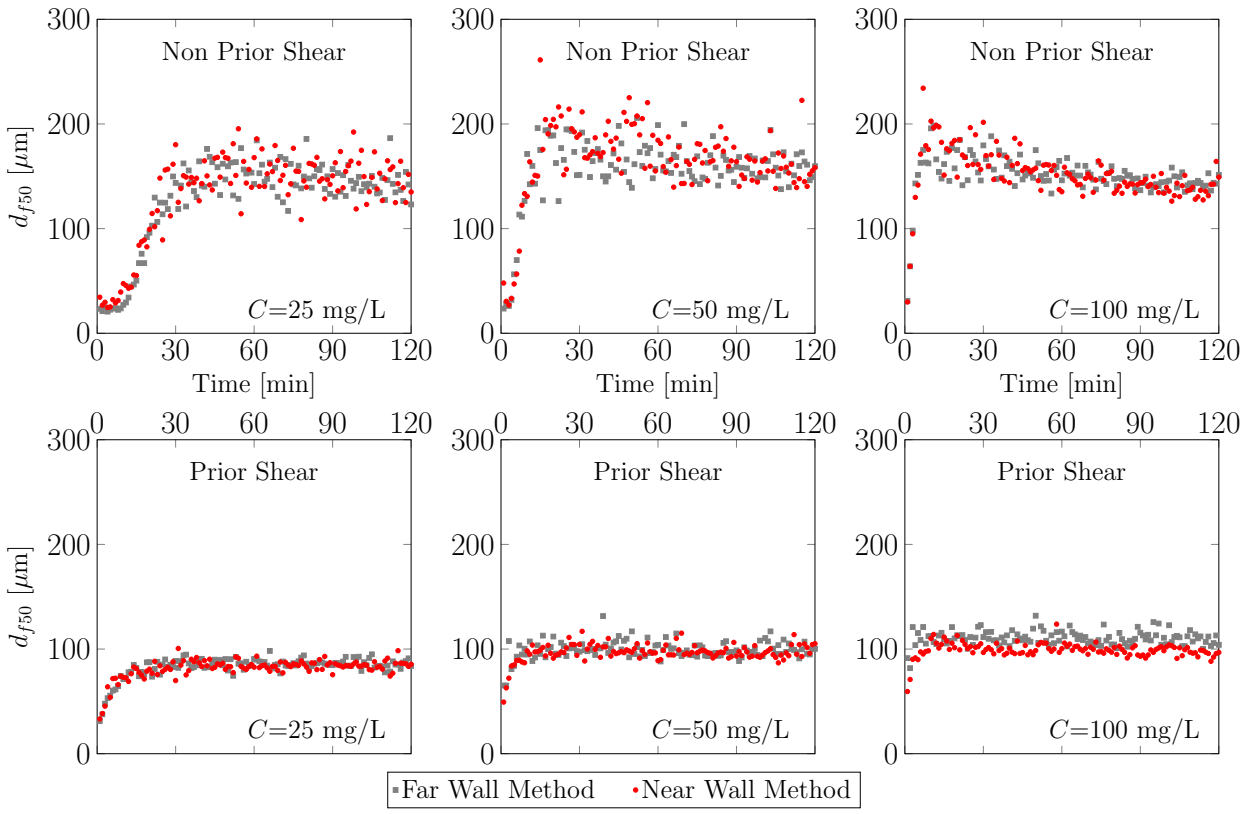


**Figure 2.9:** Time series of the average floc size, $d_{f50}$, from the near and far wall setups for both the NPS and PS phases of floc growth.

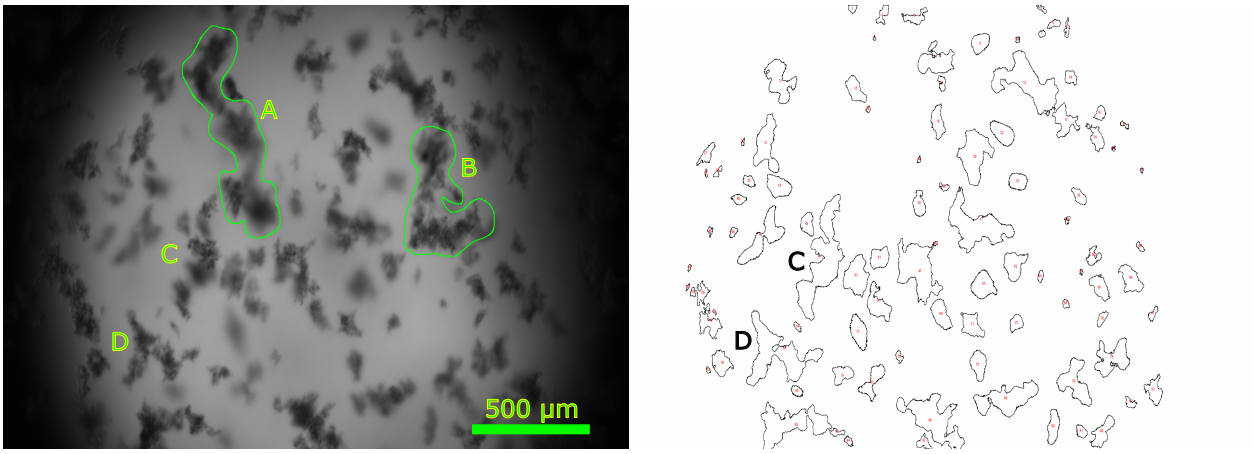


**Figure 2.10:** Examples of overlap flocs. The overlap flocs A and B were eliminated during the automated image processing based on the circularity threshold. Overlap flocs C and D, which were not detected by the automated code, were taken into account when computing floc size. The overlap causes overestimation of about 3 to 11 $\mu$m for concentration ranging from 100 to 400 mg/L, respectively.

### 2.7.3 Floc-overlap at Higher Concentration

Even with the near-wall flow-through cell, images of flocs at higher concentrations, e.g. $C$ = 200, 300, and 400 mg/L, resulted in a significant number of flocs within the imaged plane. This can lead to what we refer to as "overlap" issues when running the automated image processing routines. The term overlap refers to automatically identified flocs in the image processing routines that are really the superposition projection of two or several individuals, detached flocs in a 2-D plane (Fig. 2.10). These overlap "flocs" are often larger and far more irregularly shaped than the true flocs in suspension, and the inclusion of them in the size statistics could lead to overestimation of the average floc size.

A circularity filter was included in our standard image processing routines to help reduce the impact of overlapping flocs on the measured size distribution. Here circularity was defined as $C_{circ} = 4\pi(A_f/(P_f)^2)$ where $A_f$ is the floc area and $P_f$ is the floc perimeter. In this way, all

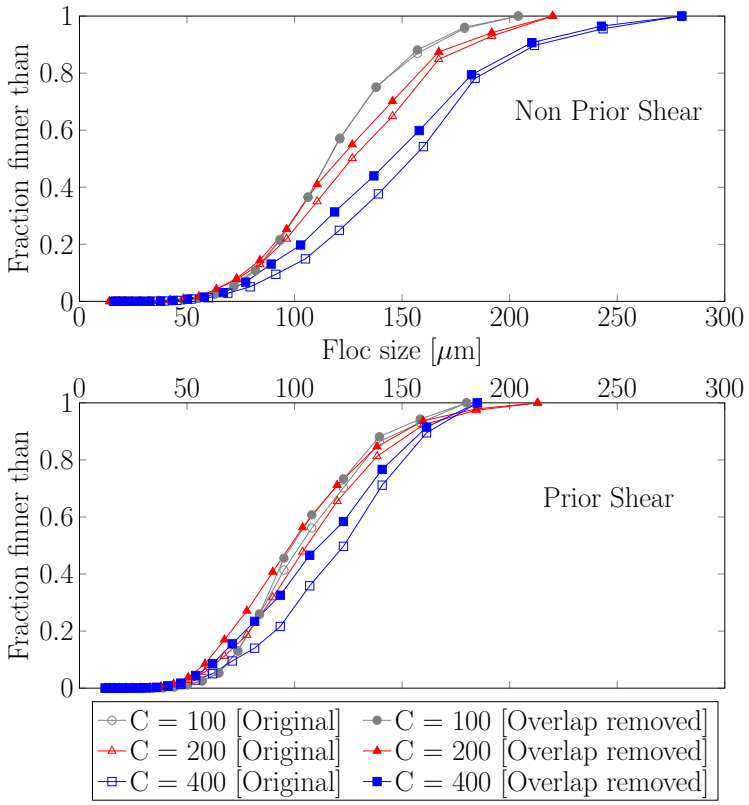


**Figure 2.11:** Comparison of floc size distribution with automated procedure and manually removal of overlap flocs. Each distribution curve was plotted from a population of 500 individual flocs. The total number of flocs that were manually examined were 3,000 flocs.

flocs identified by the automated procedures with circularity values that fell outside the range of $C_{circ}$ = 0.09 - 0.65 were removed from the results. These filter values were based on analysis of approximately one million flocs for which we knew that overlap was not an issue. Adding this filter removed the majority of the bias in sizes at higher concentration. For example, the criteria led to the removal of flocs A and B in Figure 2.10 from the results. Nevertheless, even with the circularity filter, testing showed that some overlapping flocs still made it through to the results (e.g., C and D in Fig. 2.10).

Other criteria were extensively explored to aid in removal of overlapping flocs from the

| [1]NPS | $C$ = 100 [mg/L] original | $C$ = 100 [mg/L] overlap removed | Diff. | $C$ = 200 [mg/L] original | $C$ = 200 [mg/L] overlap removed | Diff. | $C$ = 400 [mg/L] original | $C$ = 400 [mg/L] overlap removed | Diff. |
|---|---|---|---|---|---|---|---|---|---|
| $d_5$ [$\mu$m] | 71 | 70 | 1 | 66 | 66 | 0 | 79 | 72 | 7 |
| $d_{16}$ [$\mu$m] | 88 | 87 | 1 | 88 | 86 | 2 | 107 | 95 | 12 |
| $d_{50}$ [$\mu$m] | 117 | 117 | 0 | 127 | 121 | 6 | 154 | 145 | 9 |
| $d_{84}$ [$\mu$m] | 153 | 151 | 2 | 167 | 164 | 3 | 197 | 197 | 5 |
| $d_{95}$ [$\mu$m] | 177 | 176 | 1 | 201 | 197 | 4 | 241 | 238 | 3 |
| [1]PS | $C$ = 100 [mg/L] original | $C$ = 100 [mg/L] overlap removed | Diff. | $C$ = 200 [mg/L] original | $C$ = 200 [mg/L] overlap removed | Diff. | $C$ = 400 [mg/L] original | $C$ = 400 [mg/L] overlap removed | Diff. |
| $d_5$ [$\mu$m] | 64 | 64 | 0 | 58 | 53 | 5 | 62 | 56 | 6 |
| $d_{16}$ [$\mu$m] | 76 | 76 | 0 | 74 | 67 | 7 | 85 | 72 | 13 |
| $d_{50}$ [$\mu$m] | 103 | 100 | 3 | 106 | 98 | 8 | 123 | 112 | 11 |
| $d_{84}$ [$\mu$m] | 137 | 135 | 2 | 144 | 138 | 6 | 156 | 151 | 5 |
| $d_{95}$ [$\mu$m] | 164 | 161 | 3 | 173 | 168 | 5 | 174 | 172 | 2 |

**Table 2.4:** Comparison of floc size with and without removal of overlap flocs. The grain size characteristics obtained from 3,000 individual flocs (500 flocs for each condition) of which were used to manually quantify the overestimation of floc size causing by overlap. [1]NPS stands for non prior shear. [2]PS stands for prior shear.

size results. However, no other suitable filter parameter was found. In the end, we simply quantified the impact of overlapping flocs on the size measurements. This was done by manually checking 500 individual flocs identified by the automated procedures at concentrations of 100, 200, and 400 mg/L during minute 720 of each phase of the Set A experiments (i.e., during equilibrium for both the NPS and PS phase); in all, 3,000 flocs were manually checked. In each case, any floc that appeared to be an overlap projection of two or more flocs were broken down into their individual floc components. We used ImageJ, a program that was developed by National Institutes of Health and has been widely used in image processing, to trace the shape of the particle to measure its size.

For example, overlap flocs C and D in Figure 2.10 consists of three and four individual in-focus flocs, respectively. The sizes of flocs C and D were therefore eliminated from the size distribution and replaced by the sizes of the three and four in-focus individual flocs that comprise flocs C and D. The floc size distribution as well as the mean floc size, $d_{f50e}$, were calculated

for both with and without the removal of the overlap flocs. Figure 2.11 and Table 2.4 illustrate the original data and the modified data after removal of the overlapping flocs. In Figure 2.11, the frequency distributions have been normalized by the total number of measured flocs to allow for better comparison between the "with" and "without" overlap size distributions. The results of this analysis show that the overlap flocs do not significantly alter the shape of the size distribution, but that they do lead to slight overestimation of the average floc sizes, $d_{f50e}$; average overestimation of the $d_{f50e}$ was +3 $\mu$m for a concentration of 100 mg/L, up to +11 $\mu$m for concentrations of 400 mg/L (Table 2.4). Fitting a curve to the bias gives,

$$+\Delta d_{f50e} = 5.12\ln(C) - 20.74, \quad (R^2 = 0.90) \tag{2.12}$$

Here, $C$ is in mg/L and $\Delta d_{f50}$ is in $\mu$m. It must be noted that this curve is limited to $C$ in the range of 50 to 400 mg/L and that it is specific to our particular data; there is no reason to expect it to be more generally applicable.

## Bibliography

Ariathurai, R. and Krone, R. B. (1976). Finite element model for cohesive sediment transport. *Journal of Hydraulics Division*, 102(3):323–338.

Berhane, I., richard W. Sternberg, Kineke, G. C., Milligan, T. G., and Kranck, K. (1997). The variability of suspended aggregates on the Amazon Continental Shelf. *Continental Shelf Research*, 17(3):267–285.

Braithwaite, K. M., Bowers, D. G., Nimmo Smith, W. A. M., and Graham, G. W. (2012). Controls on floc growth in an energetic tidal channel. *Journal of Geophysical Research: Oceans*, 117(C2).

Burban, P.-Y., Lick, W., and Lick, J. (1989). The flocculation of fine-grained sediments in estuarine waters. *Journal of Geophysical Research*, 94(C6):8323–8330.

Burt, T. N. (1986). Field settling velocities in estuarine muds. In Mehta, A. J., editor, *Estuarine Cohesive Sediment Dynamics*, pages 126–150. Springer New York.

Chen, S. and Eisma, D. (1995). Fractal geometry of in situ flocs in the estuarine and coastal environments. *Netherlands Journal of Sea Research*, 33(2):173 – 182.

Chen, S.-N., Geyer, W. R., Sherwood, C. R., and Ralston, D. K. (2010). Sediment transport and

deposition on a river-dominated tidal flat: An idealized model study. *Journal of Geophysical Research*, 115(C10040).

Cuthbertson, A. J. S., Ibikunle, O., McCarter, W. J., and Starrs, G. (2016). Monitoring and characterisation of sand-mud sedimentation processes. *Ocean Dynamics*, 66:867–891.

Dietrich, W. E. (1982). Settling velocity of natural particles. *Water Resources Research*, 18(6):1615–1626.

Dyer, K., Christie, M., and Manning, A. (2004). The effects of suspended sediment on turbulence within an estuarine turbidity maximum. *Estuarine, Coastal and Shelf Science*, 59:237–248.

Dyer, K. R. (1989). Sediment processes in estuaries: future research requirements. *Journal of Geophysical Research*, 94(C10):14327–14339.

Eisma, D., Bernard, P., Cadee, G., Ittekkot, V., Kalf, J., Laane, R., Martin, J., Mook, W., van Put, A., and Schuhmacher, T. (1991). Suspended-matter particle size in some West-European estuaries; Part II: A review on floc formation and break-up. *Netherlands Journal of Sea Research*, 28(3):215–220.

Eisma, D. and Kalf, J. (1996). In situ particle (floc) size measurements with the Nioz in situ camera system. *Journal of Sea Research*, 36(1-2):49–53.

Eisma, D. and Li, A. (1993). Changes in suspended-matter floc size during the tidal cycle in the Dollard estuary. *Netherlands Journal of Sea Research*, 31(2):107–117.

Ferguson, R. and Church, M. (2004). A simple universal equation for grain settling velocity. *Journal of Sedimentary Research*, 74(6):933–937.

Geyer, W. R., Hill, P. S., and Kineke, G. C. (2004). The transport, transformation and dispersal of sediment by buoyant coastal flows. *Continental Shelf Research*, 24(7-8):927 – 949.

Gratiot, N. and Manning, A. J. (2004). An experimental investigation of floc characteristics in a diffusive turbulent flow. *Journal of Coastal Research*, 41:105–113.

Guo, C., He, Q., Prooijen, B., Guo, L., Manning, A., and Bass, S. (2018). Investigation of flocculation dynamics under changing hydrodynamic forcing on an intertidal mudflat. *Marine Geology*, 395:120–132.

Harris, C. K., Traykovski, P. A., and Geyer, W. R. (2005). Flood dispersal and deposition by near-bed gravitational sediment flows and oceanographic transport: A numerical modeling study of the Eel River shelf, northern California. *Journal of Geophysical Research*, 110(C09025).

Hill, P. S., Milligan, T. G., and Rockwell Geyer, W. (2000). Controls on effective settling velocity of suspended sediment in the Eel River flood plume. *Continental Shelf Research*, 20(16):2095–2111.

Huang, H. (1994). Fractal properties of flocs formed by fluid shear and differential settling. *Physics of Fluids*, 6(10):3229–3234.

Hwang, K. N. (1989). Erodibility of fine sediment in wave dominated environments. Master's thesis, University of Florida, Gainesville, FL USA.

Hwang, K.-N. and Mehta, A. J. (1989). Fine sediment erodibility in Lake Okeechobee, Florida. Report ufl/coel-89/019, Department of Coastal and Oeanographic Enginnering, University of Florida.

Keyvani, A. (2013). *Flocculation processes in river mouth fluvial to marine transitions*. PhD thesis, University of Houston, Houston, TX.

Keyvani, A. and Strom, K. (2013). A fully-automated image processing technique to improve measurement of suspended particles and flocs by removing out-of-focus objects. *Computers & Geosciences*, 52:189–198.

Keyvani, A. and Strom, K. (2014). Influence of cycles of high and low turbulent shear on the growth rate and equilibrium size of mud flocs. *Marine Geology*, 354(0):1 – 14.

Kranenburg, C. (1994). The fractal structure of cohesive sediment aggregates. *Estuarine, Coastal and Shelf Science*, 39(5):451 – 460.

Krone, R. B. (1962). Flume studies of the transport of sediment in estuarial shoaling processes. Technical report, Hydraulic Engineering Laboratory and Sanitary Engineering Research Laboratory, University of California, Berkely, CA.

Krone, R. B. (1963). A study of rheological properties of estuarine sediments. Committee on Tidal Hydraulics Final Report 63-88, Waterways Experiment Station, Corps of Engineers, US Army.

Krone, R. B. (1978). Aggregation of suspended particles in estuaries. In Kjerfve, B., editor, *Estuarine transport processes*, pages 177–190. University of South Carolina Press.

Kumar, R. G., Strom, K. B., and Keyvani, A. (2010). Floc properties and settling velocity of San Jacinto Estuary mud under variable shear and salinity conditions. *Continental Shelf Research*, 30(20):2067–2081.

Kuprenas, R., Tran, D., and Strom, K. (2017). A shear-limited flocculation model for dynamically predicting average floc size. *Journal of Geophysical Research: Oceans*, page Under review.

Law, B., Milligan, T., Hill, P., Newgard, J., Wheatcroft, R., and Wiberg, P. (2013). Flocculation on a muddy intertidal flat in willapa bay, washington, part i: A regional survey of the grain size of surficial sediments. *Continental Shelf Research*, 60, Supplement(0):S136 – S144.

Li, B., Eisma, D., Xie, Q., Kalf, J., Li, Y., and Xia, X. (1999). Concentration, clay mineral composition and Coulter counter size distribution of suspended sediment in the turbidity maximum of the Jiaojiang river estuary, Zhejiang, China. *Journal of Sea Research*, 42:105–116.

Lick, W. and Lick, J. (1988). Aggregation and disaggregation of fine-grained lake sediments. *Journal of Great Lakes Research*, 14(4):514 – 523.

Logan, B. E. (1999). *Environmental Transport Processes*. John Wiley & Sons.

MacDonald, D. G., Goodman, L., and Hetland, R. D. (2007). Turbulent dissipation in a near-field river plume: A comparison of control volume and microstructure observations with a numerical model. *Journal of Geophysical Research*, 112(C07026).

Maggi, F. (2015). Experimental evidence of how the fractal structure controls the hydrodynamic resistance on granular aggregates moving through water. *Journal of Hydrology*, 528:694–702.

Manning, A. J. and Dyer, K. R. (1999). A laboratory examination of floc characteristics with regard to turbulent shearing. *Marine Geology*, 160(1-2):147 – 170.

McAnally, W. H. and Mehta, A. J. (2000). Aggregation rate of fine sediment. *Journal of Hydraulic Engineering*, 126(12):883–892.

Mehta, A. J. and McAnally, W. H. (2008). *Sedimentation Engineering: Processes, Measurements, Modeling, and Practice*, chapter 4, pages 253–306. ASCE Manuals and Reports on Engineering Practice No. 110. American Society of Civil Engineering.

Mietta, F., Chassagne, C., and Winterwerp, J. (2009). Shear-induced flocculation of a suspension of kaolinite as function of pH and salt concentration. *Journal of Colloid and Interface Science*, 336(1):134–141.

Mikeš, D. and Manning, A. J. (2010). Assessment of flocculation kinetics of cohesive sediments from the Seine and Gironde estuaries, France, through laboratory and field studies. *Journal of Waterway, Port, Coastal, and Ocean Engineering*, 136(6):306–318.

Milligan, T. (1995). An examination of the settling behaviour of a flocculated suspension. *Netherlands Journal of Sea Research*, 33(2):163–171.

Milligan, T. and Hill, P. (1998). A laboratory assessment of the relative importance of turbulence,

particle composition, and concentration in limiting maximal floc size and settling behaviour. *Journal of Sea Research*, 39(3–4):227 – 241.

Milligan, T., Hill, P., and Law, B. (2007). Flocculation and the loss of sediment from the po river plume. *Continental Shelf Research*, 27(3-4):309 – 321.

Oles, V. (1992). Shear-induced aggregation and breakup of polystyrene latex-particles. *Journal of Colloid and Interface Science*, 154(2):351–358.

Partheniades, E. (2009). *Cohesive Sediments in Open Channels*. Butterworth-Heinemann/Elsevier, Burlington, MA.

Rubey, W. W. (1933). Settling velocity of gravel, sand, and silt particles. *American Journal of Science*, 25(148):325–338.

Safak, I., Allison, M., and Sheremet, A. (2013). Floc variability under changing turbulent stresses and sediment availability on a wave energetic muddy shelf. *Continental Shelf Research*, 53(0):1 – 10.

Sahin, C., Guner, Anil, A. H., Ozturk, M., and Sheremet, A. (2017). Floc size variability under strong turbulence: Observations and artificial neural network modeling. *Applied Ocean Research*, 68:130–141.

Shi, J. Z. (2010). Tidal resuspension and transport processes of fine sediment within the river plume in the partially-mixed changjiang river estuary, china: A personal perspective. *Geomorphology*, 121(3–4):133 – 151.

Shi, Z. and Zhou, H. J. (2004). Controls on effective settling velocities of mud flocs in the changjiang estuary, china. *Hydrological Processes*, 18:28772892.

Smith, J. and Friedrichs, C. (2015). Image processing methods for in situ estimation of cohesive sediment floc size, settling velocity, and density. *Limnology and Oceanography: Methods*, 13:250–264.

Smith, S. J. and Friedrichs, C. T. (2011). Size and settling velocities of cohesive flocs and suspended sediment aggregates in a trailing suction hopper dredge plume. *Continental Shelf Research*, 31(10, Supplement):S50 – S63.

Strom, K. and Keyvani, A. (2011). An explicit full-range settling velocity equation for mud flocs. *Journal of Sedimentary Research*, 81(12):921–934.

Strom, K. and Keyvani, A. (2016). Flocculation in a decaying shear field and its implications for mud removal in near-field river mouth discharges. *Journal of Geophysical Research: Oceans*, 121:2142–2162.

Tambo, N. and Watanabe, Y. (1979). Physical aspect of flocculation process–I: fundamental treatise. *Water Research*, 13(5):429 – 439.

Tang, F. H., Alonso-Marroquin, F., and Maggi, F. (2014). Stochastic collision and aggregation analysis of kaolinite in water through experiments and the spheropolygon theory. *Water Research*, 53:180 – 190.

Tang, F. H. and Maggi, F. (2016). A mesocosm experiment of suspended particulate matter dynamics in nutrient- and biomass-affected waters. *Water Research*, 89:76 – 86.

Teeter, A. M. (2001). Clay-silt sediment modeling using mulitple grain classes. part I: Settling and deposition. In McAnally, W. H. and Mehta, A. J., editors, *Coastal And Estuarine Fine Sediment Processes*, pages 157–171. Elsevier.

Tran, D. and Strom, K. (2017). Suspended clays and silts: Are they independent or dependent fractions when it comes to settling in a turbulent suspension? *Continental Shelf Research*, 138:81–94.

Tsai, C.-H., Iacobellis, S., and Lick, W. (1987). Flocculation of fine-grained lake sediments due to a uniform shear stress. *Journal of Great Lakes Research*, 13(2):135–146.

Van Der Lee, W. T. B. (1998). The impact of fluid shear and the suspended sediment concentration on the mud floc size variation in the Dollard estuary, The Netherlands. *Geological Society Special Publication*, 139:187–198.

van Leussen (1997). *Cohesive Sediments*, chapter The Kolmogorov microscale as a limiting value for the floc sizes of suspended fine-grained sediment in estuaries, pages 45–62. John Wiley Sons.

van Leussen, W. (1994). *Estuarine macroflocs and their role in fine-grained sediment transport*. PhD thesis, University of Utrecht, The Netherlands.

van Leussen, W. (1999). The variability of settling velocities of suspended fine-grained sediment in the Ems estuary. *Journal of Sea Research*, 41:109–118.

Verney, R., Lafite, R., Brun-Cottan, J. C., and Hir, P. L. (2011). Behaviour of a floc population during a tidal cycle: Laboratory experiments and numerical modelling. *Continental Shelf Research*, 31(10):S64–S83.

Wendling, V., Legout, C., Gratiot, N., Michallet, H., and Grangeon, T. (2016). Dynamics of soil aggregate size in turbulent flow: Respective effect of soil type and suspended concentration. *Catena*, 141:66–72.

Winterwerp, J. C. (1998). A simple model for turbulence induced flocculation of cohesive sediment. *Journal of Hydraulic Research*, 36(3):309–326.

Winterwerp, J. C. (2002). On the flocculation and settling velocity of estuarine mud. *Continental Shelf Research*, 22:1339–1360.

Winterwerp, J. C., Manning, A. J., Martens, C., de Mulder, T., and Vanlede, J. (2006). A heuristic formula for turbulence-induced flocculation of cohesive sediment. *Estuarine, Coastal and Shelf Science*, 68:195–207.

Winterwerp, J. C. and van Kesteren, W. G. M. (2004). *Introduction to the physics of cohesive sediment in the marine environment*, volume 56 of *Developments in Sedimentology*. Elsevier, Amsterdam, The Netherlands.

Wolanski, E., Asaeda, T., and Imberger, J. (1989). Mixing across a lutocline. *Limnology and Oceanography*, 34(5):931–938.

Xia, X. M., Li, Y., Yang, H., Wu, C. Y., Sing, T. H., and Pong, H. K. (2004). Observations on the size and settling velocity distributions of suspended sediment in the Pearl River Estuary, China. *Continental Shelf Research*, 24(16):1809–1826.

Xu, J., Sequeiros, O., and Noble, M. (2014). Sediment concentrations, flow conditions, and downstream evolution of two turbidity currents, Monterey Canyon, USA. *Deep-Sea Research I*, 89:11–34.

Zhang, J.-F. and Zhang, Q.-H. (2011). Lattice Boltzmann simulation of the flocculation process of cohesive sediment due to differential settling. *Continental Shelf Research*, 31:S94–S105.

# 3 Suspended clays and silts: Are they independent or dependent fractions when it comes to settling in a turbulent suspension?

## 3.1 Introduction

### 3.1.1 Overview

Many riverine, coastal, and marine environments produce conditions where suspended sediment contains a mixture of cohesive clay minerals and non cohesive silt in the size range of $0.1-63$ $\mu$m. Examples include, low land rivers such as the lower Mississippi (Galler and Allison, 2008), river mouth plume discharges (Walsh and Nittrouer, 2009), turbidity currents (Xu et al., 2014), and deep ocean currents (McCave and Hall, 2006). Understanding and predicting the vertical distribution of such sediment mixtures and the resulting zones and rates of deposition requires one to know the settling velocity of the particles, $w_s$. Without the presence of clay, the settling velocity of silt, and therefore the settling velocity of the mixture, can be defined using standard terminal settling velocity equations such as Stokes equation or that of Ferguson and Church (2004). However, the settling velocity of a pure clay suspension can be more difficult to define due to the aggregation and breakup process of flocculation. The flocculation process can produce flocs (or clay aggregates) that have sizes, densities, and shapes that are vastly different

Chapter 3 was published in Continental Shelf Research as Tran and Strom (2017)

from the original constitutive, or primary clay particles. Moreover, flocs can grow or shrink in size as the turbulent properties of the flow change (Milligan and Hill, 1998; Manning and Dyer, 1999; Kumar et al., 2010; Wang et al., 2013). This makes the settling velocity of suspended clay potentially dependent on, at least, clay mineral type, flow conditions, water chemistry, and suspended sediment concentration.

A common starting point for modeling mixtures of suspended clay and silt is to assume that the silt fraction is non cohesive, that the clay fraction is cohesive, and that the two fractions mix and settle independent of one another. That is, that the settling velocity of the silt can be defined by the terminal settling velocity of a solid particle, and that the settling velocity of the clay fraction can be defined using empirical floc-modified settling velocity equations (e.g. Hwang, 1989; van Leussen, 1994; Teeter, 2001; Soulsby et al., 2013) or through modeling of the average floc size (e.g. Winterwerp, 1998) or population (e.g. Hill and Nowell, 1995; Verney et al., 2011) coupled with a floc settling velocity equation (e.g. Strom and Keyvani, 2011). This framework allows one to treat the two mud fractions independently using our knowledge of sand transport for the silt and our flocculation models that have been developed for pure clay, and then to calculate the total mixture properties through a simple linear addition. For example, if concentration profiles are linearly additive, then the effective settling velocity of a size distribution is equal to the summation of each size fraction's settling velocity, $w_{s,i}$, multiplied by the fraction of the distribution contained within the size class, $p_i$; that is, $w_{s,avg} = \sum_{i=1}^{n} p_i w_{s,i}$. With sand or pure silt, this assumption is likely very reasonable because particles in suspension only interact through a slight transfer of momentum during collisions, and these particle collisions do not re-

sult in a change in the particle size or density. However, the reasonableness of this assumption for mixes of silt and clay is suspect due to the fragile nature of flocs and the potential for flocs to bind around silt particles. The broad goal of this paper is to explore whether or not clay and silt size fractions can be treated independently when it comes to settling velocity calculations.

### 3.1.2 Past Work

The general question of whether or not clay and silt or clay, silt, and sand settle independently or together in mass has been a topic of past interest. In some cases, the mixtures have simply been treated as independent fractions. That is, the suspension was considered as having either cohesive-like or non-cohesive-like behavior, and flocculation processes were included through empirical relationships between $w_s$ and the suspended concentration (Van Ledden, 2003; Merckelbach and Kranenburg, 2004; Hir et al., 2011; Carniello et al., 2012). Other laboratory studies have focused on bulk settling of high concentration mixtures of mud in settling columns, with the aim of identifying rates of interface descent and segregation or mixing of the clay and silt fractions in the resulting deposit texture (Amy et al., 2006; Cuthbertson et al., 2016). For instance, Amy et al. (2006) examined five settling regimes that resulted in five distinct sand-mud sedimentation textures in an effort to better understand processes that lead to sandstones with bimodal mud content. The study showed a strong dependence between the bed deposit characteristics and the concentration and ratio of cohesive to non-cohesive sediment in the suspension. Their experiments, however, were conducted in a stagnant column of water void of sustained turbulent shear. In cases where the water is stagnant and concentration of clay is high, flocs can grow to sizes that are much larger than they would be if turbulent

shear existed. Hence, in such experiments, the flocculation process will possibly exaggerate its impacts on the suspension and dictate the deposit behavior in comparison to the same type of experiment with dynamic turbulent shear stress environments, e.g., river plumes and turbidity current. Another example is that of Cuthbertson et al. (2016). Employing a non-invasive, electrical resistivity measurement and time-lapsed imaging Cuthbertson et al. (2016) showed that the bulk settling velocity and bed profile varied with the ratio of clay and sand in the mixture. As such, a sharp interface with sand-dominated deposit layer turned to a mixed clay-sand transition layer with the increase of clay fraction in the mixture. Furthermore, it required a longer time to form the transition layer under the clay-dominated condition. Yet, the authors did not address the mechanism of how sand and clay interact in either a field of turbulent shear or at the particle scale.

While these studies show that there are cases where clays and silts do and do not settle as a mixture, they do not, as a whole, discuss whether or not the presence of silt and clay together in turbulent suspensions can modify the individual floc settling velocity or the settling velocity of the individual silt grains. This is important in more dilute suspensions as might be found in estuaries, plumes, and turbidity currents. The only study we know of that has attempted to look at this was the study of Manning et al. (2013). In their work, Manning et al. (2013) compared the settling velocity of clay flocs with particles and flocs formed in a mixtures of sand, silt, and clay. They concluded that the presence of sand increased the settling speed of microflocs (flocs with diameters <160 $\mu$m), but that the presence of the sand decreased the settling velocity of larger, so-called macroflocs. The Manning et al. (2013) study suggests that the presence of sand may

alter the settling velocity of flocs. Yet the study does not discuss the fundamental mechanism by which sand modifies the settling speed of flocs of different sizes.

### 3.1.3 Important Properties that Could be Impacted by Size Fraction Interaction

The settling velocity of any particle, whether it be a solid or porous aggregate, is largely dictated by the particle or aggregate density and size. Consider the following general relation for the settling velocity of a solid particle or floc aggregate based on a balance between fluid drag and submerged weight Ferguson and Church (2004); Strom and Keyvani (2011):

$$w_s = \frac{g R_f d_f^2}{b_1 \nu + b_2 \sqrt{g R_f d_f^2}} \tag{3.1}$$

where $g$ is the acceleration of gravity, $R_f = (\rho_f - \rho)/\rho$ is the submerged specific gravity of the floc or particle, $\rho_f$ is the density of the particle or floc, $\rho$ is the density of the ambient water, $d_f$ is the equivalent diameter of the floc or particle, and $b_1$ and $b_2$ are coefficients that are dependent on particle shape and porosity. For a floc aggregate, $R_f$ is a function of floc size, $d_f$, raised to a negative power (Dyer and Manning, 1999; Markussen and Andersen, 2013). For convenience, one can relate $R_f$ to $d_f$ using a 3D fractal dimension, $n_f$:

$$R_f = R_s \left( \frac{d_f}{d_p} \right)^{n_f - 3} \tag{3.2}$$

where, $R_s$ is the submerged specific gravity of the sediment itself making up the particle or floc, $d_p$ is the size of the solid particles that any floc may be made of, i.e., the primary particles. Note that $n_f = 3$ yield $R_f = R_s$. Therefore, for a solid particle, $n_f = 3$. For flocs, $n_f < 3$; typically

falling between $n_f = 1.8$ and $n_f = 2.5$ (Khelifa and Hill, 2006; Strom and Keyvani, 2011).

Equation 3.1 highlights that the floc or particle size, $d_f$, and density, tied up in $R_f$, are the two primary parameters that set the value of $w_s$. For silt, it is unlikely that the presence of clay will impact the settling velocity of an isolated silt grain. However, it is possible that the presence of silt could potentially alter either the size or density of a clay floc relative to that of flocs formed in a suspension of pure clay. Figure 3.1 illustrates how increases in floc particle density or size leads to changes in the settling velocity. These increases are expressed in terms of percent change to better highlight the sensitivity of the parameters for flocs of different sizes. For the figure, the changes in floc density are achieved by increasing the floc fractal dimension, $n_f$ (Eq. 3.3). Of note in the figure is the sensitivity of $w_s$ to changes in density. For example, for a floc size of 95 $\mu$m, a 50% increase in $w_s$ (going from 0.36 mm/s to 0.54 mm/s) can be achieved through an increase in density of 4%. That is, by going from 1,108 kg/m$^3$ to 1,152 kg/m$^3$. This is equivalent to an increase of fractal dimension from $n_f = 2$ to 2.14. Holding the fractal dimension constant, a 50% increase in $w_s$ is achieved only after a near 50% change in the floc size.

This short analysis highlights the fact that small changes in density or size of a floc can lead to substantial changes in the settling velocity. Whether or not silt impacts a floc size or density is not known. However it is possible that the presence of silt in clay suspension could impact either. For example, silt particles could become lodged within clay flocs and increase their overall density and settling velocity. It is also possible that the presence of silt could suppress flocculation due to the added force of silt to clay floc collision or weaker bonds between

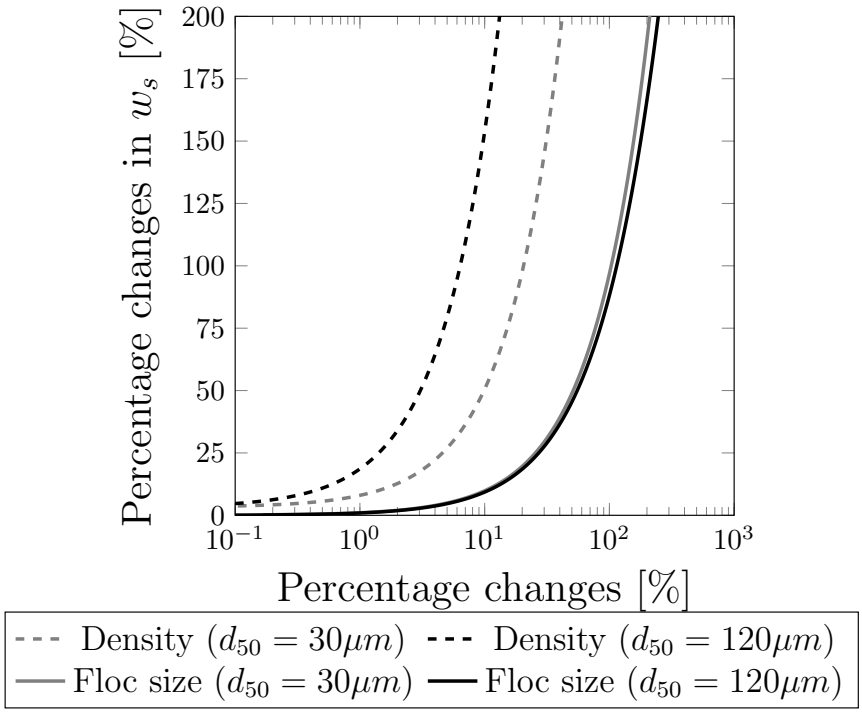


**Figure 3.1:** Settling velocity variation with increase of density and floc size.

silt and clay particles. The added force of collisions, or the weakening of bonds within the flocs, could both lead to a reduction in the flocs size and, hence, a reduction in the overall average settling velocity.

### 3.1.4 Study Objectives

In this paper, we examine the question of whether or not mixtures of clay and silt in suspension act independent of each other. More specifically, we examine the following three questions: (1) does the presence of silt in suspension alter the size of mud flocs relative to that from a pure clay suspension of equivalent concentration? (2) can silt particles become bound inside clay flocs?; and (3) if silt is bound within flocs, how does this change the settling properties of the clay and silt? Our three hypotheses are: (1) that the addition of silt will decrease the equilibrium

floc size; (2) that a fraction of the silt will be bound within the flocs; and (3) that the addition of silt particles within the floc will produce an increase in the overall floc density and settling velocity.

### 3.2 Material and Methods

Two series of laboratory experiments were conducted using different suspensions of clay, silt, and clay-silt mixtures to test our hypotheses. In the first set (Set A), the floc and silt size distributions were measured as a function of time within a turbulent suspension. The second series of experiments (Set B), measured the settling velocity of individual sediment particles or flocs in a stagnant column of water at the end of the Set A experiments. Floc cameras and image processing techniques were used in both cases to measure the floc and silt sizes as a function of time in the turbulent suspension (Set A), and the settling velocity in the stagnant settling column (Set B). Images from experimental Set A also allowed for data to be collected on the capture of silt particles within individual flocs. Table 3.1 summarizes the clay to silt ratios, concentrations, and turbulent shear rates used in each experiment. In Table 3.1 and throughout this paper, the notation clay:silt 1:1, 1:3 and C:S 1:1, C:S 1:3 refer to experimental conditions of which clay was mixed with silt in dry mass/mass ratio of 1:1 and 1:3 respectively. The terms “Pure silt 1:1,” and “Pure silt 1:3” refers to experiments that used only silt, but with the mass equivalent to that of the silt in clay:silt ratio 1:1 or 1:3 experiments.

### 3.2.1 Experimental Equipment

The sizing experiments were run on 13 liter suspensions in a mixing chamber with dimensions of 27.5 x 27.5 x 25 cm. Turbulent shear was generated using a variable speed paddle mixer. Two paddle rotation rates were used to examine the impact of turbulent shear on the stated hypotheses. These paddle speeds were chosen based on two criteria. First, the rate had to be high enough to keep the majority of the silt in suspension. Second, the paddle speed had to produce equilibrium floc sizes that were significantly larger than the silt particles. That way, the floc aggregates and silt particles could be distinguished in the image processing procedures. Based on the geometry of the paddle and mixing chamber, and the mixing tank turbulent shear relation of Logan (1999), the shear stress inside the mixing tank can be calculated as:

$$G = \left( \frac{52.3 b_{d,p} A_p s^3 R_p^3}{\nu_w V_T} \right)^{1/2} \tag{3.3}$$

Where $b_{d,p}$ is the drag coefficient, $A_p$ is the area of the paddle, $R_p$ is the radius of the paddle, $s$ is the paddle speed (rotation in second), $\nu$ is the fluid kinematic viscosity, and $V_T$ is the total volume of the fluid in the chamber. Our selected paddle rotation rates, 35 and 52 rotation per minute, produced tank-averaged turbulent shears in the range of $G$ = 50 $s^{-1}$ and $G$ = 95 $s^{-1}$, respectively.

Two Campbell Scientific OBS-3+ sensors were installed inside the mixing chamber to track the concentration of the suspension with time. Before being used in our experiments, each OBS was calibrated using the same sediment mixture and concentration as those used

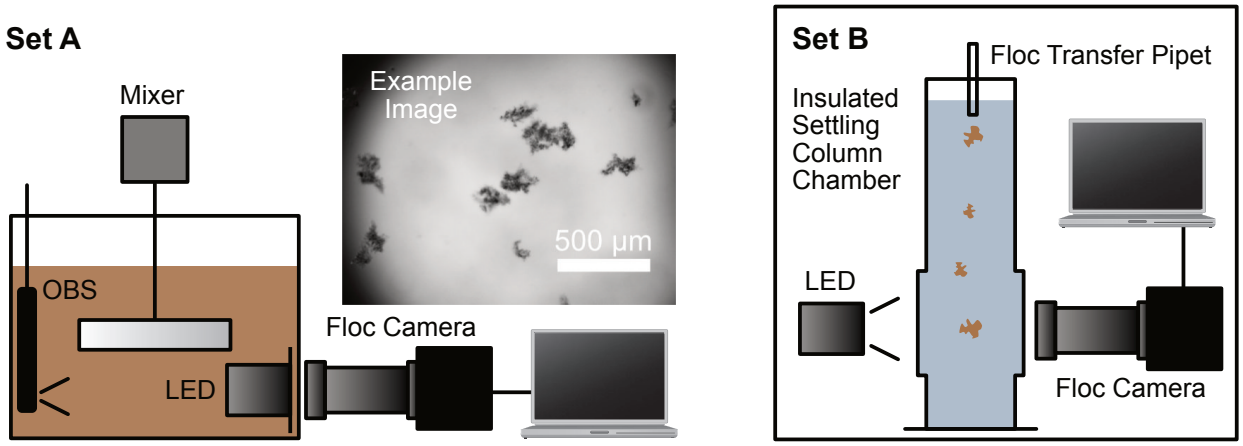


**Figure 3.2:** Experimental apparatus. Left diagram: Particle size experiment setup and a sample image. Right diagram: Settling velocity measurement experiment setup.

in the experiments; the calibration was done at a shear rate high enough to ensure that no sediment settled in the tank during data collection. During the calibration, the OBS data was recorded until the signal stabilized. For the pure clay condition, the relationship between the suspension concentration in [mg/L] and the OBS measurement of NTU is: $C = 0.9761(\text{NTU}) - 3.5794$ with the coefficient of determination, $R^2 = 0.99$. For the pure silt suspensions the relation is: $C = 11.717(\text{NTU}) - 22.735$ with $R^2 = 0.99$.

A floc camera system was used to collect still images of flocs and silt particles within the turbulent mixing chamber. The camera used in the system has a 2080 x 1552 pixel progressive scan, monochrome 8 mm CMOS sensor fitted with a 2X primary magnification objective lens that has a 34 mm working distance. The measured size of each pixel in the image with these optics is 1.3 $\mu$m/pixel, and the field of view is 2.4 × 1.4 mm; the depth of field is 0.1 mm. The camera and optics allow for quantification of particle sizes over the range of 10 to 1000 $\mu$m. To provide illumination, a LED was fitted inside waterproofed housing, sealed inside with a

round glass plate, and placed inside the tank. The glass plate served two functions. First, it allowed light to pass out of the waterproofed housing. Second, placing the LED in the tank such that the glass plate was parallel to the mixing tank wall produced a thin, ($\approx$ 1 mm) flow-through cell where flocs could be imaged. The flow-through cell both slowed the speed of the flocs and reduced the number of flocs between the light source and tank wall. The combined effect was that flocs could be imaged with a constant (as opposed to flashed) light source, and flocs could be imaged in concentrations up to 400 mg/L. Without the glass plate, the maximum concentration in which flocs could be imaged is $\approx$ 100 mg/L (Strom and Keyvani, 2016). We tested the impact of the 1 mm gap between the wall and the glass plate to ensure that a distance of 1 mm was not altering the size of the imaged flocs relative to those throughout the mixing tank. To cary out this test, we used two identical floc cameras and light sources. Both light sources were fitted with the glass plate and placed within the tank. One was placed at 1 mm from the wall, and the other was placed at 8 mm from the wall. We ran the experiments on floc growth with this camera setup under concentrations of $C$ = 25, 50, and 100 mg/L; note that the camera with the light source 8 mm away cannot capture any meaningful data at concentrations greater than 100 mg/L. The data from the three experiments showed no difference in size or rate of growth between the two cameras. We take the results of this experiment as a verification that the flow-through cell created by the glass plate on the light sources and the mixing tank wall did not filter out larger flocs, cause breakup, or increase floc size due to congestion in the cell.

The settling velocity measurements were made in a 1 m tall settling column using a floc camera identical to the one described above, but with a different location for the light source

(Fig. 3.2). The settling column and camera system were all placed within an insulated chamber. This chamber was constructed atop an optics table to create a constant temperature environment with no air motion or table vibration during the settling velocity measurement process. By trial and error, we found that the insulated box was absolutely necessary for obtaining repeatable and reasonable settling velocity measurements; the reasons for this will be discussed in more detail at section 3.4.2. The settling column consists of three main sections. The top and the bottom sections are made of circulate PVC pipe with a 4.5 cm internal diameter and 5 cm external diameter. The 40 cm long middle section is made of clear acrylic with internal cross-sectional dimensions of 3x3 cm and external dimensions of 6x6 cm. Images of the falling particles and flocs were captured near the bottom of the rectangular section. Suspension samples were transferred from the mixing tank to the settling column using a 6 mm inner diameter pipet.

### 3.2.2 Sediment Type and Water Conditions

The three suspensions tested in the experiments consisted of, (1) pure clay minerals, (2) pure silica silt, and (3) mixtures of clay and silt with 1:1 and 1:3 ratios of clay and silt by dry weight. The concentration of clay in all experiments was kept constant at 100 mg/L; the ratio of clay and silt was varied by increasing the amount of silt in the mixture. The clay fraction in all experiments consisted of a mixture of 80% kaolinite and 20% montmorillonite; a mixture that has been used in past studies to mimic estuarine mud Keyvani and Strom (2014). For the silt, we used crushed silica quartz with a density of 2650 kg/m$^3$ with grain sizes ranging from 5 to 63 $\mu$m was used. The background water for all test was a base of distilled water with enough salt

| | | | | Number of replicates | | | |
|---|---|---|---|---|---|---|---|
| Sediment Mixture | Shear $G$ [s$^{-1}$] | Clay added mg/L (g) | Silt added mg/L (g) | Sizing (Set A) NPS[1] | PS[2] | $w_s$ (Set B) NPS | PS |
| Pure Silt 1:1 | 50 | 0 (0) | 100 (1.3) | 3 | - | - | - |
| | 95 | 0 (0) | 100 (1.3) | 3 | - | - | - |
| Pure Silt 1:3 | 50 | 0 (0) | 300 (3.9) | 3 | - | - | - |
| | 95 | 0 (0) | 300 (3.9) | 3 | - | 1 | - |
| Pure Clay 1:3 | 50 | 100 (1.3) | 0 (0) | 3 | 3 | 1 | 1 |
| | 95 | 100 (1.3) | 0 (0) | 3 | 3 | 1 | 1 |
| Clay:Silt 1:1 | 50 | 100 (1.3) | 100 (1.3) | 3 | 3 | 1 | 1 |
| | 95 | 100 (1.3) | 100 (1.3) | 3 | 3 | 1 | 1 |
| Clay:Silt 1:3 | 50 | 100 (1.3) | 300 (3.9) | 3 | 3 | 1 | 1 |
| | 95 | 100 (1.3) | 300 (3.9) | 3 | 3 | 1 | 1 |

**Table 3.1:** Summary of experimental conditions highlighting the sediment mixture concentrations and total mass added for each mixture. Note that the value outside of the parentheses in the "Clay added" and "Silt added" columns represents the initial concentration of the clay or silt fractions. The value within the parentheses is the total added mass. [1]NPS stands for non prior shear; [2]PS stands for prior shear.

added to bring the salinity to 8 ppt. The distilled water and salt combination was used to minimize variability in ion and pH levels that may be present in tap water. Preliminary tests showed that, all else being equal, there was no change in the flocculation behavior or floc sizes between tests run with salinities of 5 ppt and 35 ppt. Therefore, the 8 ppt test can be considered to be representative of estuarine or marine conditions as far as flocculation with this particular mud mix is concerned.

### 3.2.3 Procedures

Each of the five sediment mixtures (pure silt 1:1, pure silt 1:3, pure clay, clay:silt 1:1, and clay:silt 1:3) were run through the sizing experiments (Set A) at shear rates of $G = 50$ s$^{-1}$ and $G = 95$ s$^{-1}$ (Table 3.1). Each suspension and shear rate experiment was replicated three times for a total of 30 sizing experiments.

For experimental Set A, the preparation of each mixture varied depending on whether or not clay was being used. For the pure silt runs, the desired mass was simply added to the clear water as it mixed in the mixing chamber. The suspension was mixed at the desired shear rate for 12 hours. Throughout this time, images of the suspension were taken at 0.5 Hz.

When using clay, 1.3 gr of the 80%/20% kaolinite and montmorillonite mixture were first well mixed in 150 mL of water in a beaker. This suspension was then sonicated for 15 minutes to break apart any large clay aggregates that were not broken down when initially mixing the clay with the 150 mL of clear water. This procedure produced an average initial size of the clay suspension of near 5 $\mu$m. In the pure clay experiments the suspension was then introduced directly to clearwater fluid mixing at a rate of $G = 50\ \mathrm{s}^{-1}$; for the clay:silt experiments, silt was also added to the mixing chamber at this time. The suspension was then left to mix for 12 hours to allow the flocs to reach and equilibrium size distribution. During this time, the suspension was imaged at 0.5 Hz. At the end of the 12 hours of mixing, the paddle rotation rate was significantly turned up ($G \approx 500\ \mathrm{s}^{-1}$) and left for 30 minutes. The purpose of this period of high shearing was to disaggregate the flocs and produce a turbulent-shear-generated initial condition for the suspension. Following the 30 minutes of high shear, the suspension was again returned to a mixing condition of $G = 50\ \mathrm{s}^{-1}$ for another 2.5 hours and imaged at 0.5 Hz (Fig. 3.3). This procedure was also followed for the $G = 95\ \mathrm{s}^{-1}$ runs.

The sequence of sediment preparation and mixing outlined above leads to two phases within each sizing experiment. Following previous work, we refer to these phases as the “non prior” and “prior” shear phases (Keyvani and Strom, 2014). The non prior shear (NPS) phase

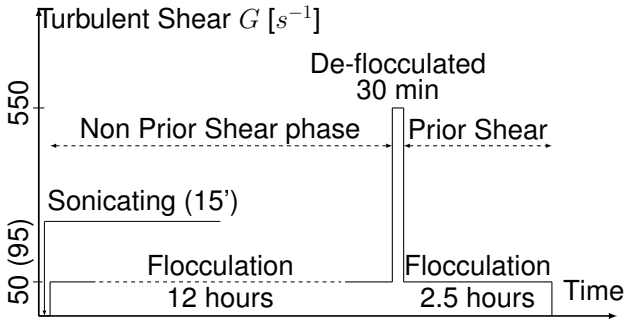


**Figure 3.3:** Experimental procedures (not to scale).

refers to the growth of flocs from the sonified suspension up to some equilibrium size during the first 12 hours of mixing (Fig. 3.3). The prior shear (PS) phase refers to the growth of flocs during the last 2.5 hrs of the experiment following the end of vigorous mixing. A key difference between the two phases is that the non prior shear phase starts with smaller clay particles ($d_p \approx 5$ $\mu$m) relative to the prior shear phase ($d_p \approx 10-15$ $\mu$m).

A few notes regarding the Set A experiments are in order. First, both shear rates ($G = 50$ and 95 $s^{-1}$) were able to keep the vast majority of the pure clay in suspension for the entire 12 hrs. However, neither of the two shear rates were able to keep all of the silt in suspension for the the entire 12 hours. Mixing at $G = 95$ $s^{-1}$ did keep more of the silt in suspension than the $G = 50$ $s^{-1}$ run, but there was still some settling of silt at this rate. The result is that the actual mass of silt in suspension at the time of equilibrium for the clay:silt 1:1 and clay:silt 1:3 tests was only around 0.6 and 1.8 times the mass of clay. Nonetheless, to maintain notational consistency, we still referred to the clay to silt ratios as 1:1 and 1:3. Secondly, because the silt did not aggregate, we did not run a "prior" shear phase for either of the pure silt experiments. This resulted in a total of 30 complete Set A experiments with 30 non prior shear time series and 18 prior shear time series (Table 3.1)

The settling velocity experiments (Set B) were conducted using pure silt and the flocs produced at the end of each phase in the Set A experiments containing clay. To make the measurements, very small samples were taken from the mixing tank and gently transferred to the top of the settling column. Care was taken to ensure that the density of the clear stagnant fluid in the settling column was the same as the density of the suspension in the mixing tank (this is discussed in greater detail in the discussion). Small background particles present in the clear fluid were used to ensure that circulation was absent from the column before the sediment was released from the pipet. Images were collected with the camera at a rate of 3 Hz. The settling velocity experiments were very labor and computationally intensive. Because of this, we collected settling velocity data from only one of the replicates in each of the six different experimental conditions containing clay for each of the two phases. This resulted in a total of 13 sets of settling velocity data, with each set containing many different 40 individual settling velocity measurements.

### 3.2.4 Image Processing

The methods used in these experiments produced a very large volume of images. For example, each experiment in the Set A runs generated 26,100 images ($\approx$ 50 GB). In total, over 3 TB of images were used to build the size distribution time series and settling velocity data reported in this paper.

Three types of information were extracted from the images to test the hypotheses. The first was simply whether or not silt particles were found bound within the flocs. This data came from the Set A experiments. Pure visual inspection was used to determine that silt particles

were indeed bound within the flocs. All further quantitative data on the number and size of silt particles within the flocs were then obtained through manual inspection of the images. The other two quantities used to test the study hypotheses were the time series of silt and floc size distributions, and the silt and floc settling velocities. Both of these quantities were extracted from the images using automated procedures. For Set A, the size distribution time series were extracted using the automated processing routines of Keyvani and Strom (2013). The routines remove out-of-focus flocs, or particles, and then combine the results from 30 images to yield size distributions of suspended particles every minute. Each 1-minute distribution contains several hundred to a few thousand particle measurements – depending on concentration and floc size. The floc identification and measurement routines used to obtain the size distributions in Set A were also used to identify and measure floc sizes in the settling velocity experiments. However, a second set of Matlab routines where then run on the output to identify the same particle in multiple images and extract the distance traveled by the particle in sequential images in units of pixels. Knowing the resolution of the camera and the time gap between images, set by the 3 Hz sample frequency, the settling velocity and size of the particle or floc was extracted and written to an output file.

## 3.3 Results

### 3.3.1 Observations from Visual Inspection of the Images

Visual inspection of the images from the Set A experiments yielded two prominent observations. First, in the runs with clay and silt, it was easy to see that most of the silt was bound up within the clay aggregates. Second, it seemed, at least qualitatively, that the size of the floc

aggregates was not dependent on the amount of silt present. Figure 3.4 shows images from all experiments at the lower shear rate of $G = 50\ s^{-1}$ at three different time windows (minute 4, 180, and 720). From the pure silt runs, it is visually evident that both the number and the size of silt grains reduces with time. This happens because the mixing condition was not vigorous enough to keep all the silt in suspension; leading to selective deposition of the largest silt grains. For the pure clay experiments (during the non-prior shear phase), flocs grow very rapidly at first (reaching a peak in size around minute 4) and then decay in size with time down to an equilibrium value. This decay in size is accompanied by an increase in the number of flocs with time since the total concentration of clay remains nearly constant. Images from the clay and silt mixture show that a trend similar to the one described for the pure clay occurs regardless of silt concentration. In fact, from visual inspection alone, one cannot say that there is really any difference in size between the flocs formed in pure clay or those formed in the clay/silt suspension at any given minute (comparison by row in Fig. 3.4). However, contrasting the images from the run with pure silt to the run with silt and clay at minutes 180 and 720, one can see that it is difficult to find any silt particles within the background suspension for the clay/silt runs. That is, the majority of the silt particles were bound within the flocs. Note that the lack of unbound silt was the norm in all images from these time periods. It seems then, at least from initial inspection, that the presence of silt had little impact on floc size, but that nearly all of the silt eventually became bound within the floc. Therefore, any impact of clay and silt interaction will likely come through modification of the floc density and not from modification of floc size. In what follows, we first quantify the amount and maximum size of silt bound within the flocs. We then present

the detailed size distribution data and then the settling velocity results from the experimental Set B.

### 3.3.2 The Capture of Silt within Flocs

Figure 3.5 illustrates the capture of silt within the clay-silt aggregates. The image was taken at minute 4 of the clay:silt 1:1, shear rate of $G = 50\ s^{-1}$ experiment. In Figure 3.5 there are three clay-silt aggregates with sizes of 338 $\mu$m (top left), 527 $\mu$m (top right) and 184 $\mu$m (bottom). A first observation is that the silt grains are distributed fairly evenly throughout the flocs. Some grains are lodged deep inside the floc whereas others nest at the edge. In this particular case, the largest silt grains captured (60 $\mu$m and 62 $\mu$m for the top left and bottom right) happened to be near the perimeter of the flocs. The capture of silt within the clay flocs was a ubiquitous outcome among all of the experiments run with both clay and silt. Under this observation, at least four further questions emerge: (1) on average, how many silt particles are captured in a floc of a given size? (2) does this value change as a function of the amount of silt added to the suspension? (3) what is the largest silt size that can be captured by a floc? And (4), does the bound silt modify the settling velocity of the flocs? Question 4 is addressed with experimental Set B. Questions 1, 2, and 3 are here investigated by manually counting the number of silt grains within flocs of different sizes, and noting the maximum silt size captured in a given floc.

400 individual flocs were chosen at random from the clay and silt suspensions of 1:1 and 1:3 at minutes 4 and 720 in the $G = 50\ s^{-1}$ experiments for the purpose of quantifying the number, and maximum size, of silt particles present within flocs. The flocs chosen for this analysis

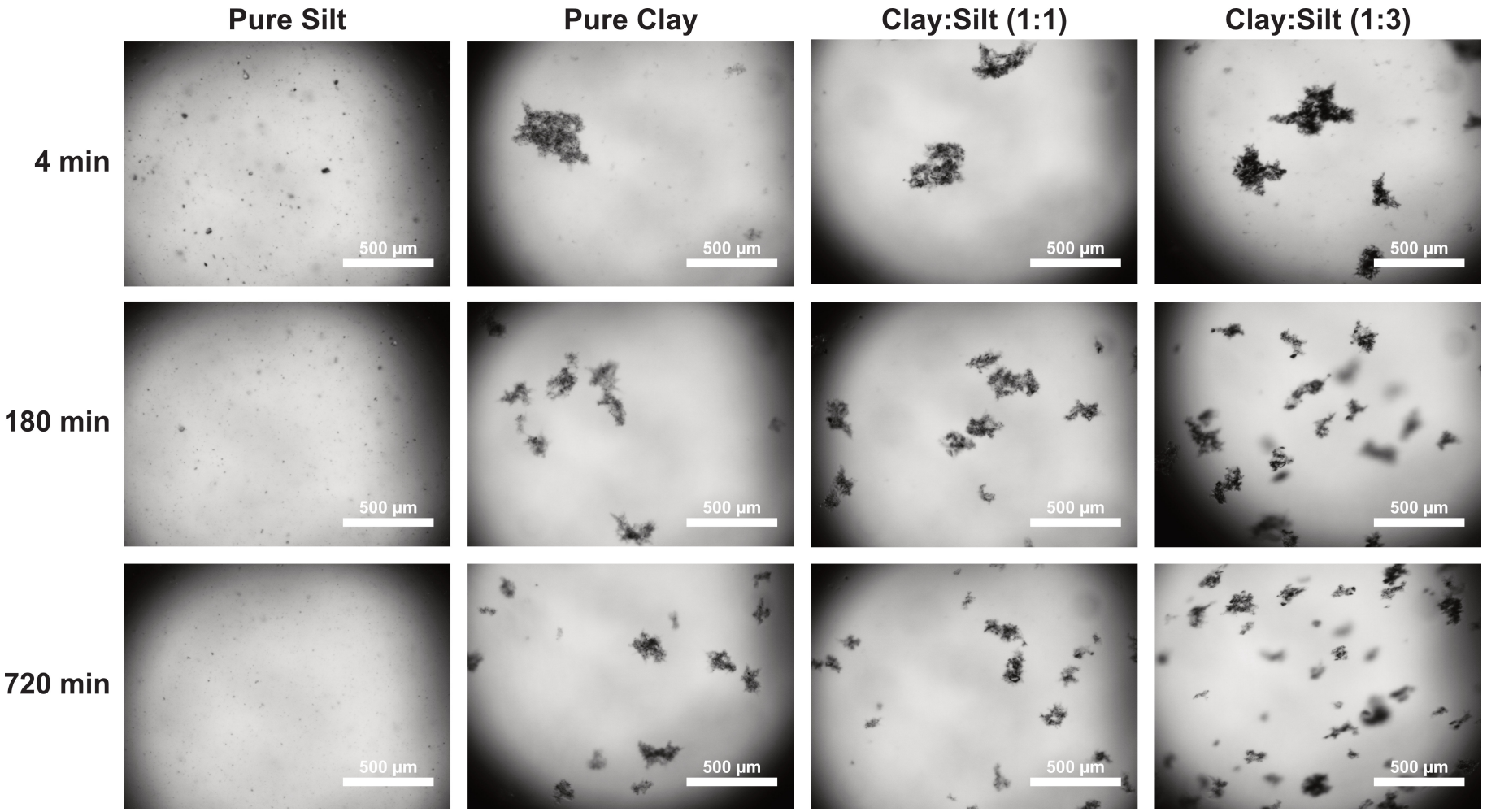


**Figure 3.4:** Sample images from the floc camera at minutes 4, 180 and 720 for each mixture at a shear rate of $G = 50\ s^{-1}$.

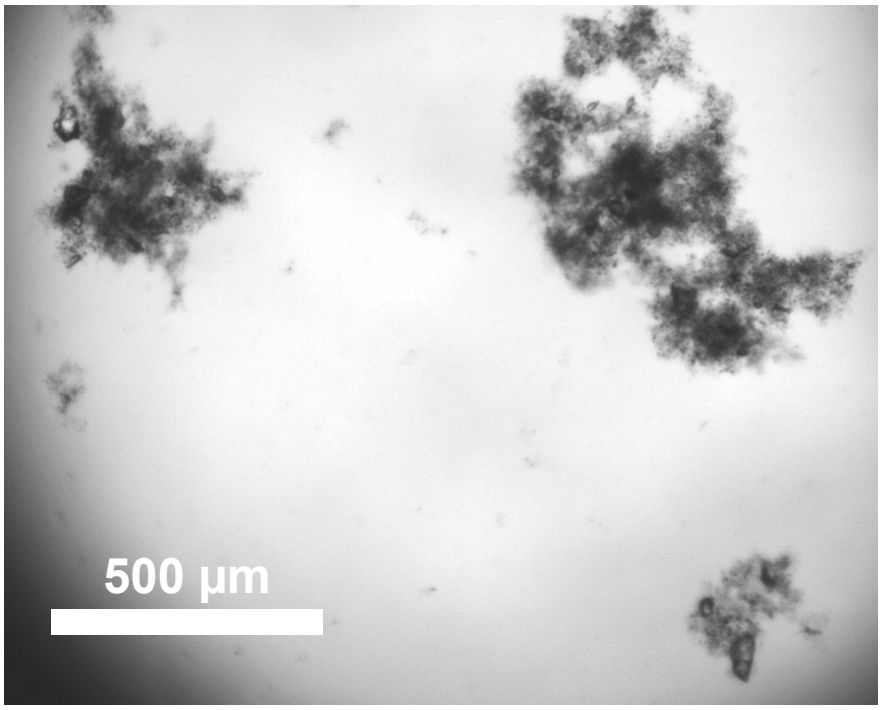


**Figure 3.5:** Sample image at minute 4, Non prior shear phase of experiment condition: clay:silt ratio 1:1, shear rate of $G = 50\ s^{-1}$. Particle size of 338 $\mu$m (top left), 527 $\mu$m (top right) and 184 $\mu$m (bottom).

ranged in size from 10 $\mu$m to 170 $\mu$m. Data on both the number and maximum size of silt within the flocs was sorted by floc size in 10 $\mu$m wide bins to allow for presentation of the number and max silt diameter as a function of floc size. Results from this showed that, on average, the number of silt particles present within a floc was a function of floc size, time, and the quantity of silt available in suspension. We also found no size limit on the diameter of silt that could be captured within a floc. The flocs were able to capture the largest silt particles in the suspension at any point in time. Figure 3.6 shows the data for the average number and maximum size of silt particles within flocs of different size ranges.

Figure 3.6 reveals that both the average number of silt particles, $N_s$, and the average maximum silt size, $d_{sm}$ that can become bound within a floc were directly proportional to the size

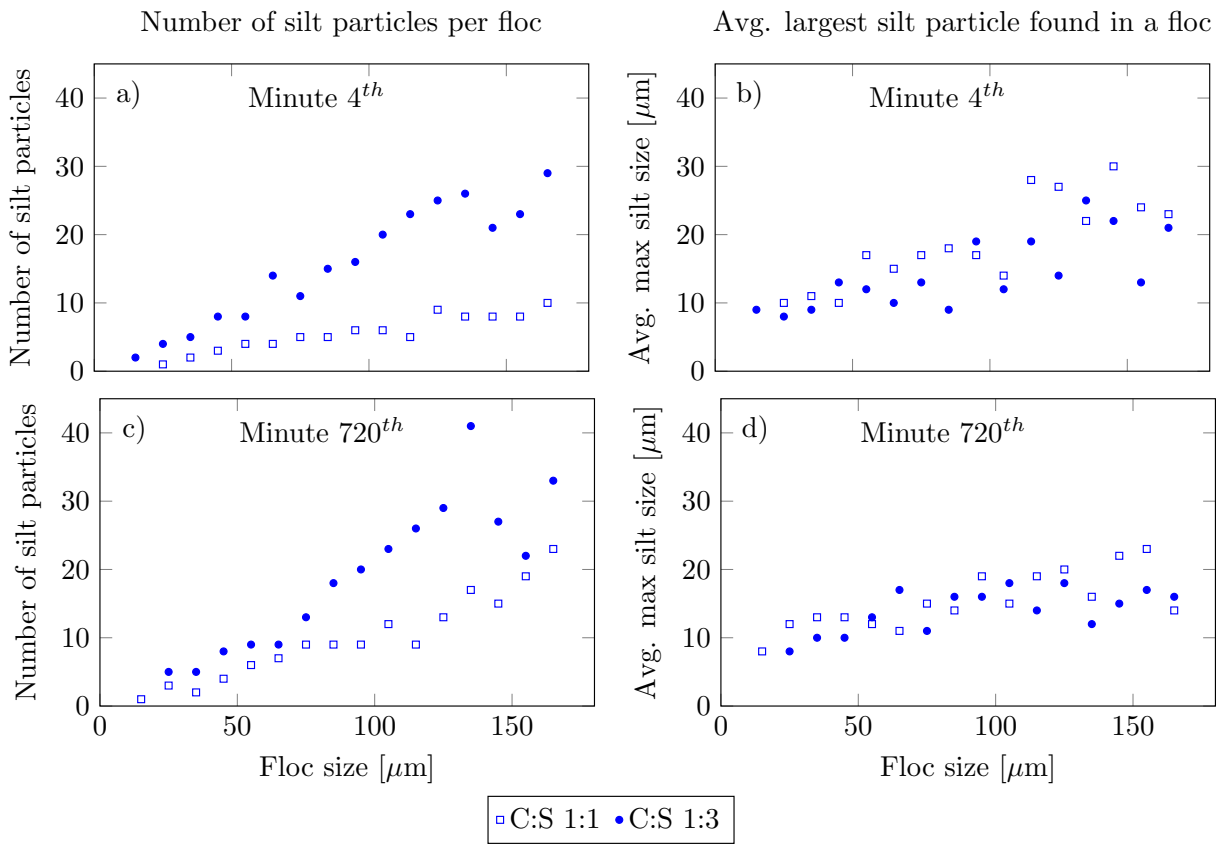


**Figure 3.6:** Manually counted and measured number of silt particles and silt grain size that gets bound within a floc. Each point in all plots is the average of at least 8 individual floc. Data used for this manual data processing from experiments under shear rate of $G = 50\ s^{-1}$.

of that floc. This observation holds for both the 1:1 and 1:3 clay to silt mixture ratios. While all of the $N_s$ data was linear with $d_f$, the slope of this functionality was greater for the clay to silt mixture ratio of 1:3 when compared to that of 1:1. This difference was particularly strong for minute 4 (Fig. 3.6a). It is likely that the larger slope in the $N_s$ vs $d_f$ functionality for the 1:3 data has to do with the larger number of silt particles being present in suspension for capture in the early phases of the experiment (minute 4) in the clay:silt 1:3 suspension relative to the 1:1 suspension. The difference in the $N_s = N_s(d_f)$ line between the 1:1 and 1:3 suspension decreased with time. In fact, there was little change in the slope of the line for the 1:3 case from minute 4

to minute 720 (Fig. 3.6a,c). The difference in behavior of $N_s$ with $d_f$ for the different clay to silt mixture ratios suggests that there might be some maximum volume of silt that can be captured by a floc of a given size and still remain in suspension. Contrary to the $N_s$ data, no difference was observed in the average maximum silt size captured, $d_{sm}$, between the two mixture ratios (Fig. 3.6b,d). Larger flocs had the ability to capture larger silt grains for both mixture ratios of clay and silt. The data shows, however, that $d_{sm}$ does tend to reduce with time for floc sizes over $d_f \approx 100$ $\mu$m.

### 3.3.3 Floc Sizes in the Presence of Suspended Silt

In this section we compare the data obtained from the pure clay, the clay:silt 1:1, and the clay:silt 1:3 runs to examine the impact of the presence and quantity of silt in suspension on flocs size under different shear rates ($G = 50$ and 95 $s^{-1}$) and different initial conditions (i.e., non prior or prior shear). The general behavior of all experiments were identical. In the NPS runs, flocs grow in size up to some peak value at around minute 4 and then decrease down to an equilibrium value. In the PS runs, the "peaking" behavior is absent. Instead, flocs quickly grow to their equilibrium size within the first few minutes of the test and then remain unchanged for the remainder of the experiment.

Each experimental condition was replicated three times to quantify the natural uncertainty of each run and better distinguish any true shift in the floc size distribution between treatments. Values of the average, maximum, and minimum differences in $d_{f50}$ of the replicate distributions are given in Table 3.2 to aid in quantifying the amount of inherent variability in experiments run with identical conditions. In general, the NPS runs showed a slightly higher

| | Shear rate G = 50 $s^{-1}$ | | | Shear rate G = 95 $s^{-1}$ | | |
|---|---|---|---|---|---|---|
| [1]NPS | Pure clay | C:S 1:1 | C:S 1:3 | Pure clay | C:S 1:1 | C:S 1:3 |
| $\Delta d_{f50,avg}$ ($\mu m$) | (23) 11 | (49) 6 | (32) 11 | (26) 5 | (19) 10 | (6) 4 |
| $\Delta d_{f50,max}$ ($\mu m$) | (34) 17 | (50) 9 | (48) 17 | (38) 7 | (29) 15 | (9) 7 |
| $\Delta d_{f50,min}$ ($\mu m$) | (7) 1 | (7) 2 | (4) 3 | (16) 1 | (6) 0 | (3) 1 |
| [2]PS | Pure clay | C:S 1:1 | C:S 1:3 | Pure clay | C:S 1:1 | C:S 1:3 |
| $\Delta d_{f50,avg}$ ($\mu m$) | (16) 9 | (12) 6 | (8) 6 | (13) 4 | (9) 14 | (4) 3 |
| $\Delta d_{f50,max}$ ($\mu m$) | (25) 13 | (17) 9 | (12) 9 | (16) 6 | (14) 21 | (6) 4 |
| $\Delta d_{f50,min}$ ($\mu m$) | (3) 6 | (8) 3 | (1) 2 | (8) 2 | (4) 0 | (2) 1 |

**Table 3.2:** The average, maximum, and minimum difference in the $d_{f50}$ of the distribution at the beginning and end of each replicate experiment. Numbers in the brackets are for the fourth minute of each experiment, and numbers outside of the brackets are for the last minute of each experiment. [1]NPS stands for non prior shear. [2]PS stands for prior shear.

degree of variability than the PS runs. $\Delta d_{f50}$ was also larger in the first few minutes of the experiments near the peaking time than it was at equilibrium. At equilibrium, the average $\Delta d_{f50}$ among both the NPS and PS runs was 7 $\mu$m; the maximum observed difference between replicates for any condition or initial condition was 21 $\mu$m (for the PS, clay:silt 1:1 run).

To reduce within treatment variability and make presentation of the data easier, we averaged the $d_{f50}$ time series for each of the three replicates to yield a single $d_{f50}$ time series for each sediment mixture, shear rate, and initial condition. Figure 3.7 shows the change in the average floc size, $d_{f50}$, as a function of time for the three different sediment mixtures containing clay, i.e., pure clay, clay:silt 1:1 and clay:silt 1:3, during the non prior and prior shear phase (top two panels in Fig. 3.7). Table 3.3 summarizes the size distribution statistics of the first ten minutes (in parentheses) and the last ten minutes for each condition. Data from all three replicates for each of the 10 min intervals were combined to produce the size distribution statistics given in the table.

As mentioned earlier, floc sizes peak early in the experiment in the non prior shear phase

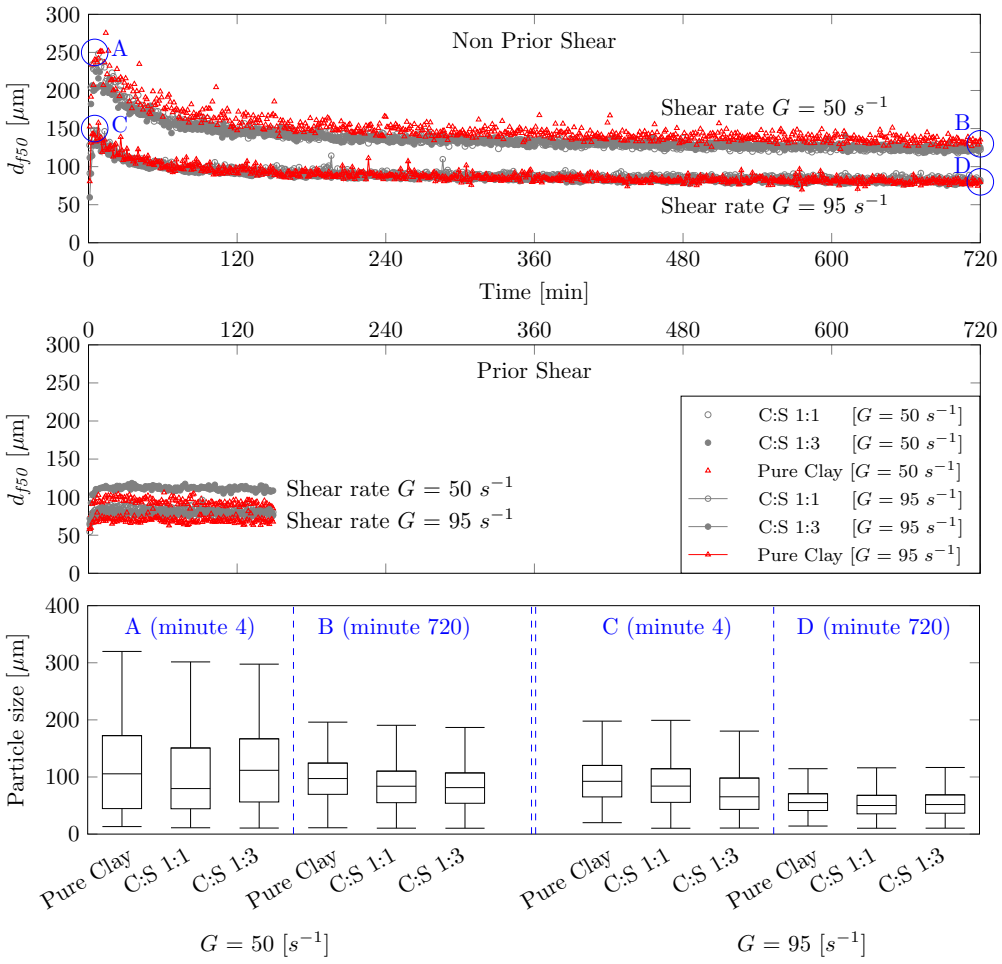


**Figure 3.7:** Measured $d_{f50}$ time series for the pure clay and clay:silt mixtures at two different shear rates. In all experiments, 100 mg/L of clay is used. Bottom row: Boxplots of particle size at minute 4 and 720.

and then decay down to some nearly constant equilibrium value. In all three sediment mixtures, the average peak size at minute 4 was between 200 and 250 $\mu$m at $G = 50$ s$^{-1}$ and between 125 and 150 $\mu$m when $G = 95$ s$^{-1}$. After 720 minutes of mixing, the $d_{f50}$ reduced down to 125 $\mu$m for $G = 50$ s$^{-1}$, and 80 $\mu$m for $G = 95$ s$^{-1}$. An immediate observation from the time series data is that $d_{f50}$ is more dependent on $G$, and whether or not it is a non prior shear or a prior shear experiment, than it is on the presence of silt in suspension. For example, in the non prior shear phase at $G = 95$ s$^{-1}$, there is no noticeable difference in $d_{f50} = d_{f50}(t)$ trend or values

| | Shear rate G = 50 $s^{-1}$ | | | | | Shear rate G = 95 $s^{-1}$ | | | | |
|---|---|---|---|---|---|---|---|---|---|---|
| [1]NPS | Pure clay | C:S 1:1 | C:S 1:3 | Pure silt 1:1 | Pure silt 1:3 | Pure clay | C:S 1:1 | C:S 1:3 | Pure silt 1:1 | Pure silt 1:3 |
| $d_5$ ($\mu m$) | (102) 80 | (103) 72 | (93) 69 | (8) 5 | (8) 4 | (70) 44 | (67) 42 | (56) 44 | (9) 6 | (10) 7 |
| $d_{16}$ ($\mu m$) | (154) 100 | (148) 92 | (135) 89 | (13) 7 | (14) 7 | (94) 56 | (92) 56 | (80) 57 | (16) 10 | (17) 10 |
| $d_{50}$ ($\mu m$) | (226) 132 | (222) 124 | (203) 123 | (26) 13 | (28) 13 | (134) 79 | (136) 81 | (121) 83 | (31) 19 | (33) 22 |
| $d_{84}$ ($\mu m$) | (303) 169 | (301) 158 | (273) 162 | (45) 21 | (45) 23 | (185) 107 | (187) 112 | (169) 114 | (50) 34 | (53) 41 |
| $d_{95}$ ($\mu m$) | (198) 352 | (360) 185 | (321) 192 | (58) 28 | (57) 32 | (217) 130 | (229) 132 | (202) 141 | (63) 44 | (63) 54 |
| [2]PS | Pure clay | C:S 1:1 | C:S 1:3 | Pure silt 1:1 | Pure silt 1:3 | Pure clay | C:S 1:1 | C:S 1:3 | Pure silt 1:1 | Pure silt 1:3 |
| $d_5$ ($\mu m$) | (44) 49 | (38) 45 | (49) 59 | - | - | (35) 37 | (34) 35 | (36) 41 | - | - |
| $d_{16}$ ($\mu m$) | (60) 62 | (53) 56 | (69) 76 | - | - | (47) 48 | (47) 47 | (50) 54 | - | - |
| $d_{50}$ ($\mu m$) | (91) 88 | (81) 80 | (106) 110 | - | - | (68) 69 | (71) 72 | (77) 80 | - | - |
| $d_{84}$ ($\mu m$) | (131) 122 | (115) 112 | (150) 153 | - | - | (93) 95 | (100) 101 | (109) 111 | - | - |
| $d_{95}$ ($\mu m$) | (158) 147 | (143) 135 | (184) 180 | - | - | (114) 115 | (120) 123 | (134) 135 | - | - |

**Table 3.3:** Grain size statistics for all experimental conditions at two different times in each experiment. The numbers in the brackets are for first ten minute of the experiment, and numbers outside of brackets are for last ten minute. Each number represents that average from the three replicates of each experimental condition. [1]NPS stands for non prior shear. [2]PS stands for prior shear.

between the pure clay, clay:silt 1:1, or clay:silt 1:3 data. This is nearly true for the $G = 50$ s$^{-1}$ data as well where $d_{f50}$ of the pure clay suspension is slightly larger than that for either of the two clay:silt mixtures. However, the difference between the mixtures is small relative to the difference created by changing the shear rate.

The reason for the slightly larger floc sizes in the pure clay runs at $G = 50$ s$^{-1}$ could be a result of a change in floc density due to the incorporation of silt particles within the floc; and not necessarily due to the silt particles modifying the size of the flocs under a condition of no settling. If we consider that a particular mixing condition can only keep flocs below a particular threshold settling velocity in suspension, then increases in floc density (through the addition of bound silt) would result in flocs reaching that threshold settling velocity at smaller sizes. Hence, the size of the flocs in suspension may go down as silt becomes bound within flocs. The OBS data from the experiments leads us to conclude that this explanation makes the most sense for our floc size and concentration time series data for the non prior shear case at $G = 50$ s$^{-1}$.

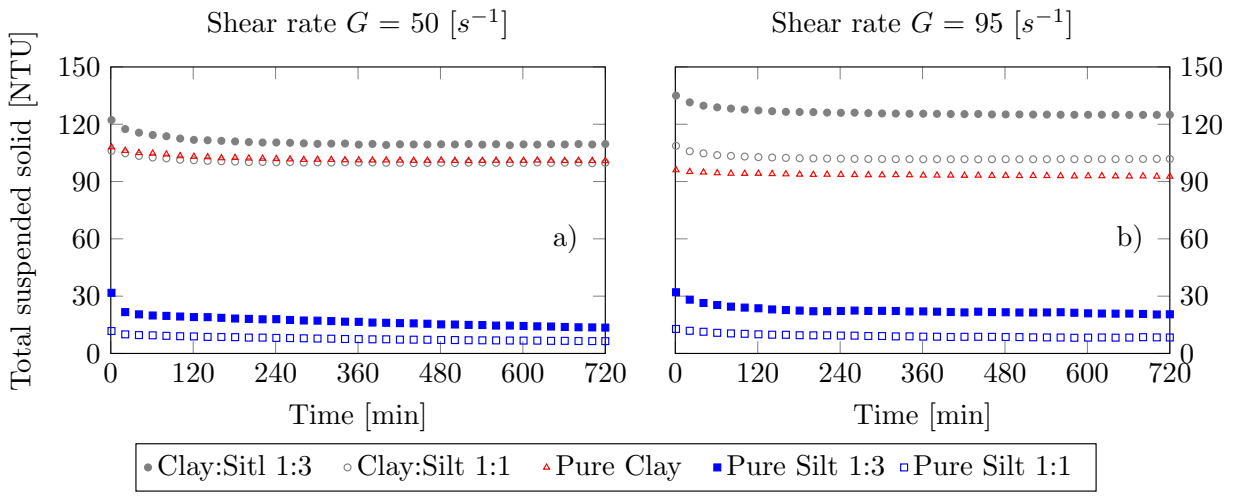


**Figure 3.8:** Measured concentration time series of Non prior shear phase for all experiment conditions.

OBS data for the various experiments performed at $G = 50$ and 95 $s^{-1}$ are presented in Figure 3.8. At $G = 50$ $s^{-1}$, notice that the clay:silt 1:1 concentration is equivalent to, or a little less than, the pure clay experiments (Fig. 3.8a). Under conditions of no settling, one would expect the concentration of the clay:silt 1:1 experiment to be roughly equivalent to the addition of the pure clay and the pure silt 1:1 concentration time series; as they are for the $G = 95$ $s^{-1}$run (Fig. 3.8b). The fact that concentration for the clay:silt mixtures at $G = 50$ $s^{-1}$ do not exhibit as large of a shift upward as one would expect seems to indicate that more of the clay is settling in the clay and silt mixture cases than is settling in the pure clay case. If this is true, then it is likely that it is the largest flocs that are settling out with the aid of bound silt grains, leading to an overall slight reduction in the floc size relative to the pure clay case. This phenomena was not observed for the higher shear condition.

Looking at the prior shear phase data, one can conclude that the runs with clay and silt produce flocs sizes that are, on average, slightly larger than those produced in the pure clay sus-

pension. The difference between the equilibrium $d_{f50}$ sizes in the clay:silt and clay ranged from $-8$ to $+12$ $\mu$m for the NPS data and from $+3$ to $+11$ $\mu$m for the PS data. The magnitude of these differences are not that great, and they certainly fall within the range of variability experienced within the replicates themselves. However, since the differences exist in the averages, it would appear that the image processing routines are yielding slightly larger sizes for the clay-silt flocs. Differences on this order cannot be seen by eye in the images, and it is difficult to say whether they should be taken as true differences or simply experimental variability.

### 3.3.4 Silt Particle Impact on Floc Settling Velocity

The settling velocity measurements were collected using pure silt and the flocs produced from each of the different conditions in the Set A experiments (Table 3.1). Because the pure silt grains are solid and should roughly follow Stokes settling, we used the measured silt settling velocity as a test of the settling column and image processing procedures. Results from the silt measurements showed that the data was parallel to the line set by Stokes relation. However, the measured $w_s$ was less than that predicted by Stokes by a factor of $\approx 2$. To account for this unknown bias in our procedures, we multiplied all of the settling velocity measurements (both silt and floc data) by a factor of 2.

Measured settling velocity from the 13 Set B experiments are plotted in Figures 3.9, and 3.10. Figure 3.9 shows settling velocity as a function of floc size, and Figure 3.10 plots the values from different sediment mixtures and mixing conditions against each other as one to one plots. Each point represents an average of about four individual floc settling velocity measurements (in some cases more, and in others less).

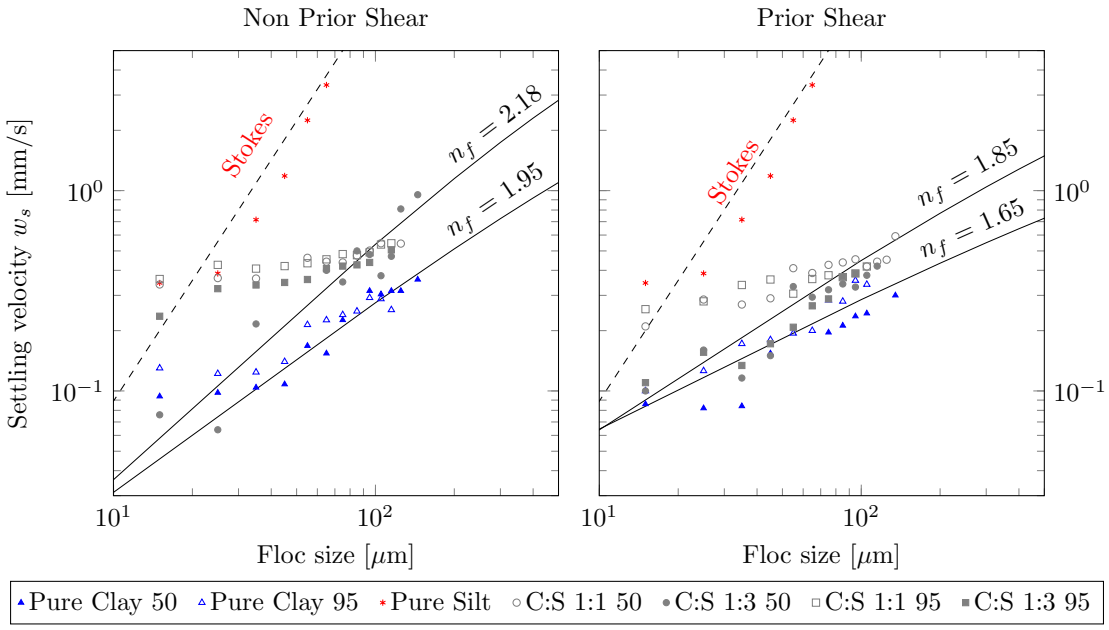


**Figure 3.9:** Measured functionality of $w_s = w_s(d_f)$ for flocs formed under different turbulent shear rates and with different sediment mixtures. Each point is the average of several measurements.

The measured $w_s$ values for the flocs fell well within the rather large range of values that have been reported elsewhere in laboratory experiments (Gibbs, 1985; Lick et al., 1992; Huang, 1994; Gratiot et al., 2005; Kumar et al., 2010) and field work (Dyer et al., 1996; Van der Lee, 2000; Fox et al., 2004; Manning and Bass, 2006). As expected, measured $w_s$ increased with flocs size at a rate less than that of the solid silt particles (Fig. 3.9). The data also clearly shows that the settling velocity of flocs formed in the presence of suspended silt is higher than that of flocs formed in pure clay suspensions (Figs. 3.9 and 3.10a,b). This indicates that the silt particles bound within the flocs do indeed increase the overall floc density.

The settling velocity data can be further subdivided into two zones based on size. Zone 1 consists of flocs with $d_f < 45$ $\mu$m; that is, the size range where there is significant overlap between the floc aggregates and the individual silt particles. Manual processing of the images

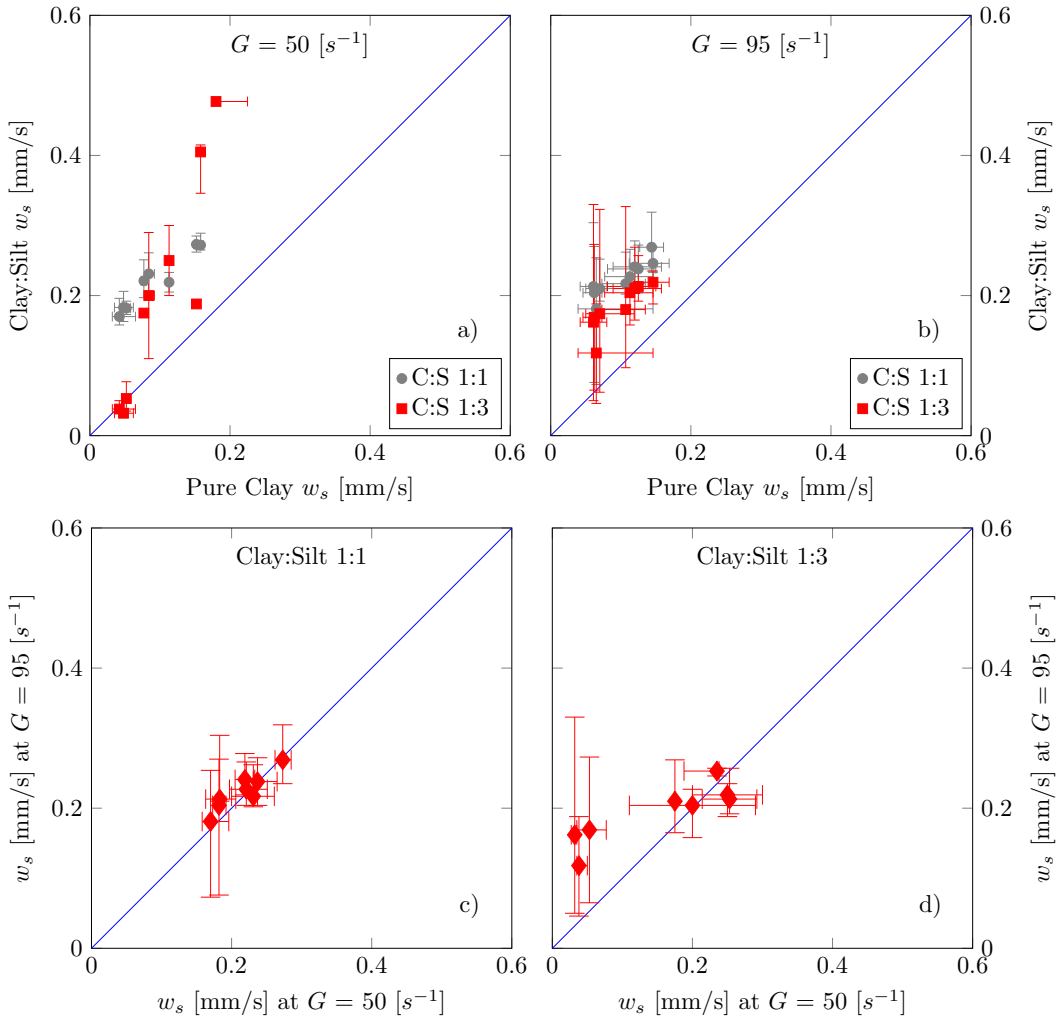


**Figure 3.10:** Top row: 1 to 1 comparison of pure clay floc settling velocity to those formed in mixtures of clay and silt. Bottom row: 1 to 1 comparison of floc $w_s$ for different shear rates.

revealed that within this size range, a floc can capture 1 to 3 small silt particles. When this happens, the addition of the 1 to 3 silt particles can result in drastic changes to the overall floc density and $w_s$. Manual calculation of the settling velocity of 10 clay:silt aggregates in the size range of 20 to 35 $\mu$m yielded $w_s$ values from 0.05 to 0.1 mm/s. Comparing these values to $w_s$ measures of pure clay flocs in an equivalent size range showed that the clay-silt flocs $w_s$ values could be up to 250% greater than the pure clay flocs. The combination of the large influence

that a few bound silt grains can have on a floc in this size range, coupled with the inability of the image processing routines to distinguish between pure clay flocs, clay-silt flocs, and pure silt particles at this scale, resulted in significant variability in settling velocity in Zone 1.

For Zone 2, $d_f > 45$ $\mu$m, the processing algorithms are able to exclude isolated silt particles from the reported settling velocity measurements based on the differences in shape between silt grains and flocs. Because of this, and the natural smaller effect of the added silt particles on density at larger sizes, variability in measured $w_s$ tended to decrease with floc size. Within this size range, clay-silt flocs settle considerably faster than pure clay flocs of the equivalent size. For example clay-silt flocs in this size range were, on average, 91% faster than the pure clay flocs in the non prior shear phase and 52% faster in the prior shear phase. This increased settling speed due to the addition of silt is also reflected in the change in the calculated fractal dimension of the suspensions. Using eq. 3.1 and 3.3 with a primary particle size of $d_p = 5$ for the non prior shear phase and $d_p = 10$ $\mu$m for the prior shear phase, and treating $n_f$ as a regression parameter yields $n_f = 1.95$ for the pure clay flocs and $n_f = 2.18$ for the clay and silt aggregates. The values for the prior shear phase are both smaller than those for the non prior shear phase, but the trend is the same in that $n_f$ goes up with the addition of silt by $\approx 0.2$.

An interesting observation from the $w_s = w_s(d_f)$ data is that the addition of silt at the smaller sizes results in a flattening of the response of $w_s$ with $d_f$. That is, not only does the addition of silt increase the overall settling velocity of a mud floc of size $d_f$, it also tends to make $w_s$ less dependent on size. This is particularly true of the experiments run at $G = 50$ s$^{-1}$. In fact, the settling velocity of all clay-silt floc sizes for $G = 50$ s$^{-1}$ is reasonably approximated at

$w_s \approx 0.35$ mm/s.

Figure 3.10 illuminates the variation of settling velocity of different mixtures and shear rates in the NPS experiments. The top row shows 1 to 1 comparison of pure clay floc settling velocity to those formed in mixtures of clay and silt, and the bottom row illustrates the clay:silt flocs $w_s$ for different shear rates. In Figure 3.10, the vertical bars show the minimum and maximum of the parameters of the y axis. Likewise, the horizontal bars show the minimum and maximum of the parameters of the x axis. Figure 3.10a and 3.10b again highlight that $w_s$ of the clay:silt flocs is higher than that of the pure clay aggregates. Figure 3.10b also suggests that flocs formed with the clay:silt 1:1 ratio have a slightly higher average settling velocity than those formed with the 1:3 mixture under conditions of $G = 95$ s$^{-1}$. This result is unexpected since flocs formed in the 1:3 mixture had, on average, more grains of silt per floc for a given size (Fig. 3.6a,c). There are at least two potential explanations for this shift. The first explanation is that the shift falls within the inherent variability of the experiments. Note that the max and min variability bars on the 1:3 data in Fig. 3.10b encompass the clay:silt 1:1 data. Additionally, the trend of higher settling velocities for flocs formed in the 1:1 mixture over those formed in the 1:3 mixture was not observed at lower shear rates (Fig. 3.10a). A second explanation might be that the added silt grains in the 1:3 flocs resulted in more fragile flocs broken and released silt particles in the transfer of flocs from the mixing tank to the settling column. We think that the first explanation is the more likely. Figure 3.10c and 3.10d show that the shear conditions under which the flocs were formed did not significantly influence the density, and hence settling velocity, of the flocs.

## 3.4 Discussion

### 3.4.1 Potential Changes to the Depositional Flux

The turbulent shearing conditions used in this study were picked to ensure that silt remained in suspension and that flocs could grow to sizes on the order of 100 $\mu$m. Within the conditions we tested, nearly all of the silt in suspension at a given mixing rate was found to bind with the clay in the formation of flocs; thereby increasing the floc density. Fitting a settling velocity equation to the measured settling velocity and size data showed that the increase in density had a larger effect on the smaller flocs (Fig. 3.9). As floc size increased, the changes in settling velocity brought on by the change in density were tempered. Even so, for the largest flocs, a change in the settling speed was evident. This increase in settling speed with the addition of silt for the larger particles could be described by a shift in the fractal dimension of $\Delta n_f \approx +0.2$. In this section we compare how big of an impact a $\Delta n_f = +0.2$ would make on the total average settling velocity of a suspended mixture. That is, we look at how big of a difference it makes if we consider the silt and clay to be dependent fractions instead of independent fractions. To do this, we compute the average settling velocity of the mixture,

$$w_s = \sum_{i=1}^{n} p_i w_{s,i} \tag{3.4}$$

for the pure silt, the pure clay, and the clay and silt mixture using particle and floc size distribution data from $G = 50$ and 95 $s^{-1}$ cases for each of the clay:silt ratios. In eq. 3.4, $p_i$ is the fraction of material associated with a grain or floc size of $d_i$ and $w_{s,i}$ is the settling velocity of that size.

| Condition | Avg. Settling Velocity, $w_{s,avg}$ [mm/s] | | | | |
|---|---|---|---|---|---|
| | Silt Particles | Clay Flocs | Clay:Slit Flocs | $w_{s,I}$ | $w_{s,D}$ |
| NPS ($G = 50$ s$^{-1}$, C:S 1:1) | 0.21 | 0.30 | 0.64 | 0.26 | 0.64 |
| NPS ($G = 50$ s$^{-1}$, C:S 1:3) | 0.21 | 0.30 | 0.64 | 0.24 | 0.64 |
| NPS ($G = 95$ s$^{-1}$, C:S 1:1) | 0.54 | 0.21 | 0.40 | 0.37 | 0.40 |
| NPS ($G = 95$ s$^{-1}$, C:S 1:3) | 0.54 | 0.21 | 0.41 | 0.43 | 0.41 |

**Table 3.4:** Average settling velocities for the different particle and flocs types along with the total mixture settling velocity taking the clay and silt as independent, $w_{s,I}$, and dependent, $w_{s,D}$, fractions.

In all calculations, we used data from the end of the NPS runs with a total of six size classes ($n = 6$). Size statistics for each of the mixtures at this time are given in Table 3.3. For the pure silt measurement, $w_{s,i}$ was calculated using Stokes equation for natural grains, which can be obtained from eq. 3.1 with $n_f = 3$, $b_1 = 20$, and $b_2 = 0.91$ (Ferguson and Church, 2004). For the pure clay settling velocity, we used the floc size distribution from the clay:silt 1:1 and 1:3 runs, with $n_f = 1.95$ and $d_p = 5$ $\mu$m. For the clay and silt mixture, $w_{s,i}$ calculations were made using the same size and $d_p$ conditions but with a $n_f = 2.15$ in each run. In all floc calculations, the shape coefficients $b_1$ and $b_2$ (eq. 3.1) were set to 18 and 0.548 respectively (Strom and Keyvani, 2011). Table 3.4 summarizes the results from the analysis.

The analysis shows that for the lower shear runs ($G = 50$ s$^{-1}$), the average settling velocity of the clay-silt flocs, $(w_{s,avg})_{clay:silt}$, is higher than that of both the silt left in suspension and the pure clay flocs. Whereas, at the higher shear condition ($G = 95$ s$^{-1}$), the overall average settling velocity of the clay-silt flocs falls between $w_{s,avg}$ of the pure silt and pure clay. The reason for this is that in moving from $G = 50$ to 95 s$^{-1}$, the flocs become smaller while the silt left in suspension becomes larger. The result indicate, as expected, that the settling velocity, and hence settling flux, of the clay is certainly enhanced (by a factor of about 2) when silt is captured within

flocs. However, another interesting implication of the calculation is that it seems possible for the binding of silt particles within the clay floc to actually slow the settling velocity of the silt fraction.

If the majority of the silt in suspension is captured by the flocs, then the settling velocity of the clay and silt mixture will be identical to the settling speed of the clay-silt flocs. We can think of this as the dependent settling velocity of the mixture, $w_{s,D}$:

$$w_{s,D} = (w_{s,avg})_{clay:silt} \tag{3.5}$$

An independent, mixture settling velocity of a suspension of clay and silt particles can be calculated using:

$$w_{s,I} = f_s(w_{s,avg})_{silt} + f_c(w_{s,avg})_{clay} \tag{3.6}$$

where $f_s$ is the fraction of silt in the mixture and $f_c$ is the fraction of clay. A useful comparison between the dependent (eq. 3.5) and independent settling velocity (eq. 3.6) can be made using $(w_{s,avg})_{silt}$ and $(w_{s,avg})_{clay}$ calculated from the pure clay and pure silt data (Table 3.4). Calculated $w_{s,I}$ values for $f_c = 0.5$ and 0.333 with $f_s = 1 - f_c$ are given in Table 3.4. The comparison shows that $w_{s,D} \approx w_{s,I}$ for $G = 95$ s$^{-1}$, and that $w_{s,D} \approx 2w_{s,I}$ for $G = 50$ s$^{-1}$. The implication from this is that clay and silt fractions can potentially be treated as independent fractions when mixing conditions are high, but that the dependence or binding of the two fractions could be important for moderate shear conditions that are not able to keep the largest silt fractions in suspension.

It seems then that whether or not the two basic size fractions, clay and silt, can be treated as independent fractions depends, at least to some extent, upon the shear rate. For very high shear rates $G > 100$ s$^{-1}$, flocs will approach the size of the silt grains that can be maintained in suspension. When this happens it is likely that flocs will not be able to capture many silt particles; recall that the number of captured silt particles was a function of floc size (Fig. 3.6). Furthermore, the presence of larger silt particles in suspension will likely dominate the settling flux of the material if $f_s \gtrsim f_c$. The combination of the smaller flocs and the significant contributions to the settling flux from the larger silt grains would tend to make the assumption that the clay and the silt are independent fractions more applicable. For low shear rate, $G < 20$ s$^{-1}$, silt cannot be maintained in suspension for very long and therefore will tend to disassociate with the flocs. In such cases, it is also likely that the assumption of clay and silt being independent fractions is reasonable. However, at moderate shear stresses, perhaps in the range of $G = 20$ to 70 s$^{-1}$, it is quite possible that silt in suspension may become bound within flocs, thereby altering the floc density and significantly modifying the average mixture settling velocity compared to that obtained from the assumption of independent fractions.

The exact bounds on this middle range where interaction between silt and clay maybe important has not been precisely defined in this study. Rather, the study simply suggests that such a range may exist. If it does exist, it is of interest to consider what type of flow environments produce this range. Based on simple calculations and field and laboratory observations from the literature, we have compiled a table listing approximate ranges of depth averaged $G$ that may exists in different flow environments (Table 3.5). It is worth mentioning that in Table

| Environment | $G$ [s$^{-1}$] | Notes |
|---|---|---|
| Steep rivers | 75-300 | [1]Based on $S = O(0.001)$; e.g., the Elwha |
| Mild rivers | 20-120 | [1]Based on $S = O(0.0001)$; e.g., the Mississippi |
| Estuaries and bays | 1 - 50 | e.g., Dyer et al. (2004) |
| River mouth plumes (field) | 1 - 50 | e.g., MacDonald et al. (2007) |
| River mouth plumes (lab) | 1 - 10 | e.g., Yuan and Horner-Devine (2013) |
| Turbidity currents (field) | 5 - 60 | e.g., Xu et al. (2014) |
| Turbidity current (lab) | 1 - 40 | e.g., Garcia and Parker (1993) |
| Deep ocean boundary currents | 1 - 5 | Estimated from velocities of 5 to 30 cm/s |

**Table 3.5:** Approximate ranges of depth-averaged turbulent shear rate, $G$, in various flow environments. [1]Values of $G$ of the steep and mild rivers were obtained by depth averaging the vertical profile of $G$ defined by: $G = [u_*^3((1-\zeta)/\zeta)/(\kappa\nu h)]^{1/2}$, where the friction velocity $u_*$ is approximated from $u_* = \sqrt{ghS}$; $h$ is flow depth, $\kappa$ is the von Karman constant, and $\zeta$ is the vertical coordinate scaled with depth. A range of reasonable depths and slopes about the order shown in the table were used to develop the estimates.

3.5, we assumed that a $G = 20$ s$^{-1}$in the field has the same impact on floc size and collision rate as $G = 20$ s$^{-1}$in the laboratory. This is because $C$ scales directly between the lab and field, and because $G$ is related to the size of the smallest eddies (or the dissipation rate); the association with the smallest scales of motion imply that information that is associated with the larger turbulent scales of a particular flow environment will theoretically gets lost in the cascade process. If this is the case, then all the flocs "feel," in a sense, is the total energy input, resulting in a particular shear and smallest eddy size (which limits the size of the flocs). Hence, if we take the range of $G$ from 20 to 70 s$^{-1}$to define the approximate conditions in which the interaction of silt and clay might be important, we would suggests that mild muddy rivers, energetic estuaries and bays, and turbidity currents would be the environments most likely to have potential interaction between the clay and silt fractions.

### 3.4.2 Uncertainty in Settling Velocity Measurements

The use of camera systems and settling columns have been widely used to obtain the settling velocity and back-calculated density of flocs in both the field and laboratory (Fennessy et al., 1994; Syvitski et al., 1995; Gratiot and Manning, 2004; Winterwerp et al., 2006; Kumar et al., 2010; Maggi, 2015). The basic procedure involves transferring a sample of suspended flocs to a clear and stagnant column of water, and then extracting the velocity and size of the aggregate as it moves through a series of images. This process is typically taken to be a reliable, state-of-the-art method for measuring settling velocity. One might expect this method to be rather straightforward. In fact, for the settling velocity of larger particles with $w_s > 1$ mm/s, such as sand, the authors have found the method to be fairly resistant to methodological variability. However, this is not the case when it comes to measuring the settling speed of individual flocs. Yet the difficulties and uncertainties present in this method when it comes to measuring floc settling velocities are rarely discussed.

The major issues that lead to uncertainty or error in the measured floc settling velocity with the settling column method are primarily two fold. The first is that when dealing with suspensions of small particles one is forced to introduce a small suspension of particles to the settling column instead of a single particle. This leads to the potential for group settling due to the added mass of the particles in the suspension. That is, the tiny suspension added to the settling column may flow downward as a small turbidity plume due to gravity acting on the particles. In such cases, the measured speed of the individual flocs flowing in the small current is higher than that of a single floc settling in identical background fluid. In such cases, the speed

of the descending flocs is a function of the overall density difference between the column fluid and the small suspension, which is set by the difference in temperature, salinity, and suspended sediment concentration. This is particularly problematic when trying to measure the settling speed of the flocs since it is impossible to capture a single floc to drop into the settling column. To mitigate settling driven by the difference in suspended sediment in the experiments reported on in this paper, we slightly increased the salinity of the fluid in the settling column relative to that in the mixing chamber. The increase in salinity was set such that the increase in density due to the presence of the suspended sediment was offset by the increase in salt within the settling column. The density of the mixture can be defined using: $\rho_{mixture} = \rho_{saltwater}(1 + \beta^{'} C_o)$ where $\beta^{'}$ is the volumetric expansion coefficient defined as $\beta^{'} = \delta\rho/\rho\delta C_o$ and $C_o$ is the initial salinity in the mixing tank ($C_o$ = 8 ppt). This increase in salinity kept the sample from settling in mass.

The second major issue that confounds floc settling velocity measurements is the development of small circulation currents within the settling column itself. These currents can be driven by temperature gradients, vibration, air currents, or the natural return flow that commences as falling particles drive and drag fluid down in the center of the column. The velocity of such currents are fairly small (0.06 to 0.2 mm/s), and they do not impact the measurement of the settling velocity of larger sediment such as sand since $w_{s,sand}$ is much greater than the velocity of the current. However, the velocity of such currents tends to be about the same as the $w_s$ of flocs. Therefore, if such currents exist, they can significantly increase or decrease the measured settling velocity depending on whether the floc is in a downward or up flowing current (Fig. 3.11). We tested small and large settling columns in many different locations within our labora-

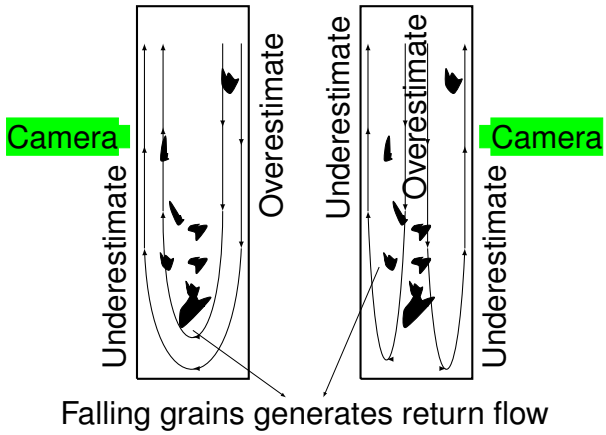


**Figure 3.11:** Circulation flow within a settling column, causing both underestimate and overestimate measurement of settling velocity.

tory and with many different techniques for setting up the column and transferring the sample from the mixing tank to the settling column. The only way found to eliminate the circulation currents in the settling column was to place both the mixing tank and the settling column in a fully enclosed and insulated chamber atop an optics table. Additionally, a time gap of at least three hours between filling of the settling column and the settling velocity measurements was required to dampen the circulation motion created from filling the column.

The broad point we are trying to make in this discussion is that extreme care must be taken when making these types of measurements. We suspect that the large range of variability in reported floc settling velocity measurements likely has as much to do with variations in the methods used to extract the data as they do with the differences in floc properties and sizes. For example reported variation in floc $w_s$ for a given floc size sometimes varies up to two orders of magnitude. In field work, Van der Lee (2000) reported Ems-Dollard estuary clay flocs with sizes of $d_f \approx 100$ $\mu$m was $w_s = 2$ mm/s, while Fennessy et al. (1994) reports River Tamar mud flocs with $d_f \approx 100$ $\mu$m of nearly $w_s = 0.25$ mm/s. In laboratory experiments, Adachi and Tanaka

(1997) used kaolinite and acquired $w_s$ = 0.075 mm/s for a floc of $d_f \approx 100$ $\mu$m while Gratiot and Manning (2004) reported $w_s \approx 10$ mm/s for natural muds at Gironde and Tamar estuaries. Undoubtedly the differences in the mud composition and floc structure are responsible for some of the variability in these settling velocities. But it is quite possible that a large fraction of the variability is due to the difficulty in making consistent measurements of floc $w_s$ in settling columns.

### 3.5 Conclusions

This study sought to explore the question of whether or not clay and silt size fractions can be treated independent of one another when it comes to modeling or predicting the settling velocity of a mixture. That is, does the presence of silt in suspension modify the settling properties of the clay, and/or does the presence of clay modify the settling properties of the silt? To begin to answer this broader question, we tested the following hypotheses: (1) the addition of silt will decrease the equilibrium floc size; (2) a fraction of the silt will become bound within the clay flocs; and (3) the addition of silt particles within the floc will produce an increase in the overall floc density and therefore the floc settling velocity.

These hypotheses were tested in a laboratory mixing chamber and settling column where the size, composition, and settling speed of the flocs could be observed and measured. Based on this data, we conclude that the presence of silt does not significantly modify the size or time-rate of development of flocs relative to a suspension of pure clay mineral; at least for the range of conditions tested in this study. While silt does not appear to modify floc size, the data did show that the majority of silt particles that remained in suspension at a given mixing condition

will eventually become bound within the clay flocs. In fact, clay flocs were able to capture silt of diameters up to 63 $\mu$mif they were in suspension. Additionally, the number of silt grains captured within a floc and the average maximum size of captured silt increased linearly with floc diameter. The addition of silt within the flocs in our study modified the floc density and led to at least a doubling of the floc settling velocity relative to flocs of equivalent sizes formed in a pure clay suspension.

This study has only looked at the interaction of one type of clay mineral mixture and one type of silt for a limited range of concentrations and turbulent shear rates. Several questions regarding how to treat mixtures of suspended silt remain. Some of these questions include: what exactly is the range of shear conditions for which one might expect to see the binding of silt in clay? Is there an upper limit to the capture of silt within flocs and what governs this limit? And, can a single settling velocity be used for all sizes of clay-silt flocs?

## Bibliography

Adachi, Y. and Tanaka, Y. (1997). Settling velocity of an aluminium-kaolinite floc. *Water Research*, 31(3):449 – 454.

Amy, L. A., Talling, P. J., Edmonds, V. O., Sumner, E. J., and Lesueur, A. (2006). An experimental investigation of sand–mud suspension settling behaviour: implications for bimodal mud contents of submarine flow deposits. *Sedimentology*, 53(6):1411–1434.

Carniello, L., Defina, A., and D'Alpaos, L. (2012). Modeling sand-mud transport induced by tidal currents and wind waves in shallow microtidal basins: Application to the Venice Lagoon (Italy). *Estuarine, Coastal and Shelf Science*, 102-103:105 – 115.

Cuthbertson, A. J. S., Ibikunle, O., McCarter, W. J., and Starrs, G. (2016). Monitoring and characterisation of sand-mud sedimentation processes. *Ocean Dynamics*, 66:867–891.

Dyer, K., Christie, M., and Manning, A. (2004). The effects of suspended sediment on turbulence within an estuarine turbidity maximum. *Estuarine, Coastal and Shelf Science*, 59:237–248.

Dyer, K. R., Cornelisse, J., Dearnaley, M. P., Fennessy, M. J., Jones, S. E., Kappenberg, J., McCave, I. N., Pejrup, M., Puls, W., Van Leussen, W., and Wolfstein, K. (1996). A comparison of in

situ techniques for estuarine floc settling velocity measurements. *Journal of Sea Research*, 36(1/2):15–29.

Dyer, K. R. and Manning, A. J. (1999). Observation of the size, settling velocity and effective density of flocs, and their fractal dimensions. *Journal of Sea Research*, 41:87–95.

Fennessy, M. J., Dyer, K. R., and Huntley, D. A. (1994). INSSEV: An instrument to measure the size and settling velocity of flocs in situ. *Marine Geology*, 117:107–117.

Ferguson, R. and Church, M. (2004). A simple universal equation for grain settling velocity. *Journal of Sedimentary Research*, 74(6):933–937.

Fox, J. M., Hill, P. S., Milligan, T. G., Ogston, A. S., and Boldrin, A. (2004). Floc fraction in the water of the Po River prodelta. *Continental Shelf Research*, 24:1699–1715.

Galler, J. J. and Allison, M. A. (2008). Estuarine controls on fine-grained sediment storage in the Lower Mississippi and Atchafalaya Rivers. *Geological Society of America Bulletin*, 120(3-4):386–398.

Garcia, M. and Parker, G. (1993). Experiments on the entrainment of sediment into suspension by a dense bottom current. *Journal of Geophysical Research*, 98(C3):4793–4807.

Gibbs, R. J. (1985). Estuarine flocs: Their size, settling velocity and density. *Journal of Geophysical Research*, 90(C2):3249–3251.

Gratiot, N. and Manning, A. J. (2004). An experimental investigation of floc characteristics in a diffusive turbulent flow. *Journal of Coastal Research*, 41:105–113.

Gratiot, N., Michallet, H., and Mory, M. (2005). On the determination of the settling flux of cohesive sediments in a turbulent fluid. *Journal of Geophysical Research*, 110(C06006).

Hill, P. S. and Nowell, A. R. M. (1995). Comparison of two models of aggregation in continental-shelf bottom boundary layers. *Journal of Geophysical Research*, 100(C11):22749–22763.

Hir, P. L., Cayocca, F., and Waeles, B. (2011). Dynamics of sand and mud mixtures: A multiprocess-based modelling strategy. *Continental Shelf Research*, 31:S135–S149.

Huang, H. (1994). Fractal properties of flocs formed by fluid shear and differential settling. *Physics of Fluids*, 6(10):3229–3234.

Hwang, K. N. (1989). Erodibility of fine sediment in wave dominated environments. Master's thesis, University of Florida, Gainesville, FL USA.

Keyvani, A. and Strom, K. (2013). A fully-automated image processing technique to improve measurement of suspended particles and flocs by removing out-of-focus objects. *Computers & Geosciences*, 52:189–198.

Keyvani, A. and Strom, K. (2014). Influence of cycles of high and low turbulent shear on the growth rate and equilibrium size of mud flocs. *Marine Geology*, 354(0):1 – 14.

Khelifa, A. and Hill, P. S. (2006). Models for effective density and settling velocity of flocs. *Journal of Hydraulic Research*, 44(3):390–401.

Kumar, R. G., Strom, K. B., and Keyvani, A. (2010). Floc properties and settling velocity of San

Jacinto Estuary mud under variable shear and salinity conditions. *Continental Shelf Research*, 30(20):2067–2081.

Lick, W., Lick, J., and Ziegler, C. K. (1992). Flocculation and its effect on the vertical transport of fine-grained sediment. *Hydrobiologia*, 235/236:1–16.

Logan, B. E. (1999). *Environmental Transport Processes*. John Wiley & Sons.

MacDonald, D. G., Goodman, L., and Hetland, R. D. (2007). Turbulent dissipation in a near-field river plume: A comparison of control volume and microstructure observations with a numerical model. *Journal of Geophysical Research*, 112(C07026).

Maggi, F. (2015). Experimental evidence of how the fractal structure controls the hydrodynamic resistance on granular aggregates moving through water. *Journal of Hydrology*, 528:694–702.

Manning, A. J. and Bass, S. J. (2006). Variability in cohesive sediment settling fluxes: Observations under different estuarine tidal conditions. *Marine Geology*, 235:177192.

Manning, A. J. and Dyer, K. R. (1999). A laboratory examination of floc characteristics with regard to turbulent shearing. *Marine Geology*, 160(1-2):147 – 170.

Manning, A. J., Spearman, J. R., Whitehouse, R. J., Pidduck, E. L., Baugh, J. V., and Spencer, K. L. (2013). *Flocculation Dynamics of Mud:Sand Mixed Suspensions*. InTech, UK.

Markussen, T. N. and Andersen, T. J. (2013). A simple method for calculating in situ floc settling velocities based on effective density functions. *Marine Geology*, 344:10 – 18.

McCave, I. N. and Hall, I. R. (2006). Size sorting in marine muds: Processes, pitfalls, and prospects for paleoflow-speed proxies. *Geochemistry, Geophysics, Geosystems*, 7(10):n/a–n/a.

Merckelbach, L. M. and Kranenburg, C. (2004). Equations for effective stress and permeability of soft mud-sand mixtures. *Geotechnique*, 1(4):235–243.

Milligan, T. and Hill, P. (1998). A laboratory assessment of the relative importance of turbulence, particle composition, and concentration in limiting maximal floc size and settling behaviour. *Journal of Sea Research*, 39(3–4):227 – 241.

Soulsby, R., Manning, A., Spearman, J., and Whitehouse, R. (2013). Settling velocity and mass settling flux of flocculated estuarine sediments. *Marine Geology*, 339:1 – 12.

Strom, K. and Keyvani, A. (2011). An explicit full-range settling velocity equation for mud flocs. *Journal of Sedimentary Research*, 81(12):921–934.

Strom, K. and Keyvani, A. (2016). Flocculation in a decaying shear field and its implications for mud removal in near-field river mouth discharges. *Journal of Geophysical Research: Oceans*, 121:2142–2162.

Syvitski, J. P. M., Asprey, K. W., and Leblanc, K. W. (1995). In-situ characteristics of particles settling within a deep-water estuary. *Deep-Sea Research II*, 42(1):223–256.

Teeter, A. M. (2001). Clay-silt sediment modeling using mulitple grain classes. part I: Settling and deposition. In McAnally, W. H. and Mehta, A. J., editors, *Coastal And Estuarine Fine Sediment Processes*, pages 157–171. Elsevier.

Van der Lee, W. T. B. (2000). Temporal variation of floc size and settling velocity in the Dollard estuary. *Continental Shelf Research*, 20:1495–1511.

Van Ledden, M. (2003). *Sand-mud segregation in estuaries and tidal basins*. PhD thesis, Delft University of Technology, The Netherlands.

van Leussen, W. (1994). *Estuarine macroflocs and their role in fine-grained sediment transport*. PhD thesis, University of Utrecht, The Netherlands.

Verney, R., Lafite, R., Brun-Cottan, J. C., and Hir, P. L. (2011). Behaviour of a floc population during a tidal cycle: Laboratory experiments and numerical modelling. *Continental Shelf Research*, 31(10):S64–S83.

Walsh, J. and Nittrouer, C. (2009). Understanding fine-grained river-sediment dispersal on continental margins. *Marine Geology*, 263(1-4):34 – 45.

Wang, Y. P., Voulgaris, G., Li, Y., Yang, Y., Gao, J., Chen, J., and Gao, S. (2013). Sediment resuspension, flocculation, and settling in a macrotidal estuary. *Journal of Geophysical Research*, 118(10):5591 – 5608.

Winterwerp, J. C. (1998). A simple model for turbulence induced flocculation of cohesive sediment. *Journal of Hydraulic Research*, 36(3):309–326.

Winterwerp, J. C., Manning, A. J., Martens, C., de Mulder, T., and Vanlede, J. (2006). A heuristic formula for turbulence-induced flocculation of cohesive sediment. *Estuarine, Coastal and Shelf Science*, 68:195–207.

Xu, J., Sequeiros, O., and Noble, M. (2014). Sediment concentrations, flow conditions, and downstream evolution of two turbidity currents, Monterey Canyon, USA. *Deep-Sea Research I*, 89:11–34.

Yuan, Y. and Horner-Devine, A. R. (2013). Laboratory investigation of the impact of lateral spreading on buoyancy flux in a river plume. *Journal of Physical Oceanography*, 43(12):2588 – 2610.

# 4 How Does the Deposition and Resuspension Process Alter Floc Sizes and Resuspension Rates?

## 4.1 Introduction

The transport processes of fine sediments are the same as those for sands involving advection and diffusion (in 2 or 3D) or dispersion (in 1D) in the water column and the boundary exchange processes of erosion and deposition (Mathew and Winterwerp, 2017). However, for mud, the main complicating issue is the substantial inter-particle interaction can occur in the suspension and deposit. These inter-particle forces add a layer of dynamics to the erosion, deposition, and transport of mud that is not present in the transport of sand. A 1D depth-averaged transport equation has the form of:

$$\frac{\partial(Cz)}{\partial t} + \frac{\partial(UzC)}{\partial x} - \frac{\partial}{\partial x}\left(\epsilon_{sx}\frac{\partial C}{\partial x}\right) = E - D \tag{4.1}$$

Where $C$ is the depth-averaged suspended sediment concentration (M $L^{-3}$), $U$ is the average fluid velocity (L $T^{-1}$), $z$ is the water depth [L], and $\epsilon_{sx}$ is the longitudinal sediment dispersion coefficient. $D$ is the rate of sediment mass per unit volume leaving the flow to the bed (deposition) ($ML^{-2}T^{-1}$), and $E$ is the rate of sediment mass per unit volume of fluid coming from the bed to the water column (erosion) ($ML^{-2}T^{-1}$). This study investigates the impact of deposition

and erosion processes on floc sizes and resuspension rates. In Equation 4.1, the terms $E$ and $D$ are often expressed as:

$$D = w_s C_b \tag{4.2}$$

and

$$E = M[\tau_b - \tau_{cr}(h)]^n \tag{4.3}$$

where $w_s$ is the settling velocity, $C_b$ is the sediment concentration near the bed (for a 1D case, $C_b$ is typically taken be a factor of $C$ or equal to $C$ for well-mixed conditions). $E$ is the erosion rate (kg m$^{-2}$ d$^{-1}$), $M$ is an empirical erosion rate constant with unit depending on the unit used in $E$ (kg m$^{-2}$ d$^{-1}$ Pa$^{-1}$), $\tau_b$ is the bed shear stress (Pa), $\tau_{cr}$ is critical shear stress (Pa), $h$ is distance from the bed surface (m), and $n$ is an empirical exponent. Equations 4.1, 4.2, and 4.3 can be applied for both cohesive and non-cohesive sediment transport. For sand, the use of these equations is straightforward since the grain size, density and shape are independent of the flow conditions. Hence, parameters such as settling velocity, $w_s$, and the critical shear stress, $\tau_{cr}$ of a certain sand size are constant, and the size of the eroded or entrained material is the same as that in the deposit. However, for cohesive sediment, the flocculation process results in dynamic changes in settling velocity through alterations to floc size, density, and shape. Furthermore, $\tau_{cr}$ may vary with depth or time, and the size of the eroded material may not be the same as it was at the time of deposition. For example, when applying Eq. 4.3 for a consolidating bed of mud, $\tau_{cr}$ is not only dependent on the grain size of the aggregates on the bed but also a function of the distance below the sediment surface (Sanford, 2008; Wiberg et al., 2013; Schoell-

hamer et al., 2017). Moreover, the knowledge of floc sizes that were detached from the bed and resuspended into the water column must also be known to model the erosion and transport processes. The complexity caused by the flocculation and consolidation processes, therefore, increases the challenge and uncertainty in prediction of transport of fine sediment. Laboratory and field studies alike have demonstrated the importance of quantifying the erosion rate and critical shear stress in order to accurately model the resuspension and transport of cohesive sediment (Tolhurst et al., 2000; Grabowski et al., 2011). For example, Moriarty et al. (2017) reveal that including the re-suspension process in their numerical model results in a more accurate prediction of the oxygen dynamics offshore of the Rhone River, France. Nevertheless, the characteristics of re-entrained flocs from freshly deposited mud has received little attention relative to the work that has been done to characterize entrainment rates of non-cohesive sand (García, 2008) or the erosion rate of muds beds of varying levels of consolidation (Grabowski et al., 2011; Wiberg et al., 2013).

Unlike cohesionless particles, cohesive sediment has the potential for the properties of the sediment to change during their time on the bed. For example, it is conceivable that during their time on the bed, flocs could dewater, increase in density or fractal dimension, and/or increase in floc strength. The consequences of the consolidation processes are reported widely in the literature as the depth-dependent critical shear stress for erosion, $\tau_{cr} = \tau_{cr}(h)$ (Sanford and Maa, 2001; Wu et al., 2017; Mathew and Winterwerp, 2017). However, these studies focused on the erosion of cohesive bed as a whole rather than investigated the size of the entrained material. Knowledge of how consolidation activities on the bed impact floc characteristics once

they resuspend are not fully understood yet. From the flocculation modeling perspective, in order to account for the re-suspension process of mud, data and understanding surrounding the change in the size of freshly deposited flocs, and their change in size after resuspension are needed.

In this study, we experimentally investigate the question: How does the deposition and resuspension process in alter floc sizes and resuspension rates? We hypothesize that flocs' characteristics changed once deposited on a bed. We further hypothesize that the conditions of the suspension at the time of deposition, the flow conditions present while the sediment is on the bed, and the duration of time the sediment is on the bed all influence the resuspension characteristics of the bed and therefore the floc sizes after resuspension.

## 4.2 Methods

### 4.2.1 Approach

Three sets of laboratory experiments were conducted to test the hypotheses. Using a mixing chamber, the experiments mimicked the cycle of deposition and erosion (or cycles of low and high shear stress) found in estuaries and/or between two benthic storm events. Parameters that were varied between experiments include: different time periods between the cycles of high and low turbulent shearing, different turbulent shear rates during the low to no shear period (what we will refer to as the deposition time), and the concentration of the suspension at the time of initial deposition (which also translates to the availability of sediment on the bed at the time of resuspension). In the first set of experiments (Set A), the shear was set with the pattern of high-low-high turbulent shearing at rates of $G = 40$, 0, and 40 $s^{-1}$. The length of time between the two

periods of high shearing was set to 0.25, 6, and 12 days for different experiments (4.2). We refer to the time period between the two high shear conditions as the time of low to no shear and as the period of deposition, $T$. In the second set of experiments (Set B), the shear pattern was modified by setting the shear rate to $G = 10\ s^{-1}$ during the period of deposition as $G = 40 - 10 - 40 - 10 - 40\ s^{-1}$ with $T = 0.25$ days. Therefore, the difference between Set A and Set B is that there is still some mixing occurring during the Set B runs when sediment has deposited to the bed. In both Set A and B, the sediment concentrations were relatively low ($C$ = 25, 100, and 400 mg/L), leading to a limited sediment supply at the time of resuspension. In the third set of experiments (Set C), the imposed shear stress steps were $G = 550 - 0 - 40\ s^{-1}$ with concentration up to $C$ = 10,000 mg/L. These high concentration experiments led to the development of a thicker mud bed during the time of no shear; this thicker bed then reduced in thickness with time through the period of deposition. Set C experiments were carried out with $T$ = 0.25, 6, and 12 days. Erosion of the thicker bed in the Set C runs provided a contrasting condition to the runs with limited sediment supply. These three sets of experiments were used to investigate hypothesis 1 and 2. We consider that changes to the state of the bed from the beginning to the end of the period of deposition in the Set A and B experiments to occur by growth, compaction, or binding of individual flocs to each other or the bed. However, changes to the bed during the set C experiments may also come from bed consolidation processes. Table 4.1 summarizes the experimental conditions. Data collected in all runs consisted of time series of concentration and the floc size distribution. Details on the experimental setup are given below.

| | **Set A**: $G$ = 550 – 40 – **0** – 40 | | | | | | **Set B**: $G$ = 550 – 40 – **10** – 40 – **10** – 40 | | | **Set C**: $G$ = 550 – **0** – 40 [$s^{-1}$] | | |
|---|---|---|---|---|---|---|---|---|---|---|---|---|
| $G$ * [$s^{-1}$] | 0 | | | | | | 10 | | | 0 | | |
| Cycles # | 1 | | | | | | 2 | | | 1 | | |
| $C$ [mg/L] | 25 | | | 400 | | | 25 | 100 | 400 | 10,000 | | |
| $T$ [days] | 0.25 | 6 | 12 | 0.25 | 6 | 12 | 0.25 | 0.25 | 0.25 | 0.25 | 6 | 12 |

**Table 4.1:** A summary of the experimental conditions. In this paper, a specific experiment will be referred as X:SSC:T Y where X is the experiment set A, B, or C; SSC is the suspended sediment concentration in mg/L; T is the low to no shear time or the deposition period in days; and Y is either before deposition (Y=D) or after resuspension (Y=R). For example, experiment B:25:0.25 R indicates the experiment in Set B with condition of concentration $C$ = 25 mg/L, deposition time $T$ = 0.25 days and the floc is at resuspension stage. *: shear stress during the deposition period. #: the number of high-low-high shear cycles repeated in one experiment.

### 4.2.2 Experimental Equipment

In this study, we used a mixing tank, floc camera system, and an OBS to provide the data needed to test our hypotheses; the setup is similar to the one used in our previous studies (Tran and Strom, 2017; Tran et al., 2018). Figure 4.1 shows a schematic of the mixing tank with the floc camera system and the Optical Backscatter Sensors (OBS). All experiments were run in a 13 L mixing chamber that has dimensions of 27.5 x 27.5 x 25 cm. Turbulent shear was generated by using a rotating paddle mixer. Logan (1999) proposed the relation between tank geometry, paddle speed, and turbulent shear rate have the form of:

$$G = \left( \frac{52.3 b_{d,p} A_p s^3 R_p^3}{\nu_w V_T} \right)^{1/2} \tag{4.4}$$

Where $b_{d,p}$ is the drag coefficient, $A_p$ is the area of the paddle, $R_p$ is the radius of the paddle, $s$ is the paddle speed (rotation in second), $\nu$ is the fluid kinematic viscosity, and $V_T$ is the total volume of the fluid in the chamber. Our selected paddle rotation rates, 0, 12, and 29 rpms,

produced tank-averaged turbulent shears of approximately $G$ = 0, 10, and 40 $s^{-1}$, respectively. This ranging of shear rates can be found in rivers (Tran and Strom, 2017), energetic estuaries and bays (Dyer et al., 2004), river mouth plumes (MacDonald et al., 2007), and turbidity current (Xu et al., 2014), or under extreme events like storms and hurricanes.

Floc size evolution within the suspension was monitored by a floc camera system. The floc camera has a 2080 x 1552 pixel progressive scan, monochrome 8 mm CMOS sensor fitted with a 2X primary magnification objective lens resulting in quantification of particle size over the range of 10 to 1000 $\mu$m. To provide illumination, a LED was fitted inside a waterproofed housing, sealed inside with a round glass plate, and placed inside the tank. Another floc camera with the same specification was placed underneath and perpendicular with the bottom of the tank to record the floc activities on the bed (Figure 4.1). Images from this camera provide qualitative data of deposited floc behaviors on the bed.

Two OBSs were installed inside the mixing chamber at 5 and 12 cm above the bottom to monitor the concentration and stratification of the suspension. OBS calibration followed the protocol in Operation's Manual (2008 - 2012) for OBS-3+ and OBS300 Suspended Solids and Turbidity Monitors given by Campbell Scientific, Inc. The calibration yield a relationship between $C$ in mg/L and the OBS measurement of NTU is: $C = 1.3902(\text{NTU}) - 7.3153$ with the coefficient of determination, $R^2 = 0.99$.

The suspension in all experiments consists of a mixture of 80% kaolinite and 20% montmorillonite (by dry mass), a mixture that has been used in past studies to mimic estuarine mud (Keyvani and Strom, 2014; Tran and Strom, 2017). The background water for all experiments

was a base of tap water with enough salt added to bring the salinity to 8.5 ppt; we have empirically found that adding salt at 5 ppt and greater reduces variability in floc growth that may occur from run to run with unsalted tap water. The water was left at room temperature for 24 hours before being used.

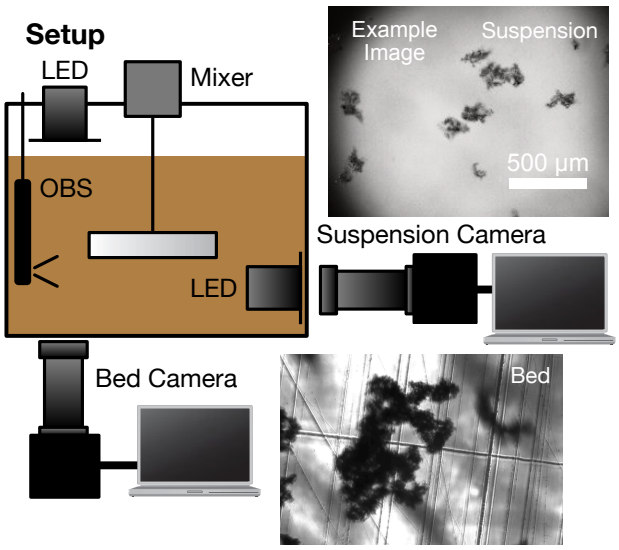


**Figure 4.1:** Schematic of the mixing chamber, including a mixer to generate turbulent shear, OBSs to measure suspension concentration, two floc camera systems to monitor floc size time series in the water column and on the bed.

### 4.2.3 Procedures

All experiments began with the preparation of the mixture. A mixture of 80%/20% kaolinite and montmorillonite (CEC = 29 meq) was first mixed with 13 L of 8.5 ppt saltwater, at shear rate of $G \approx 550$ s$^{-1}$for 30 minutes. The purpose of this period of high shearing was to disaggregate the flocs and produce a turbulent-shear-generated initial condition for the suspension. Following this vigorous mixing, the mixture was treated differently according to the purposes of each set of experiments (Table 4.1 and Figure 4.2 and 4.3).

In Set A, the shear rate was then set to $G = 40$ s$^{-1}$and left for two hours to allow flocs to

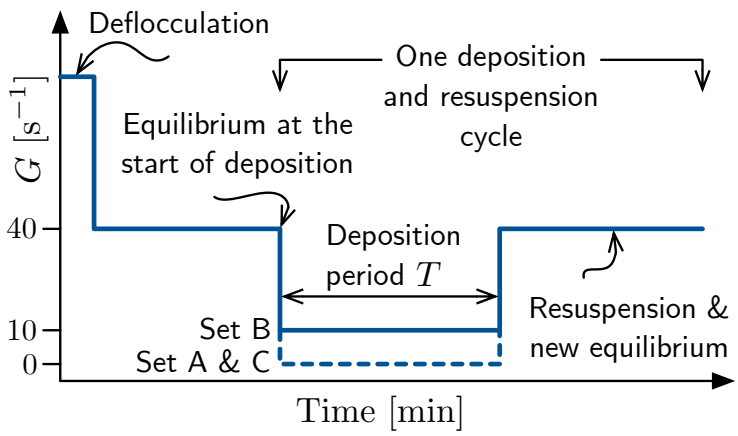


**Figure 4.2:** Procedure time series of imposed turbulent shear, $G$ and deposition time, $T$.

reach their equilibrium size. During this time, images of flocs in suspension were collected at a rate of 1 Hz. The paddle was then turned off, resulting in a shear rate of $G = 0$ s$^{-1}$during the deposition time $T = 0.25$, 6, and 12 days, respectively. In this period of time, it is possible that flocs could have bound together or compacted somewhat. However, without the presence of overlying sediment, classic consolidation was not present (Figure 4.3). (Figure 4.3). No images of flocs in suspension were collected after an approximately 30 min during the period of deposition because all sediment settled out of the water column when $G = 0$ s$^{-1}$. After this no-shear period, the paddle rotation rate was again set to produce $G = 40$ s$^{-1}$for another two hours of floc imaging. The mixture concentrations used in Set A were $C = 25$ and 400 mg/L. Set A provided data for comparison of floc size before deposition and after resuspension.

In Set B, the first two hours proceeded similarly to Set A with $G = 40$ s$^{-1}$. However, during the deposition period, there were two changes. First, instead of applying $G = 0$ s$^{-1}$(as in Set A) the shear was reduced to $G = 10$ s$^{-1}$. Mixing continued at $G = 10$ s$^{-}1$ for 6 hours ($T = 0.25$ days), before returning the shear to $G = 40$ s$^{-}1$. The low shear period also resulted in some deposition

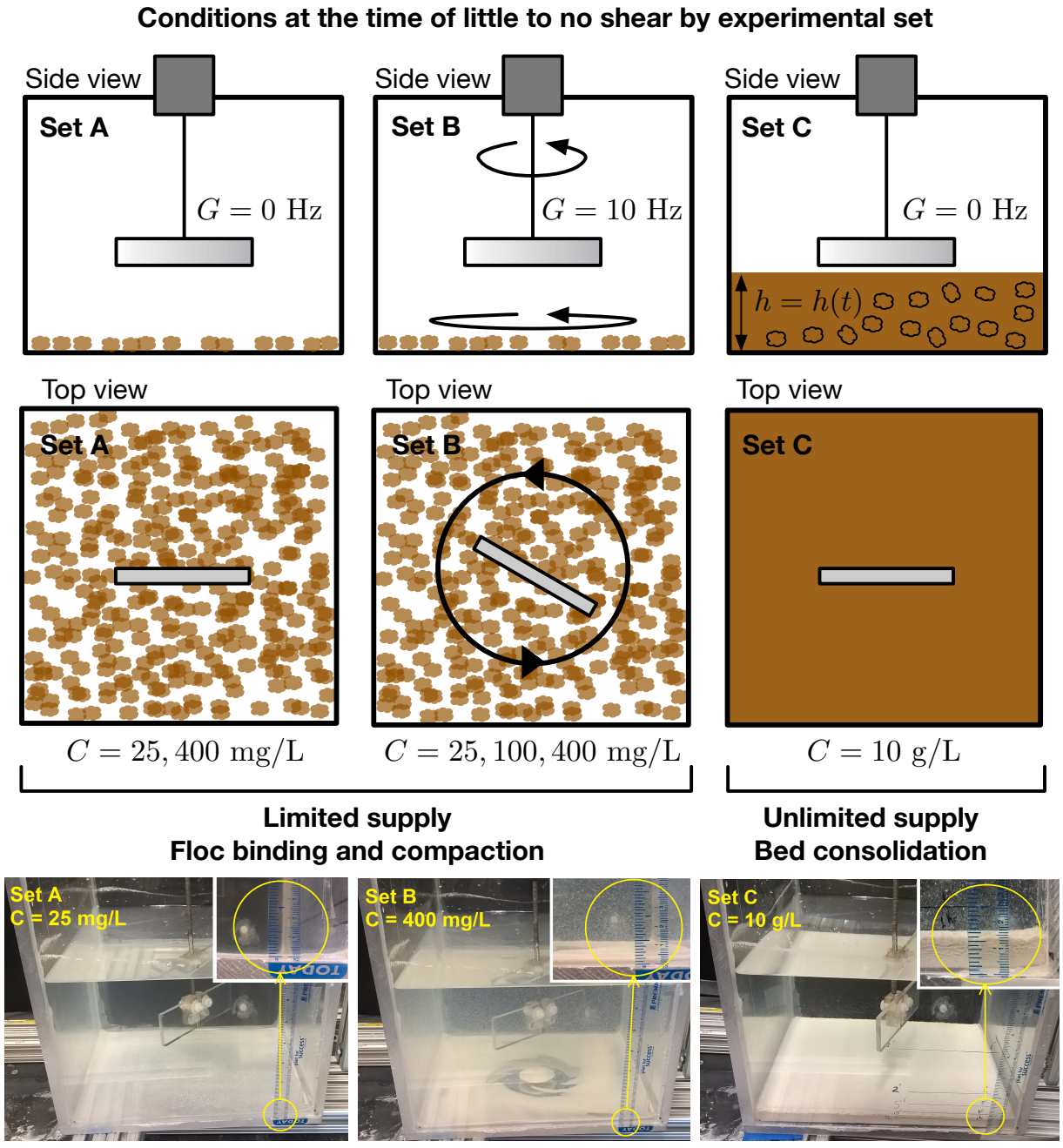


**Figure 4.3:** Schematic and photos of the period of deposition for each experimental set (organized by column). Sets A and B are considered to be conditions of limited sediment supply at the time of resuspension, whereas Set C is taken to be a condition of unlimited sediment supply in the bed at the time of resuspension. While on the bed, flocs can grow, compact, and bind to each other and/or the bed in the Set A and B runs. In Set C, the bed also undergoes compaction with time and depth (what we refer to as consolidation).

as in Set A, yet it allowed flocs in the water column and on the bed to slowly move and grow in size (Figure 4.3). Second, there were two cycles of low and high shear in the Set B runs. In Set B, three concentration conditions were examined, i.e., $C$ = 25, 100, and 400 mg/L. Set B coarsely mimics an estuarine with periods of low but non-zero shear during low and high slack.

In Set C, after the 30 min of high shearing, the shear was brought to $G$ = 0 $s^{-1}$and the suspension was left intact for $T$ = 0.25, 6, and 12 days, respectively. Following this no-shear period, the shear rate of $G$ = 40 $s^{-1}$ was applied to the suspension for five hours during which concentration and floc size were monitored.

Sets A and B are considered to be conditions of limited sediment supply at the time of resuspension, whereas Set C is taken to be a condition of unlimited sediment supply in the bed at the time of resuspension. While on the bed, flocs can grow, compact, and bind to each other and/or the bed in the Set A and B runs. In Set C, the bed also undergoes compaction with time and depth (what we refer to as consolidation).

A preliminary experiment was conducted to investigate the maximum amount of sediment that a turbulent shear rate of $G$ = 40 $s^{-1}$can keep in suspension. After the high shearing period, the shear was dropped down to $G$ = 40 $s^{-1}$for 48 hrs. The result indicated that at $G$ = 40 $s^{-1}$the turbulent can keep $C \approx$ 10,000 mg/L in suspension.

Throughout this paper, a specific experiment will be referred as X:SSC:T Y where X indicates the experiment set (i.e. A, B, or C), SSC is the concentration in mg/L, T is the low to no shear period in days, and Y is the notation for either before deposition (Y=D) or after resuspension (Y=R). For example, floc size before being deposited in an experiment in Set A that has

the condition of $C$ = 25 mg/L and consolidation time of 6 days will denote as the floc size of experiment A:25:6 D.

### 4.2.4 Image Processing

Automated image processing routines were used to extract the floc size information from collected images using the ImageJ and Matlab processing scripts of Keyvani and Strom (2013). The routines remove out-of-focus flocs and then combine the results from 60 images to yield by-volume size distributions of suspended particles every minute.

## 4.3 Results

In this study, we can have compaction, growth, or binding of individual flocs to either each other or the bed for Set A and B. And we have consolidation of the mud bed for Set C. We use the term consolidation to refer to the reduction in the void space of the bed (as evidenced by the reduction in the thickness of the bed) with time, i.e., $G = 0$ s$^{-1}$and $C$ = 10,000 mg/L. Besides consolidation, binding and compaction are other two processes that have important influence on the bed structure and behavior. The term binding refers to a process takes place on the bed in which floc either sticks to the bed or with other flocs as it rolls around in the fluff layer. Compaction refers to a process in which individual floc reduces in volume and increase in density. Binding and compaction can occur under both low shear or no shear period.

### 4.3.1 Primary Results of the Three Set of Experiments

Figure 4.4 shows the plot of the average floc size and suspension concentration with time for the Set A experiments. Figure 4.5 shows the same for sets B and C. Four observations from

the figures are in order. First, within the first 3 – 20 min of the resuspension phase, the floc sizes increase rapidly towards equilibrium. Second, in the Set A experiments, the deposited and resuspended average equilibrium floc size appear to be similar. However, in Set B, there is a slight downward trend in both floc size (in experiments B:25, and B:100) and in some cases concentration (B:400) (Figure 4.5 a,b,c). Note that the main difference between Set A and B is the shear rate during the period of deposition, $G = 0\ s^{-1}$ in Set A and $G = 10\ s^{-1}$ in Set B. Third, in Set A the floc size seems to be independent of $T$ the length for which the flocs are on the bed (Figure 4.4). Fourth, under the same turbulent shear condition, higher concentration resulted in larger floc sizes. For example, the left column in Figure 4.5 shows the results from Set B experiments in which the floc size slightly increases according to the increase of the concentration from 25 to 400 mg/L.

In the Set C experiments, the floc size after resuspension decreased slightly relative to the sizes at the time of deposition with the increase in the time for which the sediment sat on the bed $T$ (Figure 4.5 d,e,f). In all experiments, floc sizes reached equilibrium within 3 to 20 minutes.

### 4.3.2 Decrease in Resuspension Concentration

The deposition time and the availability of sediment on the floor of the tank both influence the resuspension rate and resuspended floc size. In Set A, resuspension concentration quickly goes back to the concentration value before deposition (Figure 4.4 a to f). The last experiment of Set B, B:400:0.25 shows a reduction of about 50 mg/L in resuspension concentration (Figure 4.5 c). The preliminary experiment indicates that the flow in our experiments is strong enough to keep

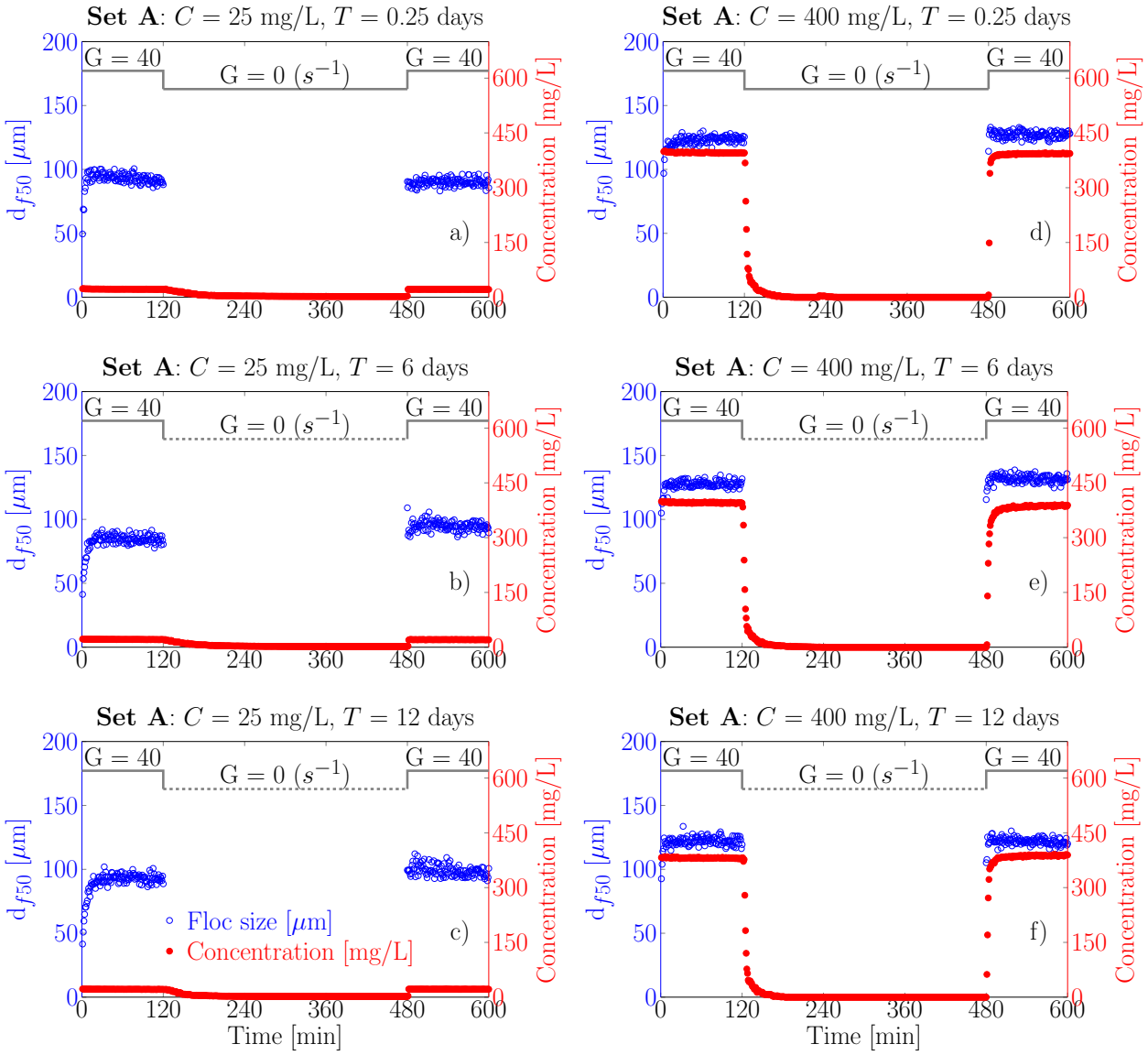


**Figure 4.4:** Measured average floc size and suspension concentration time series from the Set A experiments. The deposition period, $T$, increases from top to bottom and the concentration increases from left to right.

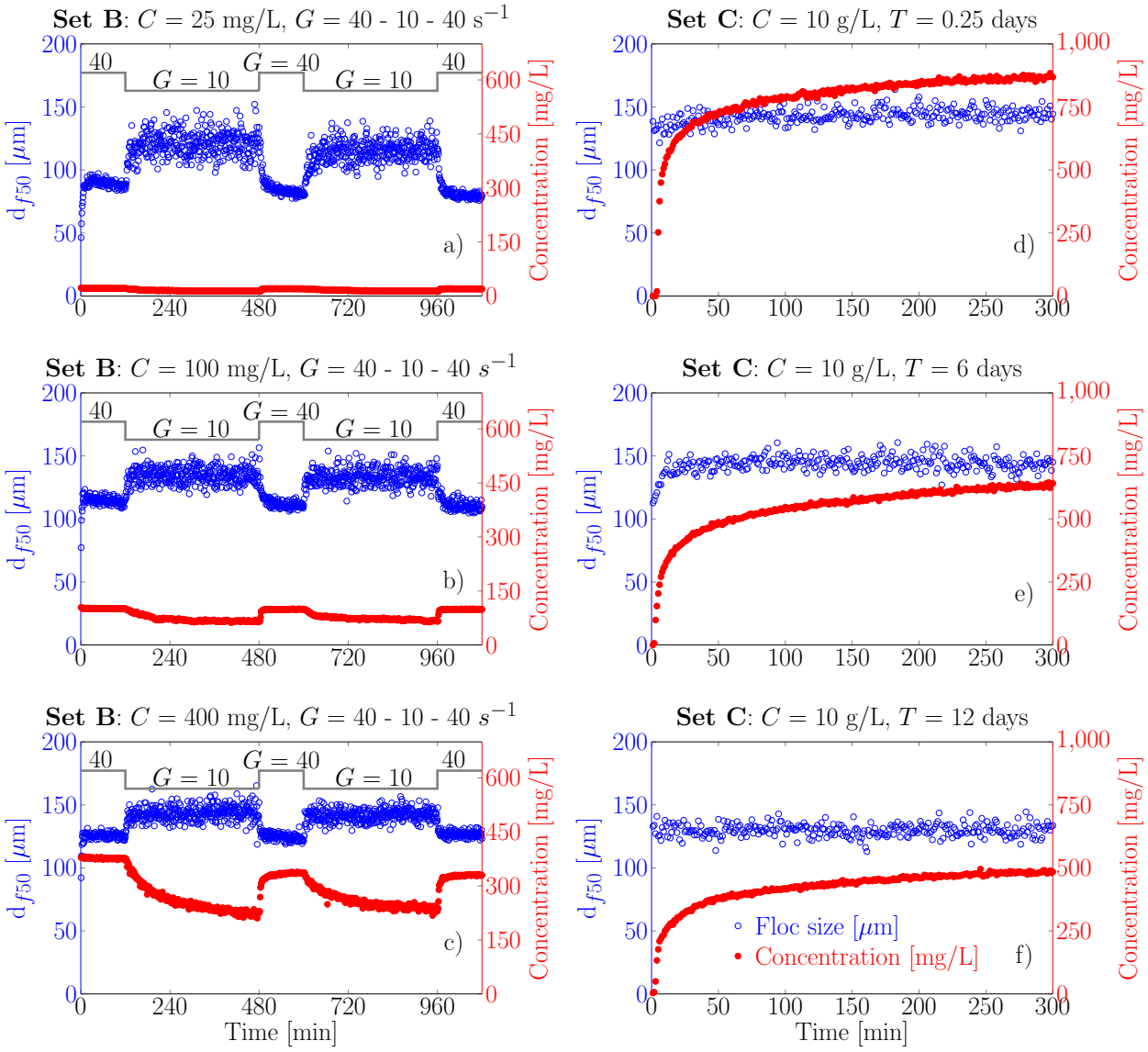


**Figure 4.5:** The left column shows floc size and concentration time series from the Set B experiments. Concentration increases from top to bottom; in all cases, $T$ = 0.25 days. The time series of average floc size and suspended sediment concentration during the resuspension phase only of the Set C experiments is given in the righthand column. For these three runs, the deposition period $T$ increases from 0.25 to 6 to 12 days from top to bottom.

about 10,000 mg/L in suspension. Hence, the deficit in concentration in the last experiment in Set B must be due to reasons other than a lack of carrying capacity of the mixing fluid. In the discussion section, we will further investigate this observation.

Figures 4.5 d,e,f illustrate the floc size and concentration evolution from the Set C experiments. The concentration time series manifest a correlation with deposition period (or the time for which the sediment was left on the bed before resuspension). For example, the equilibrium concentration after resuspension for the case of $T$ = 12 days was about 500 mg/L whereas with $T$ = 0.25 days, $C$ increased to approximate 870 mg/L. Nevertheless, amongst the three experiments in Set C, the erosion behavior is similar with a steep increase in the first 50 minutes then gradually reduce to an equilibrium. Up to this point, it seems that consolidation time does not have a significant impact on floc size but alters the behavior of the resuspension concentration. The next section will discuss in more detail the evidence of how turbulent shear, concentration, and consolidation time impact floc characteristics.

## 4.4 Discussion

### 4.4.1 The Modification of Floc Size on the Bed

Evidence that flocs grow on the bed can be seen through the reduction of resuspended floc size and concentration in both the Set B and C experiments. In Set B, the low shear, $G = 10\ s^{-1}$, allows about half of the aggregates to settle while keeping the rest in suspension. This is the time during which flocs on the bed can slowly move and grow in size. When the shear was set back to $G = 40\ s^{-1}$, most of the flocs resuspended, but some large flocs remained on the bed. Two lines of reasoning that lead us to this observation are 1) the video of floc activities on the bed

(V1), please refer to the supporting information, and 2) a decrease in floc size and $C$ compared to the first $G = 40$ s$^{-1}$ period, or the period before deposition.

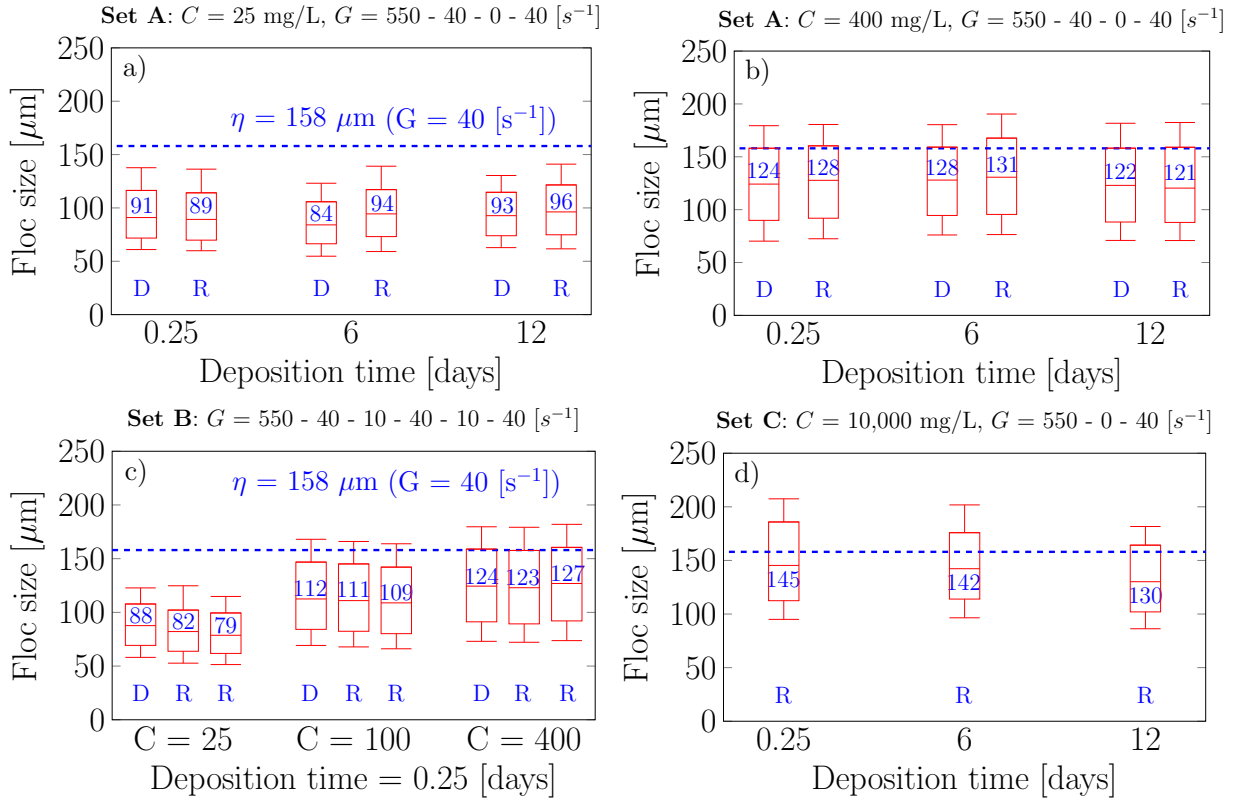


**Figure 4.6:** Data shows the floc size characteristics at equilibrium before deposition (D) and after resuspension (R) – except for Set C (figure d) where only resuspension data is shown. The horizontal bars in the box-and-whisker plots from top to bottom are: $d_{f95}$, $d_{f84}$, $d_{f50}$, $d_{f16}$, and $d_{f5}$). Each population of floc size comes from the last ten minutes of each period of $G = 40$ s$^{-1}$. On average, the number of measured flocs in the last ten minutes is around 36000 for $C = 25$ mg/L and 125000 for $C = 400$ mg/L.

First, in this paper, the second floc camera captured floc images on the bed during the low shear period. Images from this bed-camera were not used for any of the analysis in this study, such information rather used for qualitatively verifying if flocs aggregates and grows in size once they settled on the bed. The video, provided in the supporting information, reveals that flocs bind with other aggregates and grow rather quickly as soon as the shear was turned off.

Second, Figure 4.5c shows the results of the Set B experiments which unveils that the increase of floc size during the deposition time leads to a reduction in resuspended sediment concentration. For example, a deficit in resuspension concentration of 50 mg/L in each resuspension cycles is seen in experiment B:400:0.25. The reduction of resuspension sediment in lower concentration runs, i.e., B:25:0.25 and B:100:0.25, is also indirectly reflected via the resuspended floc sizes (Figure 4.6). Figure 4.6 illustrates the box-and-whisker plot of floc size characteristics at equilibrium, the last ten minutes of each $G$ = 40 $s^{-1}$period, of all experiments. The horizontal bars in the box-and-whisker plots from top to bottom are $d_{f95}$, $d_{f84}$, $d_{f50}$, $d_{f16}$, and $d_{f5}$. Figure 4.5 a,b and Figure 4.6c show that the floc size after each cycle was slightly smaller than the previous cycles. Tran et al. (2018) proposed that at low concentration floc size is very sensitive to the change in concentration. Hence, an insignificant reduction in concentration, which our OBS could not detect, can cause a small decrease of resuspended equilibrium floc size in experiments B:25:0.25 and B:100:0.25.

In Set C, observation from experiments shows that the surficial bed strata, or the fluff layer, will initially resuspend with a number of large flake shaped flocs before the turbulent shear stress takes control and reset the floc size within a few minutes. The flake flocs are only present in the longer consolidation time experiments, i.e., 6 and 12 days, where flocs have enough time to dewater and bind with other aggregates. The video V2 in the supporting information provides images of the flake flocs. This observation confirms that flocs' characteristics are a function of local conditions as shown previously in Section 4.3.1. Moreover, Figure 4.5 and 4.6d display that both the average floc size and the range between $d_{f95}$ and $d_{f5}$ after resuspen-

sion go down slightly with an increase in the period of deposition (or with an increase in the time for which the bed has a chance to consolidate).

It is noted that the presence of shear stress during the period of deposition impacts the resuspension behavior. For example, even though the experiments A:400:0.25 and B:400:0.25 have the same conditions of $C$ = 400 mg/L and $T$ = 0.25 days, the difference in magnitude of shear stress during the slack water resulted in different resuspension characteristics. Namely, only 87.5% of freshly deposited aggregates in the Set B experiment were resuspended compared to 100% resuspension in the Set A experiment (Figure 4.4f and Figure 4.5c). The importance of fluid conditions while the flocs are on the bed was also reported by Lau and Droppo (2000), who suggested that the antecedent conditions of deposition have a profound impact on the stability of the bed.

Hence, we conclude that during the low to no shear period, flocs can growth, bind, compact while on the bed and thereby slightly modify the ability of the flow to resuspend the flocs relative to the time before the flocs spent significant time on the bed. These processes seem to be rather insignificant when the fluid is stagnant while the flocs are on the bed for concentrations in the range of 400 mg/L before deposition occurs (the limited sediment supply conditions). Within this set of conditions, neither the concentration at the time of deposition or the time for which the flocs are on the bed before being resuspended have any influence on the resuspended floc size or rate of suspension. However, the presence of low shear while the flocs are on the bed in conditions of limited supply does seem to have some small influence on the resuspension characteristics of the flocs. Furthermore, increasing $C$ at the time of deposition

to create a thick mud deposit (C=10,000 mg/L, unlimited sediment supply at the time of resuspension) does produce a dependence in the resuspension characteristics on the length of time for which the bed is left undisturbed before resuspending the sediment. Such alteration in floc characteristics reflects via the reduction in resuspended floc size and concentration. The degree of modification of floc characteristics depends on the shear stress, concentration and the time of low shear period.

### 4.4.2 Resuspension Efficiency

From our data, it is not possible to quantitatively obtain the erosion coefficient or the critical shear stress, $\tau_{cr}$. Hence, in this paper, we use the time to equilibrium as a proxy of the erosion efficiency or the resuspension efficiency. Figure 4.7 shows the time for the resuspension concentration to reach its equilibrium condition in Set A and B experiments. Figure 4.8 illustrates the rates at which resuspension concentrations reach a certain value, i.e., 100, 200, 300, and 350 mg/L, in experiments in Set A and C.

**Impact of Deposition Time on Resuspension Efficiency**

It is widely reported in the literature that erosion rate goes down with an increase in time between deposition and erosion of a mud bed (Winterwerp and van Kesteren, 2004; Partheniades, 2009). Figures 4.7 and 4.8 also show that the erosion rate decrease with an increase in the deposition time. The time to equilibrium in Figure 4.7 was defined as the time that the suspension concentration needed to rise from 0 mg/L until reaching a plateau. Figure 4.7 indicates that in very low concentration in Set A experiments, i.e., $C$ = 25 and 100 mg/L, the erosion or resuspension rate is independent of deposition time with the time to equilibrium $C$ being about 3 to 4

min for all three different deposition time scenarios. The disparity in resuspension efficiency with respect to deposition time is only exposed to higher concentration experiments, $C$ = 400 mg/L. In experiments A:400, increase in deposition time from 0.25 to 6 or 12 days doubled the time to equilibrium (Figure 4.7 opened triangle markers). Figure 4.5 d,e,f also confirms that the longer the deposition time, the smaller the erosion rate will be, as evidenced by the lower concentrations. This, in turn, lead to slightly smaller resuspended floc size, since concentration also has an impact on the floc size in water column (Tran et al., 2018).

It is important to clarify that in our experiments there are two main sources causing the decrease of resuspended concentration which, in turn, leads to the reduction of equilibrium floc size in the erosion phase. First, the period of low shear, i.e., in Set B with $G$ = 10 $s^{-1}$, enhances floc binding process resulting in a small amount of floc aggregates remain on the bed during the resuspension. Such reduction of resuspended concentration leads to the decrease in floc size distribution (Figure 4.5 a,b,c and 4.6c). Second, longer deposition time improves the consolidation process making the bed stronger and more resistant to the erosion forces. Hence, the suspension concentration reentrains into the water column also reduces. Consequently, the resuspended floc size decreases (Figure 4.5 d,e,f). Impact of concentration of the mixture and turbulent shear during the slack water are discussed in more detail in the next section.

**Impact of Concentration and Shear on Resuspension Efficiency**

Figure 4.8 elucidates that in general Set C, unlimited sediment supply, takes a longer time to resuspend the same amount of sediment than in the limited sediment supply case of Set A. For example, the differences in erosion rates between experiments A:400:0.25 and C:10,000:0.25

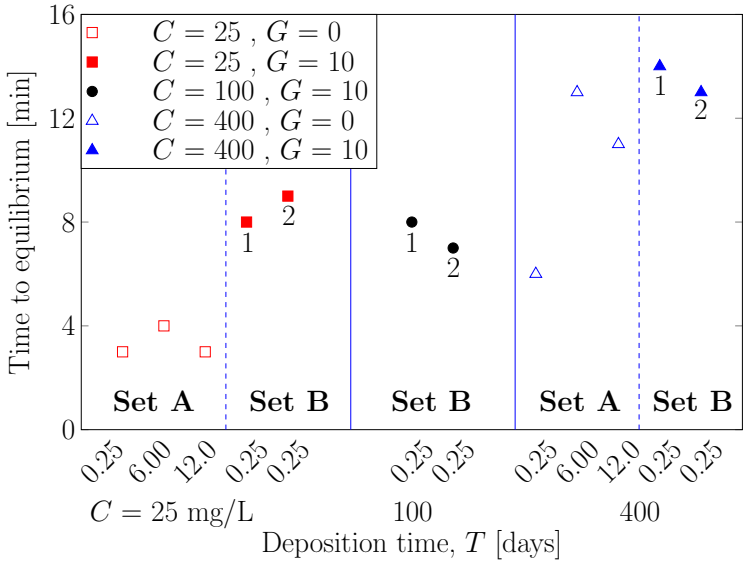


**Figure 4.7:** The time for concentration to reach equilibrium in the resuspension phase in experiments Set A and B. In the figure, $C$ is in mg/L and $G$ is in $s^{-1}$. The square, circle, and triangle markers show concentration $C$ = 25, 100, and 400 mg/L, respectively. Solid shape illustrates Set B experiments where number 1 and 2 are the first and second resuspension cycle. Opened shape indicates Set A experiments.

could only be due to differences in the concentration at the time of deposition since the other conditions such as $G$ and $T$ were the same (Figure 4.8). Unfortunately, during the deposition period due to the excessively high concentration, our floc camera was unable to obtain the floc size at the time of deposition for the Set C experiments. Nevertheless, we would argue that the floc size, shortly before deposition, of these two particular experiments, were considerably different since the floc size also a function of concentration. Such differences in prior-deposited floc size and concentration of sediment on the bed result in different aggregation, bed structure, and hence the erosion rate. If we further assume that in case of $T$ = 6 hrs, the impact of consolidation is negligible then obviously the distance between two lines A:400:0.25 and C:10,000:0.25 in Figure 4.8 caused by concentration only. Another evidence of concentration dictates erosion rate can be seen in Figure 4.7, e.g., in Set A experiments. That is, given the same deposition time,

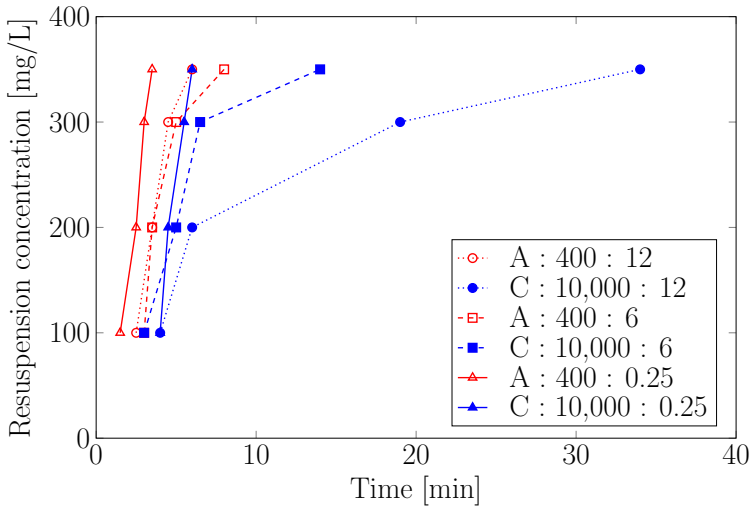


**Figure 4.8:** The time that turbulent shear under different experimental conditions in Set A and C needed to re-entrain the same amount of sediment on the bed to the water column.

higher concentration mixtures take two or four times longer to reach the equilibrium condition. Figure 4.8 also shows that higher concentrations take longer to get to equilibrium, i.e., C:10000 compare to A:400 experiments. However, what is interesting is that higher concentrations are also slower to reach to the absolute $C$ values such as the time to $C$ = 200 mg/L. Concentration, therefore, plays important role in modifying the resuspension efficiency.

In this study, the applied turbulent shear before and after deposition of the mixture is always at $G$ = 40 $s^{-1}$. However, there are two different shear rates were applied during the deposition period, $G$ = 0 $s^{-1}$in Set A and C experiments and $G$ = 10 $s^{-1}$in Set B experiments. The variation in shear during slack water period resulted in two different floc sizes on the bed. Consequently, the time to equilibrium in Set B is more than twice the time needed in Set A, given the same $T$ = 0.25 days (Figure 4.7). In other words, resuspension efficiency in Set A is double that of Set B's or at least in our experiment condition the presence of shear during the consolidation period has as much influence on resuspension efficiency as consolidation time and/or

concentration (Figure 4.7).

It is noticed that in Figure 4.8 the time to re-suspend the first 100 mg/L of sediment in all experiments are quite similar, ranging from 1.5 to 4 min, the variation becomes greater since the 200 mg/L level. For deeper layers, the values of $\tau_{cr}$ increase significantly as a function of depth results in different time to erode the same amount of sediment in different experiments. Since the $\tau_{cr} = \tau_{cr}(h)$ the erosion of the first 100 mg/L in similar time means such layer of bed deposit has similar value of $\tau_{cr}$. Thus, it seems that $C$ = 100 mg/L is the cap for flocs erosion, thenceforth, it would be the flocs or surface erosion where the turbulent shear need to break down the aggregates and/or the structure of the bed in order to bring individual floc into suspension. This observation coincides with other studies (Thomsen and Gust, 2000; Winterwerp and van Kesteren, 2004; Partheniades, 2009; Mathew and Winterwerp, 2017). Another interesting observation is that the pre-deposit condition also plays an important role in dictating the characteristics of floc aggregates on the bed which in turn impact on the resuspension coefficient.

### 4.4.3 Implication of the Findings to Resuspension Modeling

Aspects that impact the critical shear stress and erosion coefficient of pure mud or cohesive sediment have been thoroughly examined, including physical properties of the sediment (Partheniades, 1962; Dade et al., 1992; Lick et al., 2004; Mahalder et al., 2018), hydrodynamic properties (Partheniades, 2009; Mathew and Winterwerp, 2017), geochemical properties (van Ledden et al., 2004; Gerbersdorf et al., 2008; Mahalder et al., 2018), and biological properties (Dickhudt et al., 2009; Briggs et al., 2015; Li et al., 2017). Nonetheless, to the best of the authors' knowl-

edge, no studies have ever investigated the flocculation and consolidation processes of freshly deposited flocs on a bed and how such experiences can modify size and characteristics once the flocs re-entrain to the water column. Subjected to dewatering and consolidation processes the deposited flocs are expected to increase in density and fractal dimension, and decrease in size. Tran and Strom (2017) pointed out that for a floc size of 95 $\mu$m, a small increase in density (4%) or fractal dimension ($n_f$ = 2 to 2.4) can lead to an increase in settling velocity of 50%. Hence, being able to properly characterize the properties of resuspended floc is important for adequately modeling mud transport in systems that see either simultaneous erosion and deposition of flocs (such as in a river or turbidity current) or systems that have periodic erosion and deposition (such as estuaries and fresh shelf deposits that are reworked by waves). This present study is unique in that it is the first study comparing the floc characteristics before deposit and after resuspension under different condition of shear stress, suspended sediment concentration, and consolidation time.

As discussed previously, in our experimental conditions, the equilibrium floc size and floc characteristics can be altered due to two main reasons, binding and consolidation and/or the combination of both processes. The binding has a profound impact on the antecedent conditions of resuspension. First, the presence of low shear during slack water conditions was found to modify flocs on the bed relative to the case of zero shear. As shown in Figure 4.7, maintaining $G = 10\ s^{-1}$ in just 6 hours in the short deposition time experiments resulted in the same effect on the resuspension rate as of increasing the time of consolidation from 6 hours to 12 days in the case of zero shear. The importance of antecedent conditions to resuspension process was also

reported by (Lau and Droppo, 2000). Lau and Droppo (2000) conducted a series of experiments with bed deposited under quiescent conditions and under shear. Their data show that the presence of shear during the deposition increase the stability of the bed about eight times larger than without shear in the deposition process. This information shows the effect of binding either between floc and floc or between floc and the bed is a very important factor. Second, the suspension concentration at the time of deposition will define the deposited floc sizes as well as the floc sizes that will be torn off the bed and re-entrained into the water column. It is believed that the order of binding increases with the increase of suspension concentration at the time of deposition. Both binding and consolidation processes result in a stronger bed, smaller amount of large flocs and suspension concentration reentrain into the water column. This is, in turn, lead to a reduction in resuspended floc size.

Several mud erosion models are widely used in the literature include (Sanford and Maa, 2001; Sanford, 2008; Wiberg et al., 2013; Mathew and Winterwerp, 2017; Wu et al., 2017). These studies presented and discussed comprehensively the factors that affect critical shear stresses and/or erosion coefficient. Unfortunately, none of these studies illustrated how the modification of resuspended floc should be included in resuspension models. We recommend that further laboratory experiment studies to quantify the impact of antecedent conditions on the increase of fractal dimension and density of resuspended flocs are needed.

## 4.5 Conclusions

This study investigates the modification if any, of flocs after resuspension relative to their state before spending time on the bed and being resuspended. We tested two hypotheses that 1) flocs

grow on the bed and 2) resuspension efficiency dictates resuspended concentration which in turn influence the floc size. Three sets of experiments were conducted to examine the resuspended floc characteristics under different conditions of 1) consolidation time, 2) the presence of shear stress during the low shear period, and 3) limited and unlimited of sediment supply.

Overall, the data suggest that resuspended floc size is a function of local condition and independent of consolidation time. In our experiment, the floc sizes reentrain into the water column were smaller than that of the deposition phase due to either reduction in resuspended concentration or the remaining on the bed of larger flocs. The data highlights the importance of the prior-erosion condition, i.e., high concentration or the presence of low shear during the slack water period. For example, in Set B, the presence of shear during consolidation period enhances floc size on the bed and prevent some bigger flocs to resuspend which in turn influence both resuspended concentration and floc size in the water column. In Set C, a depth-limited erosion case, longer consolidation time resulted in a deficit in resuspended concentration causing smaller resuspended floc size since floc size is also a function of concentration. We conclude that for the water and sediment conditions tested in our study, the resuspended floc characteristics are could be treated as being in equilibrium with the local conditions. We also observe that in our experimental conditions, the antecedent condition of resuspension play a role as important as the duration of consolidation does.

## Bibliography

Briggs, K. B., Cartwright, G., Friedrichs, C. T., and Shivarudruppa, S. (2015). Biogenic effects on cohesive sediment erodibility resulting from recurring seasonal hypoxia on the louisiana shelf. *Continental Shelf Research*, 93:17–26.

Dade, W., Nowell, A., and Jumars, P. (1992). Predicting erosion resistance of muds. *Marine Geology*, 105(1–4):285 – 297.

de Lucas Pardo, M., Sarpe, D., and Winterwerp, J. C. (2015). Effect of algae on flocculation of suspended bed sediments in a large shallow lake. consequences for ecology and sediment transport processes. *Ocean Dynamics*, 65:889–903.

Dickhudt, P. J., Fridrichs, C. T., Schaffner, L. C., and Sanford, L. P. (2009). Spatial and temporal variation in cohesive sediment erodibility in the York River estuary, eastern USA: A biologically influenced equilibrium modified by seasonal deposition. *Marine Geology*, 267:128–140.

Dyer, K., Christie, M., and Manning, A. (2004). The effects of suspended sediment on turbulence within an estuarine turbidity maximum. *Estuarine, Coastal and Shelf Science*, 59:237–248.

García, M. H. (2008). *Sediment Transport and Morphodynamics. Sedimentation Engineering*,

chapter 2 Sediment Transport and Morphodynamics, pages 21–163. ASCE Manuals and Reports on Engineering Practice No. 110. ASCE.

Gerbersdorf, S. U., Jancke, T., Westrich, B., and Paterson, D. M. (2008). Microbial stabilization of riverine sediments by extracellular polymeric substances. *Geobiology*, 6:57 – 69.

Grabowski, R. C., Droppo, I. G., and Wharton, G. (2011). Erodibility of cohesive sediment: The importance of sediment properties. *Earth-Science Reviews*, 105(3-4):101 – 120.

Guerin, L., Coufort-Saudejaud, C., Line, A., and Frances, C. (2017). Dynamics of aggregate size and shape properties under sequenced flocculation in a turbulent Taylor-Couette reactor. *Journal of Colloid and Interface Science*, 491:167 – 178.

Keyvani, A. and Strom, K. (2013). A fully-automated image processing technique to improve measurement of suspended particles and flocs by removing out-of-focus objects. *Computers & Geosciences*, 52:189–198.

Keyvani, A. and Strom, K. (2014). Influence of cycles of high and low turbulent shear on the growth rate and equilibrium size of mud flocs. *Marine Geology*, 354(0):1 – 14.

Lau, Y. L. and Droppo, I. G. (2000). Influence of antecedent conditions on critical shear stress of bed sediments. *Water Research*, 34(2):663–667.

Li, B., Cozzoli, F., Soissons, L. M., Bouma, T. J., and Chen, L. (2017). Effects of bioturbation on the erodibility of cohesive versus non-cohesive sediments along a current-velocity gradient: A case study on cockles. *Journal of Experimental Marine Biology and Ecology*, 496:84–90.

Lick, W., Jin, L., and Gailani, J. (2004). Initiation of movement of quartz particles. *Journal of Hydraulic Engineering*, 130(8):755–761.

Logan, B. E. (1999). *Environmental Transport Processes*. John Wiley & Sons.

MacDonald, D. G., Goodman, L., and Hetland, R. D. (2007). Turbulent dissipation in a near-field river plume: A comparison of control volume and microstructure observations with a numerical model. *Journal of Geophysical Research*, 112(C07026).

Mahalder, B., Schwartz, J. S., Palomino, A. M., and Zirkle, J. (2018). Relationships between physical-geochemical soil properties and erodibility of streambanks among different physiographic provinces of Tennessee, USA. *Earth Surface Processes and Landforms*, 43:401–416.

Mathew, R. and Winterwerp, J. C. (2017). Surficial sediment erodibility from time-series measurements of suspended sediment concentrations: development and validation. *Ocean Dynamics*, 67:691–712.

Moriarty, J., Harris, C., Rabouille, C., Fennel, K., Friedrichs, M., and Xu, K. (2017). The roles of resuspension, diffusion and biogeochemical processes on oxygen dynamics offshore of the Rhone River, France: a numerical modeling study. *Biogeosciences*, 14:1919–1946.

Partheniades, E. (1962). *A Study of Erosion and Deposition of Cohesive Soils in Salt Water*. PhD thesis, University of California Berkely, Berkely, CA.

Partheniades, E. (2009). *Cohesive Sediments in Open Channels*. Butterworth-Heinemann/Elsevier, Burlington, MA.

Sanford, L. P. (2008). Modeling a dynamically varying mixed sediment bed with erosion, deposition, bioturbation, consolidation, and armoring. *Computers & Geosciences*, 34(10):1263 – 1283.

Sanford, L. P. and Maa, J. P. Y. (2001). A unified erosion formulation for fine sediments. *Marine Geology*, 179(1-2):9 – 23.

Schoellhamer, D. H., Manning, A. J., and Work, P. A. (2017). Erosion characteristics and horizontal variability for small erosion depths in the Sacramento-San Joaquin River Delta, California, USA. *Ocean Dynamics*, 67:799–811.

Sharif, A. and Atkinson, J. (2012). Model for surface erosion of cohesive soils. *Journal of Hydraulic Engineering*, 138(7):581–590.

Thomsen, L. and Gust, G. (2000). Sediment erosion thresholds and characteristics of resuspended aggregates on the western european continental margin. *Deep Sea Research Part I: Oceanographic Research Papers*, 47(10):1881 – 1897.

Tolhurst, T. J., Black, K. S., Paterson, D. M., Mitchener, H. J., Termaat, G. R., and Shayler, S. A. (2000). A comparison and measurement standardisation of four in situ devices for determining the erosion shear stress of intertidal sediment. *Continental Shelf Research*, 20:1397 – 1418.

Tran, D., Kuprenas, R., and Strom, K. (2018). How do changes in suspended sediment concentration alone influence the size of mud flocs under steady turbulent shearing? *Continental Shelf Research*, 158:1–14.

Tran, D. and Strom, K. (2017). Suspended clays and silts: Are they independent or dependent fractions when it comes to settling in a turbulent suspension? *Continental Shelf Research*, 138:81–94.

van Ledden, M., van Kesteren, W. G. M., and Winterwerp, J. C. (2004). A conceptual framework for the erosion behaviour of sand-mud mixtures. *Continental Shelf Research*, 24:1 – 11.

Verney, R., Lafite, R., and Brun-Cottan, J.-C. (2009). Flocculation potential of estuarine particles: The importance of environmental factors and of the spatial and seasonal variability of suspended particulate matter. *Estuaries and Coasts*, 32(4):678–693.

Verney, R., Lafite, R., Brun-Cottan, J. C., and Hir, P. L. (2011). Behaviour of a floc population during a tidal cycle: Laboratory experiments and numerical modelling. *Continental Shelf Research*, 31(10):S64–S83.

Wiberg, P. L., Law, B. A., Wheatcroft, R. A., Milligan, T. G., and Hill, P. S. (2013). Seasonal variations in erodibility and sediment transport potential in a mesotidal channel-flat complex, willapa bay, {WA}. *Continental Shelf Research*, 60, Supplement(0):S185 – S197.

Winterwerp, J. C. and van Kesteren, W. G. M. (2004). *Introduction to the physics of cohesive sediment in the marine environment*, volume 56 of *Developments in Sedimentology*. Elsevier, Amsterdam, The Netherlands.

Wu, W., Perera, C., Smith, J., and Sanchez, A. (2017). Critical shear stress for erosion of sand and mud mixtures. *Journal of Hydraulic Research*, 56(1):96–110.

Xu, J., Sequeiros, O., and Noble, M. (2014). Sediment concentrations, flow conditions, and downstream evolution of two turbidity currents, Monterey Canyon, USA. *Deep-Sea Research I*, 89:11–34.

# 5 Conclusions

The settling velocity, and hence floc properties, play a large role in determining where mud delivered to coastal zones ends up. Because of the difficulty in predicting how flocs change in dynamic transition zones, and because of the lack of data, flocculation is typically treated in only a very basic way in both detailed hydrodynamic models (Lesser et al., 2004; Edmonds and Slingerland, 2010) and geologic-scale deltaic and basin filling models (Syvitski and Hutton, 2001; Hutton and Syvitski, 2008). Most academic and professional studies that have included flocculation in their modeling efforts have done so using the direct modeling of $w_s$ on local conditions of $C$ and $G$ (Chapter 1). The next most common method is to use an equilibrium floc size approach (Chapter 1). Nevertheless, the flocculation data used to calibrate and validate such models are often measured in a stagnant settling column in laboratory experiments or under conditions in which multiple parameters, e.g., $C$, $G$, and salinity $S$, are co-varied during filedwork campaigns. As a consequence, the models that are developed based on such data can lead to under- or over- prediction of the floc size or floc settling velocity. Furthermore, due to the low resolution of the data sampling some important physical processes during the flocculation time might lose. For example, the aggregation and break up rate are often in the order of five minutes or less depending on the concentration and shear, hence, if the time between two sampling points is longer than five minutes the modification rate of floc to the change of

local conditions would be missing. Subsequently, in order to enhance the accuracy and to validate/calibrate any flocculation model high caliber data of flocculation evolution under different hydrodynamic conditions is required.

This dissertation examines several typical processes in coastal zones and deep ocean which have influences on the flocculation processes and hence the floc aggregates size and settling velocity. We developed a new, non-intrusive optical method, the Near Wall method, to increase the upper limit of concentration from 100 to 400 mg/L. The Near Wall method not only provides better floc images but also allow customizing the frequency at which the floc size data will be collected, every one minute in our case. Laboratory experiments also allow us full control of the hydrodynamic conditions which in turn eliminate the covariation of different parameters such as $G$, $C$, salinity and mixture of sediment. The high resolution of data collection from our laboratory experiments help to isolate the impact of each and every parameter on floc size and settling velocity. Such data is a good source of input for flocculation modeling calibration and validation. Data associated with this dissertation are also available on GitHub under https://github.com/FluidSedDynamics.

### 5.1 Summary of Primary Findings

In Chapter 2[1], the dependence of floc size on steady and decaying concentration were investigated. We hypothesized that 1) concentration has strong influences on the flocculation rate but weak impacts on equilibrium floc size and 2) the floc size adapts quickly to the change in $C$. Accordingly, two set of experiments were conducted. In the first set, different concentrations, i.e.,

[1] Published in Continental Shelf Research

$C$ = 15, 25, 50, 100, 200, 300, 400 mg/L, were kept constant in 12 h of floc size measurement. The result shows that floc size is a weak, positive function of concentration. The data also illustrate that increase in $C$ will enhance the floc growth rate, particularly when the primary particle sizes are small. In the second set of experiments, the river plume processes with the entrainment of clear water, $C$ = 0 mg/L, was mimicked using a three-tank setup. The flow rate of clear water discharged from the top tank to the mixing tank was set the same with the drain rate from the mixing tank to the bottom tank. Hence, the water level inside the mixing tank was remained unchanged during the experiment, and so was the turbulent shear. The data reveal that the equilibrium floc size response quickly to the decrease of concentration, within the range of ten minutes.

In Chapter 3[2], we examine whether mixers of silt and clay have any interaction in a turbulent suspension. Three hypotheses were tested, including 1) if the presence of silt impacts the floc size, 2) whether clay aggregates can capture silt particles, and 3) whether silt particles increase the density and thus the settling velocity of clay flocs. Subsequently, floc/particle size and settling velocity in suspension of pure clay, pure silt and mixtures of different ratio of clay:silt were measured. The data show that while silt does not has a significant impact on clay aggregate sizes, it gets bound up within the flocs and increases the density of floc which in turn lead to the increase in settling velocity. It is worth noting that under low shear ($G < 20$ $s^{-1}$)or very high shear ($G > 70$ $s^{-1}$) the number of silt particles that floc aggregates can capture reduce significantly. In other words, within the range of $G$ from 20 to 70 $s^{-1}$ silt particles and floc aggregates can be treated independently. However, within this range, the presence of silt in

[2]Published in Continental Shelf Research

suspension modified floc settling velocity considerably and the two fraction should be treated dependently. The work in Chapter 3 was published in Continental Shelf Research, volume 138, pages 81 - 94.

Chapter 4 investigates whether floc properties are modified during the resuspension process. Erosion or resuspension of floc aggregates occurs at estuary zones and/or during a benthic storm when the turbulent shear is intensive enough to break up the surficial bed strata structure, tearing off individual flocs then bringing them into suspension. We tested the hypotheses that 1) once deposited on a bed, flocs grow in size and 2) the re-entrainment efficiency dictates the resuspension concentration which in turn influences the floc growth rate and equilibrium floc sizes as floc size is also a function of concentration. To mimic the resuspension processes three sets of experiments with different turbulent shear stress patterns, consolidation times, and concentrations, were conducted. Within one experiment, the conditions at which the flocs being deposited and resuspended are always the same to make the equilibrium floc size comparable. The data show that there are unnoticeable alterations of floc characteristics before and after resuspension. The deposited flocs, however, grow in size depending on the antecedent conditions of deposition and the shear stress during consolidation time. Higher deposited concentration results in larger floc size on the bed and stronger bed structure. Consequently, the resuspension concentration reduces with the increase of concentration and/or consolidation time, leading to slight smaller resuspended floc size. A low shear stress during the slack water period also enhances the flocculation and hence the floc sizes. This improvement in flocculation also results in lower re-entrainment concentration and smaller resuspended floc sizes.

Chapter 4 is in preparation and will be submitted soon.

### 5.2 Implication and Future Work

The findings in this dissertation help to fill the gaps of knowledge in cohesive sediment transport processes. More specifically, the dissertation unveils how cohesive sediment behaves in different local conditions and also suggests how floc behaviors should be accounted for such circumstances. This information is valuable for projects such as land-building diversions on the Mississippi River. For example, we found that within the shear stress ranges $G$ 20 - 70 $s^{-1}$the interaction between silt and clay is significant. Chapter 3 suggested that in this case, settling velocity of clay:silt aggregates should be treated dependently. Another example is that better understanding of how deposition and erosion impact floc size characteristics will enhance the accuracy of cohesive sediment transport models during the resuspension process.

Currently, the findings from this dissertation have been contributing to one ongoing study. Applying the idea of the Near Wall method in the second current project, we are modifying the lens of a GoPro Hero 5 camera so that it can capture particle size ranging from 50 to 1000 $\mu$m with concentration up to 400 mg/L.

Several questions regarding the interaction of clay and silt are also under investigation. First, it is helpful to determine what exactly is the range of shear conditions for which one might expect to see the binding of silt in clay. This information important in that it suggests conditions in which the clay-silt flocs can be treated dependently or independently, i.e., can a single settling velocity be used? Second, whether the presence of silt on a cohesive bed modifies the aggregate and consolidate behavior of flocs which in turn influence the characteristics of the re-entrained

flocs. Results from such research would provide calibration data to integrate resuspended floc size and settling velocity in flocculation models.

## Bibliography

Edmonds, D. A. and Slingerland, R. L. (2010). Significant effect of sediment cohesion on delta morphology. *Nature Geoscience*, 3(2):105–109.

Hutton, E. W. and Syvitski, J. P. (2008). Sedflux 2.0: An advanced process-response model that generates three-dimensional stratigraphy. *Computers & Geosciences*, 34(10):1319 – 1337.

Lesser, G., Roelvink, J., van Kester, J., and Stelling, G. (2004). Development and validation of a three-dimensional morphological model. *Coastal Engineering*, 51(8-9):883 – 915.

Syvitski, J. P. and Hutton, E. W. (2001). 2D SEDFLUX 1.0C:: an advanced process-response numerical model for the fill of marine sedimentary basins. *Computers & Geosciences*, 27(6):731 – 753.